VASCULAR STIFFENING REGULATES ENDOTHELIAL PERMEABILITY AND SMOOTH MUSCLE CELL MOTILITY

A Dissertation

Presented to the Faculty of the Graduate School

of Cornell University

In Partial Fulfillment of the Requirements for the Degree of

Doctor of Philosophy

by

John Huynh

January 2013

VASCULAR STIFFENING REGULATES ENDOTHELIAL PERMEABILITY AND SMOOTH MUSCLE CELL MOTILITY

John Huynh, Ph. D.

Cornell University 2013

Cardiovascular diseases are the leading causes of death in the developed world. Atherosclerosis, a type of cardiovascular disease where blood vessels stiffen and accumulate lipid-laden plaques that restrict blood flow, is a major underlying cause of many cardiovascular events, including heart attack or stroke. The stiffening of blood vessels occurs also occurs with age, which is considered a significant risk factor for atherosclerosis. Although a relationship exists between age, vessel stiffening, and atherosclerosis, the exact mechanisms underlying this relationship are not well-characterized.

Herein, we demonstrate that age-related vessel stiffening promotes hallmarks of atherosclerosis, specifically endothelial permeability and vascular smooth muscle cell (VSMC) motility. Endothelial cells cultured on synthetic hydrogel substrates made to mimic the stiffness of healthy and diseased vessels exhibited increased permeability on stiffer substrates. This increase in permeability is due to the widening of endothelial cell-cell junctions and results in increased leukocyte transmigration through endothelial monolayers. Using a mouse model of aging, aged mice were also found to display increased vessel permeability and junction separation compared to young mice. Substrate stiffness induces endothelial permeability and junctional separation by upregulating cell contractility in a RhoGTPase-dependent manner.

Inhibition of cell contractility pharmacologically or with siRNA restored endothelial monolayer integrity *in vitro* and *in vivo*.

In the later stages of atherosclerosis, VSMCs migrate into the intimal layer from the medial layer of the artery and contribute to the formation of atherosclerotic plaques. Age-related vessel stiffening mediates this migration, which is also stimulated by the release of platelet-derived growth factor (PDGF) by endothelial cells or entrapped inflammatory cells. PDGF also induces the formation of circular dorsal ruffles (CDRs), actin-based structures associated with enhanced cell motility. Herein, our data demonstrate that vessel stiffening promotes the formation of CDRs by increasing cell contractility and intracellular pre-stress. When VSMC contractility was enhanced or inhibited pharmacologically, cells significantly increased or decreased CDR formation, respectively. Together, our results suggest that extracellular matrix stiffening alone, which occurs during aging, can lead to endothelial monolayer disruption, VSMC motility, and atherosclerosis pathogenesis. Our data suggest that targeting vascular stiffening and/or cellular responses to stiffening may be a promising approach to preventing atherosclerosis.

BIOGRAPHICAL SKETCH

John Huynh was born in Houston, Texas on July 26, 1984 to Anh and Quocanh Huynh. After graduating from Stephen F. Austin High School in 2002, he attended the University of Texas at Austin to pursue a Bachelors of Science in Biomedical Engineering. Upon receiving his degree in 2006, he worked at Calcitec, Inc., a start-up spine medical devices company in Austin, Texas. John joined Cornell University's Ph.D. program in Biomedical Engineering in August 2007 and was awarded a Graduate Assistant in Areas of National Need (GAANN) Fellowship. John's project on elucidating the mechanical mechanisms underlying the progression of atherosclerosis was supervised by Professor Cynthia A. Reinhart-King. He was awarded a National Science Foundation GK-12 Fellowship in 2009 and completed his doctoral degree in August 2012 before joining Merck & Co. John enjoys listening to music, playing piano and guitar, spontaneous travel, thrilling adventures, and thinks it is awesome that you just read this.

To friends and family,

For your unconditional love and support

ACKNOWLEDGMENTS

I must first thank Dr. Cindy Reinhart-King for her invaluable role in shaping me not only as a scientist, but as a mentor and a leader. Her intellect, mentorship, and unwavering support provided me ample opportunity to grow into an independent researcher. I credit her for driving me to excel, to work harder than I have ever worked, and to reach my potential as an investigator. Thank you, Cindy, for five incredible years.

I would also like to thank my dissertation committee members, Drs. Barbara Baird and Larry Bonassar. Their insights identified room for scientific growth and stimulated interesting conversations for future research.

I am immensely indebted to my collaborators, John Peloquin, Drs. Joe Califano, Christine Montague, François Bordeleau, Kuldeep Rana, Mike King, Nozomi Nishimura, and Chris Schaffer. I would not have been able to complete my projects without your friendship, expertise, and sacrifice. A special shout-out goes to Kuldeep, who maintained the most gracious attitude of any scientist I have ever had the pleasure of working with. I look forward to meeting your twins. Mike, Chris, and Nozomi, thank you for making me feel welcome in your labs and homes.

Many thanks to Belinda Floyd and Dr. Mike Shuler, who convinced me to come to Cornell and helped me transition from faraway Texas. I could not have joined a more hospitable department.

I would like to acknowledge those who have made my time here at Cornell

better-rounded. Dennis Zhou and Esther Lim, it was an honor and privilege to have you as undergraduate researchers. I have rarely met anyone as hard-working as you two, and I know you will have success wherever you go. Thanks to Nev Singhota and Drs. Shivaun Archer and Chris Schaffer who organized the GK-12 program. Thanks to Ms. Stacey Coston and Waverly High School for inviting me into their classroom. The students were an absolute inspiration for me to continue teaching science and mentoring.

I would be remiss to not express my gratitude to those who encouraged me to continue my education and pursue a Ph. D. Thanks to Drs. Nicholas Peppas and Nicki Bergmann for taking a chance on me when I had no lab experience whatsoever. Their mentorship molded my aspirations of becoming a researcher. Special thanks to Nicki, who continued to mentor me even though I showed up on my first day with an arm in a cast and sling. I would like to acknowledge Drs. Krishnendu Roy and Laura Suggs who took special interest in my development as an undergraduate. I cannot thank you enough for giving me the confidence to pursue a Ph. D. To Drs. Eric Nauman and Ed Sander, thank you for giving me the freedom to design devices and create experiments from scratch. It was immensely helpful in my growth as an engineer.

My colleagues at Calcitec, Inc. require mentioning as well. Thanks to Dr. Hai Bo Wen, Ali Ismailoglu, Peter Sargent, and Aaron Weisgerber for showing me the ropes in a start-up environment, giving me an inordinate amount of responsibilities, and stimulating my growth as a researcher. We were doing great work; unfortunately, our time was cut a bit short.

I would like to thank some old friends who have kept in contact and made sure

I was doing well from afar. Amar Shah, Brandon To, Jonathan Ng, Loc Trinh, and Najib Benhida, thank you guys for your random calls and messages. It was always a pleasure to hear about your successes or to hype up the underperforming sports teams we masochistically follow.

Thank you to the many friends in Ithaca who made this such a wonderful journey, especially those in the Reinhart-King Lab. Joe Califano, Casey Kraning-Rush, Brooke Mason, Shawn Carey, Jon Charest, and Courtney Faber, you were my surrogate family, and I will forever cherish the memories of our time in upstate New York. You were all relied upon for support, good conversations (about science and everything else), and fun times. Drs. Saumandra Bajpai and François Bordeleau, even though you have only been in Ithaca a couple of months, I thoroughly enjoyed working with you. I would also like to thank Na Young Kim and Viral Oza for their collaborations and for always keeping the lab lively. Thanks also to Blake Mason and Jason Kraning-Rush for hanging out with the CRK family and supporting all of us through thick and thin.

Special thanks to Joe Califano, who got me started in the Reinhart-King Lab and later became my roommate. We will continue our shenanigans down in West Point, PA very soon. Puifai Santisakultarm, thank you as well for being an exceptional roommate. Thanks for helping me get through tough times and making sure I was well-fed and less stressed throughout my thesis writing.

I must express my gratitude to my loving and supportive family. Mom, Dad, Sylvia, and Greg, I cannot thank you enough for everything you have done for me.

Last but not least, I must acknowledge Joanna Chen. This dissertation would not exist without her love, friendship, and devotion. Joanna, you have taught me so much about myself and helped me grow into a better person. Words cannot adequately describe what an amazing woman you are. Thank you for the memories.

TABLE OF CONTENTS

LIST OF FIGURES

Chapter 1: Introduction

Chapter 2: Real-time permeability measurements of endothelial monolayers on soft substrates

Chapter 3: Age-related intimal stiffening enhances endothelial permeability and leukocyte transmigration

Chapter 4: Substrate stiffness promotes circular dorsal ruffle formation in vascular smooth muscle cells

Chapter 5: Exploring biomechanics in the classroom

Chapter 6: Conclusions and future directions

LIST OF ABBREVIATIONS

AFM	Atomic force microscopy
BAEC	Bovine aortic endothelial cell
CDR	Circular dorsal ruffle
CVD	Cardiovascular disease
EC	Endothelial cell
ECM	Extracellular matrix
FITC	Fluorescein isothiocyanate
GAPDH	Glyceraldehyde 3-phosphate dehydrogenase
HUVEC	Human umbilical vein endothelial cell
IBL	Inquiry-based learning
ICAM	Intercellular adhesion molecule
LDL	Low density lipoprotein
MLC	Myosin light chain
MLCK	Myosin light chain kinase
MMP	Matrix metalloproteinase
PA	Polyacrylamide
PDGF	Platelet-derived growth factor
ROCK	Rho-associated kinase
TFM	Traction force microscopy
TNF-α	Tumor necrosis factor-α
VCAM	Vascular cell adhesion molecule
VEGF	Vascular endothelial growth factor
VSMC	Vascular smooth muscle cell

CHAPTER 1

INTRODUCTION

Portions of this chapter were published as a book chapter titled “Cell Generated Forces in Tissue Assembly and Disease” in *Mechanobiology of Cell-Cell and Cell-Matrix Interactions* (Huynh et al., 2011)

1.1 Atherosclerosis

Cardiovascular diseases (CVDs) are the leading causes of death in the United States, accounting for approximately 800,000 out of 2.5 million deaths per year, or nearly 33 percent (Roger et al., 2012). Atherosclerosis, a disease where blood vessels harden and thicken, is the underlying cause of CVDs (Frostegård, 2005; Noll, 1998). During the progression of atherosclerosis, white blood cells and fatty materials like low density lipoproteins (LDL) permeate through the endothelial cell (EC) layer and accumulate within the vessel wall (Ross, 1999). The release of cytokines and growth factors from endothelial cells and white blood cells stimulates the migration and proliferation of normally quiescent vascular smooth muscle cells (VSMCs) from the medial layer into the intima (Raines, 2004). This results in the formation of atherosclerotic plaques that occlude the vessel and restrict blood flow (Paraskevas et al., 2007). Rupture of these plaques often leads to the formation of thrombi, which can detach and block downstream blood flow (Badimon and Vilahur, 2012). This generally has severe consequences as the blockage of blood flow may lead to complications such as claudication, heart attack, and stroke.

Atherosclerotic vessels have increased stiffness compared to healthy, native

vessels (Zoungas and Asmar, 2007). This increase in vascular stiffness is partially due to increased deposition of extracellular matrix (ECM) proteins collagen and fibronectin (Zieman et al., 2005), collagen cross-linking caused by the accumulation of advanced glycation end-products (Basta, 2008), and elastin fatigue and fracture (Greenwald, 2007; O'Rourke, 2007). In addition to atherosclerosis, vascular stiffening also occurs in a number of other pathologies, including hypertension (Laurent and Boutouyrie, 2007) and diabetes (Laugesen et al., 2009).

Interestingly, vascular stiffening also occurs universally with age, which is considered a major risk factor for CVD. A recent study showed that aortic pulse wave velocities, a measurement of arterial stiffness, of healthy 85 year olds are double that of healthy 35 year olds (McEniery et al., 2005), clearly linking vascular stiffening to age. Additionally, according to recent statistics, only ~18% of CVD-related deaths occurred in people younger than 65 years of age, but ~67% of deaths due to CVDs occurred after the age of 75 (Roger et al., 2012). Atherosclerosis is found in half of the population over the age of 65. Notably, studies have shown that macroscale arterial stiffness, measured through pulse wave velocities, can independently predict cardiovascular events including coronary heart disease and stroke and are used for clinical diagnosis of cardiovascular risks (Blacher et al., 1999; Mattace-Raso et al., 2006; Sutton-Tyrrell et al., 2005). To perform pulse wave velocity measurements, two probes are placed on the patient—generally, one at the carotid artery and another at the femoral artery. These probes sense the pulse through the arteries and calculate the speed of blood flow by using the distance between the two probes. The slower that the pulse wave velocity is, the more elastic and distensible the arteries are. Conversely, faster pulse wave velocities indicate stiffened vessels and increased risk for CVD (Boutouyrie et al., 2009).

While vascular stiffening correlates with cardiovascular risk, little is known about how changes in vascular stiffness affect the function of the endothelial and vascular smooth muscle cells in the vessel wall. It was not until more recently that platforms were developed to rigorously study the relationship between substrate stiffness and cell behaviors like adhesion, proliferation, migration, and differentiation. These platforms will be described in the following sections, along with an overview of the forces in cell-substrate and cell-cell interactions, methods to measure cell forces and mechanical properties, and the importance of forces in disease, particularly atherosclerosis.

1.2 Biology of cell-cell and cell-substrate interactions

1.2.1 Cell structures involved in mechanosensing

Cell adhesions are critical for the maintenance and structure of tissues. Two families of structures that are important in mediating cell adhesions are cadherins and integrins. Cadherins are calcium-dependent transmembrane proteins that associate with cell-cell adhesions (Nishimura and Takeichi, 2009). Integrins, on the other hand, are transmembrane proteins that mediate cell-ECM interactions (Delon and Brown, 2007). Importantly, both cadherins and integrins are physically linked to actin (Aplin et al., 1998), a major component of the cell cytoskeleton. Due to this linkage, crosstalk between cadherins and integrins are thought to regulate mechanotransduction during development (Schwartz and DeSimone, 2008) and disease progression (Jaalouk and Lammerding, 2009).

Within the vasculature, endothelial cells line the inner surface of blood vessels and control the permeability of cells and solutes into the underlying tissue.

Perturbation of the endothelial lining may result in pathological conditions such as edema (Chavez et al., 2011) and atherosclerosis (Hirase and Node, 2012). Vascular endothelial (VE)-cadherin regulates endothelial cell-cell adhesions by forming adherens junctions, zipper-like structures along the cell border than link ECs to one another (Dejana and Giampietro, 2012). In addition to mediating cell-cell interactions, VE-cadherin interacts with the cell cytoskeleton by binding to actin through regulatory or scaffolding proteins like α-catenin, β-catenin, p120, and plakoglobin (Dejana et al., 2008). Interestingly, when VE-cadherin is phosphorylated at tyrosine residues, adherens junctions separate due to VE-cadherin degradation and internalization (Gavard, 2009), resulting in impaired endothelial barrier function. Because VE-cadherin is linked to actin, actomyosin contraction is also believed to regulate cell-cell adhesions (Dudek and Garcia, 2001).

Integrins are heterodimeric transmembrane proteins that are heavily involved in cell-substrate interactions. Although 18 α-subunits and 8 β-subunits have been identified in mammals, integrins only assemble into 24 different known pairs, each of which have specific interactions with different ECM proteins (Margadant et al., 2011). Two distinct mechanisms are involved in integrin signaling and activation. In "outside-in" signaling, the binding of integrins to its ligand or ECM causes a conformational change and activation of integrins. Conversely, in "inside-out" signaling, the binding of an intracellular activator, e.g. talin or vinculin, induces increased affinity of integrins for its ligand (Shattil et al., 2010). When activated, either by internal or external signals, integrins cluster at adhesion sites, growing in size and protein content from nascent focal complexes to focal adhesions (FAs) (Berrier and Yamada, 2007; Parsons et al., 2010).

Focal adhesions are particularly important in cell-matrix interactions and mechanotransduction (Chicurel et al., 1998; Katsumi et al., 2004; Maniotis et al., 1997). This is partially due to their role in acting as a centralized point for downstream signaling cascades. Indeed, a large number of signaling proteins involved in cell migration and proliferation are recruited to FAs, including focal adhesion kinase (FAK) (Zhao and Guan, 2011), integrin-linked kinase (ILK) (Persad and Dedhar, 2003), and Src (Kim et al., 2009). In addition to their role as signaling hubs, FAs connect the actin cytoskeleton to the underlying ECM (Shattil et al., 2010).

Actin is a ~42 kDa protein that exists in two forms in the cell: globular monomeric actin (G-actin) and filamentous actin (F-actin). G-actin can bind ATP to form a stable core which becomes the basis for spontaneous F-actin polymerization (Dominguez and Holmes, 2011). Bundles of F-actin, or stress fibers, are critically important in determining cell shape and contractility (Ingber, 2003; Pellegrin and Mellor, 2007). When treated with cytochalasin D, an inhibitor of actin polymerization, cells lose their structural integrity and ability to remain well-spread (Kraning-Rush et al., 2011). Myosin motor proteins interact with stress fibers to provide contractile forces within cells which are then transmitted to the ECM as traction forces (Kumar et al., 2006). As will be reviewed later in this chapter, traction forces are essential for many cell behaviors including migration, differentiation, and disease.

1.2.2 Signaling pathways involved in mechanosensing

The Rho family of guanosine triphosphatases (GTPases) is a family of G proteins that are intricately involved in actin cytoskeletal organization (Bishop and Hall, 2000) and the generation of cell contractile forces (Huang and Ingber, 2005). As a G protein, RhoGTPase acts as a molecular switch—it is active or inactive when

bound to GTP or GDP, respectively. Rho guanine exchange factor (RhoGEF) associates Rho with GTP so that active Rho can associate with and stimulate different effector proteins. Rho GTPase-activating protein (RhoGAP) hydrolyzes GTP to GDP, returning Rho to an inactive state.

To control actin dynamics, RhoGTPase associates with its effector, Rho-associated kinase (ROCK) to control the activity of downstream myosin (Narumiya et al., 2009). ROCK serves a dual purpose to elicit actomyosin contraction. Firstly, ROCK inactivates myosin light chain (MLC) phosphatase, which inhibits the dephosphorylation of MLC resulting in increased levels of phosphorylated MLC. Secondly, ROCK can phosphorylate MLC directly (Amano et al., 2010). Together, ROCK activity induces MLC phosphorylation which stimulates the association of myosin with stress fibers and increases actomyosin contraction.

1.2.3 Measuring cell forces

Cadherins, integrins, and actin are physically linked within the cell, and their interplay is crucial to controlling cell contractility and traction force generation (Kumar et al., 2006). Traction forces have been implicated in regulating a variety of cell behaviors (Chen, 2008; Discher et al., 2005; Orr et al., 2006; Vogel and Sheetz, 2006). Endogenous traction forces are used for motility, tissue assembly, ECM remodeling, and mechanosensing. In recent years, many different methods have been developed to quantify cellular traction forces. Here, I will briefly describe these *in vitro* methods and highlight the experiments that have characterized the nature of traction forces.

The first observations of traction forces were published by Harris and

colleagues in 1980. Using deformable silicone rubber substrates, they captured images of fibroblasts forming wrinkles in the substrate (Figure 1.1A), indicating the generation of inward forces strong enough to deform their substrate (Harris et al., 1980). Interestingly, there was no evidence of pushing forces based on the location of the cell relative to the wrinkles. The most significant drawback to the wrinkling substratum method, despite its ease to implement, is that it is only semi-quantitative. It is difficult (and perhaps impossible) to derive quantitative information about the magnitude of the forces based on the location or size of the wrinkles. This limitation was overcome by the incorporation of fluorescent beads into pre-stressed silicone substrates, which provided a more quantitative analysis of cellular traction forces (Lee et al., 1994) and set the stage for methods of measuring force through substrate displacement analysis. Regarded as an inverse problem where cell-generated stress is calculated from the measurement of underlying substrate displacement, one particular method for measuring traction forces from substrate displacements has gained prominence in recent years: traction force microscopy.

Traction force microscopy (TFM) was developed by Dembo and coworkers to measure cell-generated traction stresses (Dembo et al., 1996). Using images of fluorescent bead fields before and after a cell is released by trypsinization, TFM calculates bead displacements through an optical flow algorithm (Marganski et al., 2003). As mentioned above, these displacements can then be used to inversely calculate force generation based on the stiffness of the substrate to which cells are attached (Figure 1.1D-H) (Dembo and Wang, 1999). TFM algorithms by Dembo et al. have been packaged in a licensed software library called LIBTRC. Similar techniques that also solve the inverse problem have been published by others in recent years (Del Alamo et al., 2007; Butler et al., 2002; Sabass et al., 2008).

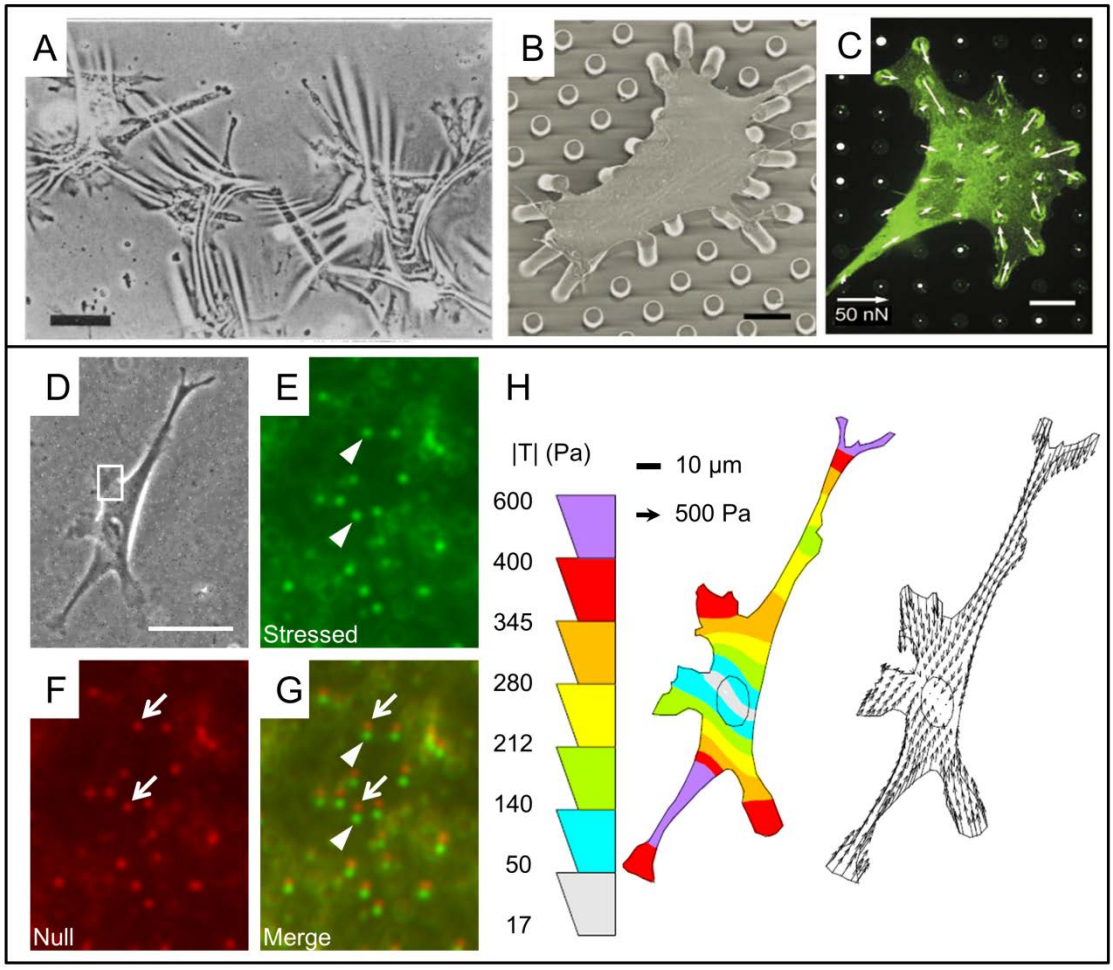
A
B
C
50 nN
D
E
Stressed
F
Null
G
Merge
H
|T| (Pa)
600
400
345
280
212
140
50
17
10 μm
500 Pa

Figure 1.1. (A) Landmark experiments with chick heart fibroblasts on deformable silicone substrates reveal the presence of cell-generated traction forces; bar is 100 μm. From Harris et al. (1980). **(B)** and **(C)** Micropost arrays: **(B)** Electron micrograph of a smooth muscle cell attached to a microfabricated post array. **(C)** Traction force vector map (white arrows) obtained by measuring post deflections spatially correlated with immunofluorescence localization of the focal adhesion protein vinculin (green); bars are 10 μm, arrow is 50 nN. From Tan et al. (2003). **(D-H)** Traction force microscopy: **(D)** A cell is plated on a deformable substrate and imaged with phase contrast microscopy. Fluorescent beads embedded in the gel substrate are imaged immediately after the phase image (e, "Stressed") and after cell removal with trypsin (f, "Null"). **(G)** Merged fluorescent images depict the displacements of the marker beads in the substrate due to cell contractile forces in the boxed region of the phase image. **(H)** Marker displacements are used to calculate the magnitude (|T| per area) and direction (arrows) of tractions that a cell exerts on the substrate. Scale bar in (D-G) is 50 μm; beads in (D-G) are 0.5 μm in diameter. From Califano and Reinhart-King (2010). Reprinted with kind permission of Springer Science and Business Media.

A second prominent method for measuring traction, first described by Tan and coworkers (Tan et al., 2003), involves cell culture on microfabricated post array detectors (mPADs, Figure 1.1B and C) (Sniadecki and Chen, 2007). Cell force and contractility causes the posts to deflect. These deflections are directly proportional to the traction forces exerted by the cell and are calculated at each post using elastic beam theory (Tan et al., 2003). The modulus of mPADs can be altered by the geometry of the posts independent of the surface ECM coating that facilitates cell adhesion. The advantage of such a technique is that computationally, cellular forces are straightforward to calculate, as the calculation is based on simple beam-bending mechanics. Moreover, the force on each post is decoupled. A drawback of these measurements is that the cells are adherent to a non-continuous surface, which deviates further from mimicking the *in vivo* environment.

Alternate methods of force quantification have also been described, including the use of microfabricated cantilevers (Galbraith and Sheetz, 1997) and micropatterned silicone elastomeric substrates (Balaban et al., 2001), but their appearance in the literature is limited.

1.3 Cell-substrate and cell-cell interactions mediate cell forces

1.3.1 Cell-substrate interactions mediate force generation

Traction force generation is sensitive to a variety of factors, including cell shape, cell size, ECM density, substrate stiffness, and growth factors present in the environment. Early work showed that traction generation is dependent on both cell shape and size (Parker et al., 2002; Wang et al., 2002). In these studies, cells were cultured on adhesive islands of different shapes to understand how cell shape affects traction force generation. The authors find that tractions on circular islands were greatest at sites of

cell protrusion but exhibit no preferred direction of force. However, on square islands, the highest tractions are associated with protrusions at the square corners, implicating shape to be an important mediator of traction force generation. In regards to cell size, Lemmon and co-workers performed a comprehensive study of traction force measurements across numerous cell types, including smooth muscle cells, endothelial cells (ECs), fibroblasts, and epithelial cells. While the magnitude of traction forces between cell types varied significantly, within each cell type traction forces increased with cell size (Lemmon et al., 2005), underscoring the importance of cell size and spreading to traction force generation. Work in our lab also shows that traction forces increase linearly with cell area (Reinhart-king et al., 2003).

Traction forces are also sensitive to substrate ECM coating and stiffness. On polyacrylamide gels derivatized with increasing concentrations of ligand, cells exhibit increased spreading and higher traction forces on substrates with higher ligand concentration (Reinhart-King et al., 2005). It is hypothesized that additional ligand on a surface increases the availability of cell-matrix adhesions to form, thereby increasing focal adhesion formation and cell contractility. Cellular force also increases with substrate stiffness and concomitant increases in cell area (Lo et al., 2000; Paszek et al., 2005). Since increasing substrate stiffness increases contractility and cell area, interplay between substrate stiffness, cell area, and traction force generation may exist. Using measurements of force, area, and stiffness coupled with linear regression modeling, our lab demonstrated that both substrate stiffness and cell area are significant predictors of traction force generation. (Califano and Reinhart-King, 2010). Together, these data suggest that both substrate stiffness and cell area, whether modulated by stiffness directly or by ligand density, contribute significantly to traction force generation.

Interestingly, growth factors present in the extracellular environment also modulate cell contractility (Ren et al., 1999). For example, vascular endothelial growth factor (VEGF), a secreted glycoprotein that stimulates endothelial cell proliferation, migration (Leung et al., 1989), and angiogenesis (Nicosia, 1998) has been shown to stimulate stress fiber and focal adhesion formation (Huot et al., 1998) through RhoGTPase and ROCK activation (van Nieuw Amerongen et al., 2003). Similarly, tissue growth factor-α (TGF-α), a ligand for epidermal growth factor receptors, stimulates RhoGTPase and ROCK activity that lead to cytoskeletal reorganization (Appleton et al., 2010). While growth factors are typically only considered in the context of their effects on cell growth on proliferation, these data indicate that they may function in part through their ability to alter cell contractility profiles. It is likely that there is significant crosstalk between cell response to growth factors, substrate stiffness, and cell-matrix adhesions, suggesting that these separate signals integrate intracellularly to produce a specific cell response.

In addition to “outside-in” events that cause cells to alter their force generation, “inside-out” events occur where cell-matrix adhesions transmit force from the cell to the substrate. Real-time measurements of cell force coupled with fluorescent imaging of focal adhesions indicate that focal adhesion area is linearly dependent on the local force exerted by a cell (Balaban et al., 2001). This relationship indicates that a constant stress is applied to focal adhesions in the cell despite variations in focal adhesion size and shape. Separate experiments with cells on mPADs confirm that cell-generated stresses onto their substrate correlate with focal adhesion size (Tan et al., 2003). Less mature focal complexes at the leading edge of a cell are capable of exerting strong transient forces that drive migration (Beningo et al., 2001). Forces

subsequently decrease as adhesions mature into large plaques that become centrally localized in the cell during migration. More recent work further illustrates the complex interaction of force generation and substrate adhesions. When 3T3 fibroblasts are seeded on magnetic microposts and deflected by an external magnetic field, changes in traction forces occur at peripheral adhesions that are located further away from the force application site (Sniadecki et al., 2007). These data suggest that cells can respond to an "outside-in" mechanical signal at one location and transmit cell-generated traction forces "inside-out" at another location. It is hypothesized that mechanical signals can be transmitted throughout the cytoskeleton, but the exact mechanism remains unknown. Together, these data emphasize the complex interplay between "outside-in" and "inside-out" signaling that controls mechanotransduction and force generation.

1.3.2 Cell-cell interactions mediate force generation

While much of the work investigating cellular traction forces have focused on cell-matrix contractility, recent work has adapted traction force microscopy methods to the study of forces exerted at cell-cell contacts as well (Ganz et al., 2006). Cadherins are intimately linked to intracellular signaling mechanisms that influence cellular contractility and force generation. For example, vascular endothelial (VE)-cadherin mediated cell-cell contact activates a RhoGTPase signaling pathway, resulting in increased intracellular tension (Nelson et al., 2004) and time-dependent adhesion strengthening (Kris et al., 2008). Interestingly, this cadherin-mediated increase in contractility is actin dependent, similar to integrin-mediated contractility.

Cadherins are capable of mediating cellular contractility, and there is growing interest in measuring these forces. To do this, recent work has coated deformable

substrates with cadherin fragments, thereby simulating cell-cell contacts on a matrix used for traction measurements. Cadherins directly transmit traction forces (Ganz et al., 2006; Ko et al., 2001) that increase with increasing substrate rigidity and require actomyosin activity (Ladoux et al., 2010). These data implicate cadherins as integral components of cellular mechanosensing.

1.4 Cell-matrix and cell-cell interactions in development, migration, and disease

1.4.1 Matrix stiffness regulates development and differentiation

Matrix rigidity, which plays a large role in the generation of traction forces, also plays a critical role in development, differentiation, and tissue formation. In a seminal study by Engler and co-workers, substrate stiffness alone has been found to direct differentiation of mesenchymal stem cells (MSCs) (Engler et al., 2006). When plated on substrates that have a rigidity similar to that of brain tissue, MSCs are directed into a neurogenic lineage, whereas on stiffer substrates that mimic the rigidities of muscle or collagenous bone, MSCs differentiate into myogenic or osteogenic lineages. Similarly, substrate elasticity has been found to modulate cell spreading, growth rate, gene expression, and osteogenic differentiation of pluripotent embryonic stem cells (Evans et al., 2009).

In addition to changes in ECM stiffness, the stiffness of cells themselves also contributes to differentiation and embryogenesis. Notably, the nuclei of human embryonic stem cells stiffens six-fold as cells progress through differentiation (Pajerowski et al., 2007), suggesting that cell stiffening plays a role in promoting differentiation. Chowdhury et al. corroborated this finding by showing that mouse embryonic stem cells are ten times softer than their differentiated counterparts (Chowdhury et al., 2010). It has been hypothesized that by remaining soft,

undifferentiated cells have the advantage of being more motile and retain the ability to migrate through solid tissues and small pores.

Cell stiffness is directly influenced by the actomyosin-dependent contraction of cells (Krieg et al., 2008). Sordella and coworkers show that modulating the activity of RhoGTPase, an integral mediator of cell force generation, is sufficient to alter the differentiation program of adipocyte and myocyte precursors (Sordella et al., 2003). The authors also show that mouse embryo-derived fibroblasts lacking p190RhoGAP, an inhibitor of RhoGTPase, have excessive Rho activity and are defective for adipogenesis, opting instead to undergo myogenesis. Subsequent studies suggest that actomyosin-dependent tension, mediated by Rho and its downstream effector Rho-associated kinase (ROCK), is required for human MSCs to commit to osteogenesis (McBeath et al., 2004). McBeath and coworkers attribute lineage commitment to mechanical cues presented by changes in cell shape—they found that unspread, round MSCs underwent adipogenesis whereas flat, spread cells committed to an osteogenic lineage.

In vivo studies also implicate the Rho-ROCK pathway as a central facilitator of differential growth in tissue assembly. In embryonic mouse lung morphogenesis, disrupting cell tension by inhibiting ROCK and other downstream effectors alters basement membrane thickness, inhibits new epithelial bud formation, and disrupts capillary blood vessels (Moore et al., 2005). Conversely, increasing cell tension by activating RhoGTPase accelerates lung branching and increases capillary elongation. Taken together, these studies highlight the critical role cell-generated forces play in the correct differentiation of stem cells and embryonic development.

1.4.2 Cell-generated forces regulate cell motility, migration, and proliferation

One of the core functions of traction force generation is to drive cell motility (Oliver et al., 1999), a process that is necessary during cell organization and tissue assembly. Differential motility among cell types is responsible for cell sorting and self-organization in tissues (Mori et al., 2009). Local ECM chemistry and mechanics that affect cell-generated forces are likely responsible for the differential motility of cells during development and assembly. Early experiments indicate that changes in cell migration may be attributed to substrate ligand density, integrin expression level, and ligand binding affinity (Palecek et al., 1997). Other studies show that in addition to substrate ligand density, substrate stiffness also mediates cell migration (Jannat et al., 2010; Peyton and Putnam, 2005). The phenomenon of durotaxis, where cells migrate in response to a stiffness gradient, was identified a decade ago in fibroblasts (Lo et al., 2000). More recent work with bovine aortic smooth muscle cells indicates that durotaxis and cell orientation increase with increasing stiffness gradient magnitude (Isenberg et al., 2009). Although more research is necessary to fully understand the role of substrate mechanics in cell migration, it is a clear parameter in dictating cell locomotion.

While much of the work in elucidating the role of cell forces in migration has been performed with single cells, there is also a significant role for traction generation in collective cell migration. Collective cell migration, the phenomenon of migration of cell groups (Rorth, 2007), occurs during development, wound healing, and metastasis. Less is known about traction forces in cell aggregates, largely because few techniques exist to make these measurements. Early work has been done to investigate collective cell migration and traction force generation in Madin-Darby canine kidney (MDCK) cell epithelial sheets as a model system for the epithelial-mesenchymal transition (de

Rooij et al., 2005). de Rooij and colleagues show that epithelial cell scatter, which recapitulates cancer cell invasion and metastasis, of MDCK cells increases with increasing concentrations of ECM protein and correlates with adhesion strength and actomyosin-dependent contractility. This contractility transmits tension to the cell periphery.

du Roure and co-workers expanded on these studies and measured traction forces of MDCK cell sheets on microfabricated PDMS pillars. They find that traction stresses are greatest at the monolayer edge and are greater than those measured in single cells (du Roure et al., 2005). Separate work indicates that large traction forces are also generated in the bulk of the cell sheet, many cell rows away from the leading edge (Trepat et al., 2009). These traction forces may act in a global tug-of-war that pulls the cell sheet toward the leading edge. Additional work on PDMS substrates of anisotropic stiffness indicate MDCK cells assembly is anisotropic along the stiffest substrate direction and correlates with traction force and actin cytoskeletal orientation (Saez et al., 2007). These data indicate that cells within cell sheets can act in concert to generate traction forces throughout the tissue and further implicate substrate stiffness as a regulator of tissue formation. As this is a nascent area, much work remains to be done to understand the role of traction generation in collective cell movements, and new technologies are required to investigate and quantify collective forces.

During tissue formation, cells migrate and proliferate into new structures. Cell-generated forces are critically important during cell proliferation and division (Scholey et al., 2003). The same interplay described earlier of cell-substrate and cell-cell interactions also mediates proliferation of cells within cell aggregate models of tissues. Recent work suggests that differential patterns of proliferation correspond to local

mechanical stresses and cytoskeletal generated tension. Localized cell proliferation within cell aggregates were found to correspond to regions of high traction stresses generated within a cell monolayer (Nelson et al., 2005). Additionally, inhibition of actomyosin contraction or cadherin-mediated adhesions disrupted the spatial pattern of proliferation. In similar experiments, fibroblast proliferation and differentiation on micropatterned PDMS islands correspond to high levels of mechanical stress at the perimeter of cell aggregates (Li et al., 2009). These data indicate that tension at the cell-matrix interface and along the edges of collections of cells can drive proliferation profiles.

Forces generated through cell-cell contacts also regulate proliferation. A biphasic proliferative response is seen when cell proliferation is regulated by the amount of neighboring-cell contact: while a single-cell neighbor increases proliferation, an increasing number of contacting cells inhibits proliferation (Gray et al., 2008). This relationship is potentially explained by the balance that exists between contractility, spreading, and proliferation. While increases in proliferation are dependent on RhoGTPase-mediated intracellular tension, cell-cell contacts may lower proliferation by decreasing cell-ECM contact. Using ECs cultured on patterned PDMS substrates, Nelson and Chen show that VE-cadherin-mediated cell-cell contact promotes opposing proliferation signals (Nelson and Chen, 2003). VE-cadherin inhibits cell spreading and proliferation when cells are physically constrained; otherwise, VE-cadherin increases proliferation through Rho-dependent changes in cytoskeletal tension. These data again point to the delicate balance between cell-matrix and cell-cell adhesion in regulating cell behavior.

1.4.3 Cell-generated force disruption in disease and atherosclerosis

Other than the hematopoietic cells, all cell types require adhesion for normal function. As such, virtually all cell types are capable of generating forces and sensing their mechanical environment. When cell-generated forces are altered due to changes in the mechanical properties of their microenvironment, cell functions such as survival, death, proliferation, adhesion, and migration may become dysregulated. The perturbation of proper force balance or mechanotransduction signaling pathways is thought to result in diseases of the liver (Wells, 2008), heart (Lammerding et al., 2004), and vasculature (Haga et al., 2007), among others. Importantly, changes in ECM elasticity and the disruption of force balance are also considered important factors in cancer progression (Butcher et al., 2009).

As an example of cell-force in disease progression, the tumor environment itself is stiffer than its surrounding tissue due to elevated interstitial fluid pressure, increased matrix deposition, and cell proliferation (Huang and Ingber, 2005). Currently, there is an emphasis in cancer research on elucidating the mechanical mechanisms that drive tumor progression and metastasis. In a study by Paszek and colleagues, increased RhoGTPase-dependent cell contractility, mediated by matrix stiffness, was found to disrupt tissue organization and enhance the malignant transformation of mammary epithelial cells (Paszek et al., 2005). Of note, reducing cytoskeletal tension by inhibiting Rho decreased tumor colony size and proliferation and the expression of the malignant phenotype. These data were critical in establishing the role of matrix stiffness and cell-generated forces in abnormal cell growth and tumorigenesis.

Oftentimes, the mechanical compliance of tissues is altered in injury. After injury of the skin, for instance, platelets aggregate and form a temporary fibrin clot,

and myofibroblasts lay down a provisional ECM comprised of collagen (Midwood et al., 2004). Although myofibroblasts quickly restore the mechanical integrity of damaged tissues, scar tissues have increased stiffness due to excessive collagen deposition, or fibrosis (Hinz, 2009). Unfortunately, fibrosis after injury can affect almost every organ in the body. For example, recent studies investigated the effects of matrix rigidity on cell differentiation in the early stages of liver fibrosis. Li et al. show that myofibroblastic differentiation of liver portal fibroblasts depends on mechanical tension and that they exhibit increasingly myofibroblastic phenotypes with increasing matrix rigidity (Li et al., 2007). Subsequent *in vivo* studies confirmed that liver stiffness is influenced by matrix quantity and cross-linking (Georges et al., 2007). This increase in stiffness was found to precede liver fibrosis and is thought to activate myofibroblast differentiation.

In the cardiovascular system, myocardial infarction is generally followed by scarring of the heart tissue and fibrosis, which leads to increased stiffness and impaired cardiac output. To compensate for this decrease in cardiac output, cardiomyocytes increase in size in order to generate more force, which leads to increased ventricular wall thickness or dilation (Grossman et al., 1975; Sun and Weber, 2000). Over time, elevated stress levels in the myocardium leads to the dysregulation of ECM remodeling resulting in myocyte apoptosis, necrosis, and cardiac failure (Barry et al., 2008; Jaalouk and Lammerding, 2009). Interestingly, optimal beating of cardiomyocytes has been found to correspond to an optimal matrix elasticity (Engler et al., 2008). Engler and colleagues cultured chick embryonic cardiomyocytes on substrates of varying compliances and observed significant differences in cardiac output and strength of beating. On stiffer matrices that mimic the modulus of fibrotic myocardium, large differences were found between cell strains

and their underlying matrix strains, suggesting that cells were overstretching and overstraining themselves. Furthermore, cardiomyocytes on stiffer substrates rarely exhibited the typical striated myofibrils throughout the cytoplasm, and 48 hours after plating, less than 10% of cells continued to beat, with cells only beating sporadically (Engler et al., 2008). In comparison, cardiomyocytes on substrates softer than striated muscle were able to continuously beat but performed very little contractile work. These results show that for cells to function properly, they must be supported by a matrix of physiologic stiffness and may lose their native phenotype on matrices that are either too soft or too stiff, as occurs in many pathologies.

Disruptions in cell-generated forces also have wide implications in disease progression of the vasculature, particularly in the development and advancement of atherosclerosis. Atherosclerosis is a multi-stage disease in which fatty deposits accumulate on the vessel wall and obstruct blood flow (Figure 1.2). Additionally, the artery stiffens, losing its elasticity due to excess ECM protein deposition by fibroblasts and smooth muscle cells (Zieman et al., 2005). Studies also suggest that advanced glycation end-products contribute to artery stiffening by crosslinking ECM proteins, particularly collagen, in the vessel walls (Soldatos and Cooper, 2006).

The endothelial cell layer, normally a non-adhesive and non-thrombotic surface, is considered the first mediator in atherosclerosis progression. Dysregulation of the EC layer leads to increased permeability, immune cell attachment and lipid deposition. Force balance, driven by the mechanical interaction between the endothelium and its basement membrane (Figure 1.2A), is implicated as a critical factor in the maintenance of a functional endothelial barrier (Ingber, 1997; Mehta and Malik, 2006).

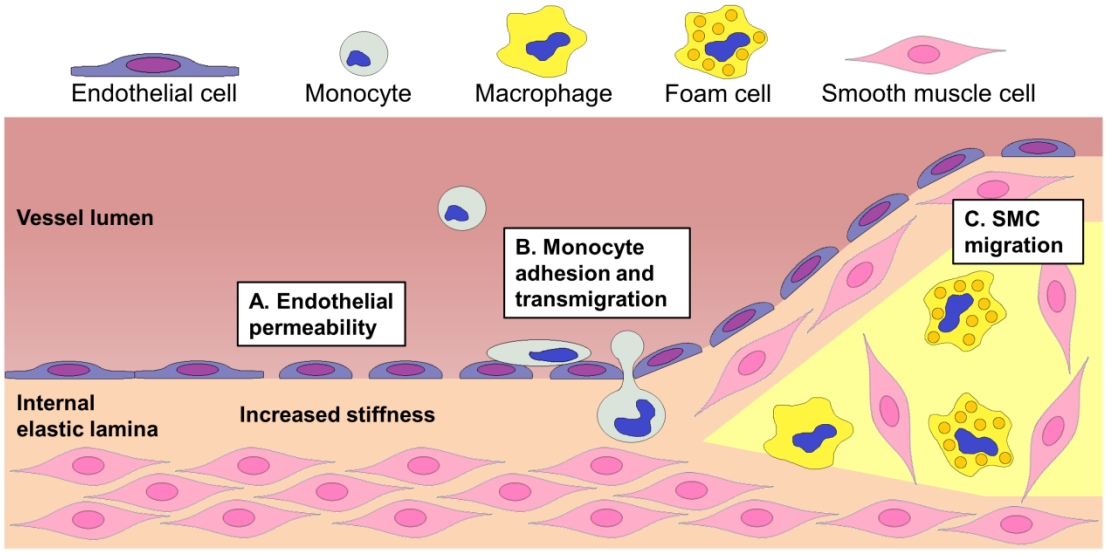

Figure 1.2. Disruption of force balance in the progression of atherosclerosis. **(A)** Increased vessel stiffness, particularly the rigidity of the internal elastic lamina, may disrupt endothelial cell force balance leading to increased cell contractility and barrier permeability. **(B)** Increased substrate and endothelial cell stiffness may recruit monocytes to adhere and transmigrate through the endothelial layer. **(C)** Increased ECM deposition and vessel stiffness causes vascular smooth muscle cells to proliferate and migrate into the intima, occluding the blood vessel. Reprinted with kind permission of Springer Science and Business Media.

It is hypothesized that RhoGTPase-dependent contractile forces drive ECs to separate, while cell-cell interactions provide tethering forces that maintain endothelial barrier integrity. In a recent study by Birukova et al., AFM was used to test this hypothesis by measuring the stiffness of human pulmonary artery ECs as they were stimulated with known barrier-disruptive or barrier-protective agonists (Birukova et al., 2009). The authors were able to show that barrier-disruptive agonists increase cell stiffness in the central region, while barrier-protective agonists increase stiffness at the cell periphery and decrease cell stiffness at the center. These results were confirmed by similar AFM studies on human umbilical vein ECs that show that cell stiffness and membrane tethering forces are directly related to the polymerization state of actin (Cuerrier et al., 2009). These results support the hypothesis that cell-generated forces maintain the endothelial barrier and directly link cell stiffness with specific permeability responses.

As the permeability of the endothelium becomes dysregulated, lipoprotein deposition initiates the inflammation cascade and recruits immune cells to attach and transmigrate through the endothelial layer (Figure 1.2B). The adhesion and migration of neutrophils are influenced in part by cell-generated forces and substrate rigidity (Oakes et al., 2009). Neutrophils are more well-spread and exert greater traction forces when allowed to adhere to stiffer substrates. Additionally, neutrophils migrate more slowly on stiffer substrates but also more persistently, resulting in longer distances being covered. Further studies show that a balance in cell-generated force corresponding to an optimal substrate stiffness maximizes neutrophil migration (Stroka and Aranda-Espinoza, 2009). These *in vitro* data suggest that matrix stiffening, which occurs in atherosclerosis, may promote leukocyte recruitment and promote the inflammatory cascade *in vivo*.

Interestingly, in this same inflammatory cascade, heterogeneous cell-cell interactions alter cell mechanics. The adhesion of neutrophils to the EC layer increases the stiffness of adjacent ECs (Kang et al., 2009). When taken together with the findings of Birukova et al. which suggest that cell-generated forces may regulate endothelial permeability, it is possible that neutrophil adhesion causes a local increase in endothelial force generation and barrier permeability in preparation for their eventual transmigration. This possibility was explored in an elegant study done by Rabodzey and colleagues. The authors measured the tangential forces exerted by neutrophils during transmigration through a confluent EC layer grown on a microfabricated pillar substrate (Rabodzey et al., 2008). In response to neutrophil transmigration, endothelial cell-cell junctions become disrupted and EC traction forces increase significantly. Moreover, traction forces induced by neutrophil transmigration increase with increasing substrate rigidity. Therefore, the relationship between matrix stiffness, EC stiffness, and EC force generation plays an integral role in regulating permeability and transendothelial migration.

In the later stages of atherosclerosis, vascular smooth muscle cells migrate from the media into the intima, largely contributing to the occlusion of the blood vessel (Figure 1.2C). Coincident with this migration is an increase in collagen deposition and increased vessel stiffness. Recent *in vitro* studies indicate that substrate stiffness has a direct effect on the migration speeds of VSMC. Data show that VSMC migration speed has a biphasic relationship with respect to substrate stiffness, suggesting that an optimal stiffness exists which maximizes cell migration speed and persistence (Peyton and Putnam, 2005). On substrates fabricated to contain well-defined stiffness gradients (Isenberg et al., 2009), VSMCs orient themselves in the

direction of the gradient and preferentially migrate from softer to stiffer regions in a phenomenon termed durotaxis. While these studies have advanced our understanding of the interplay between mechanics and cardiovascular disease, additional attention is required to fully understand the role of cell-generated forces in endothelial permeability, neutrophil transmigration, and VSMC migration *in vivo*.

1.5 Organization of the dissertation

The objective of this work is to elucidate the mechanical mechanisms that underlie to progression of atherosclerosis. Specifically, I studied how substrate stiffness and cell contractility affect critical events that occur during atherosclerosis, such as endothelial permeability and vascular smooth muscle cell migration. Herein, I present data that implicate vascular stiffening as an important factor that may initiate and exacerbate atherosclerotic phenotypes.

In Chapter 2, I describe a novel method to measure the permeability of endothelial cells that are cultured on soft, porous substrates that better mimic vessel stiffness compared to conventional permeability measurement platforms. Because endothelial permeability assays are traditionally performed on tissue culture plastic, I first developed a method to measure permeability of cells cultured on polyacrylamide gels. Due to polyacrylamide's porous nature, I developed an assay based on the accumulation of a fluorescently-labeled tracker molecule into the gels. We find that when polyacrylamide gels are immersed in a FITC-dextran solution, confocal microscopy can be used to image the amount of dye entrapped within the gel. When cells were grown to confluence on the gels, significantly less dye moved into the gel, indicating that endothelial cells were creating barrier that resisted the movement of dye. The method was then rigorously validated by treating endothelial cells with a

variety of known agonists to elicit permeability responses.

In Chapter 3, I use the method developed in Chapter 2 to determine the effects of substrate stiffness on endothelial permeability. Because the adherens junctions between endothelial cells are comprised of VE-cadherin, I studied their VE-cadherin organization in response to the stiffness of their substrate. In collaboration with the Schaffer Lab at Cornell, we also investigated permeability and VE-cadherin organization in a mouse model and found that permeability and VE-cadherin separation increases in aged, stiffer arteries. Moreover, using traction force microscopy, I present data that increased permeability and junction destabilization are the result of upregulated cell contractility. Notably, when endothelial cells were treated with a pharmacological inhibitor of cell contractility, permeability and junction separation were decreased. Importantly, we were able to recapitulate these results *in vivo*, where mouse permeability and VE-cadherin separation also decreased due to drug treatment. Lastly, in collaboration with the King Lab, we determined that leukocyte transmigration through endothelial monolayers increases with substrate stiffness, and inhibition of endothelial contractility reduces transmigration. These impactful results provide us with a better understanding of the relationship between age, vascular stiffening, and atherogenesis.

In Chapter 4, I present novel findings that substrate stiffness induces the formation of circular dorsal ruffles (CDRs) in vascular smooth muscle cells. Although these transient actin-based structures have been documented for many years, little is known if substrate stiffness affects their formation or function. Because they are widely assumed to play a role in mediating cell motility, we hypothesized that CDR formation may play a role in VSMC migration phenotypic of atherosclerotic plaque

formation. I show that more VSMCs exhibit CDRs on stiffer substrates and cell-generated forces are required for robust CDR formation. When treated with activators and inhibitors of myosin light chain, cells form more or fewer CDRs, respectively. Additionally, the pathways that regulate CDR formation in response to substrate stiffness involve the association of Src and myosin light chain kinase (MLCK).

In Chapter 5, my experience as a NSF GK-12 teaching fellow is described. During this time, I developed and executed two high school level science labs at Waverly High School in Waverly, NY. These labs were aimed to teach polymer science and arterial stiffening to rising juniors. Additionally, I developed several lectures that were given to students to stimulate interest in science, technology, and biomedical engineering. Conclusions of my dissertation and future directions of research are presented in Chapter 6. Experimental protocols and GK-12 teaching materials are provided in the appendices.

1.6 References

del Alamo JC, Meili R, Alonso-Latorre B, Rodríguez-Rodríguez J, Aliseda A, Firtel RA, Lasheras JC, Rodriguez-Rodriguez J. 2007. Spatio-temporal analysis of eukaryotic cell motility by improved force cytometry. *Proceedings of the National Academy of Sciences U S A* **104**:13343–13348.

Amano M, Nakayama M, Kaibuchi K. 2010. Rho-kinase/ROCK: A key regulator of the cytoskeleton and cell polarity. *Cytoskeleton* **67**:545–54.

Aplin AE, Howe A, Alahari SK, Juliano RL. 1998. Signal transduction and signal modulation by cell adhesion receptors: the role of integrins, cadherins, immunoglobulin-cell adhesion molecules, and selectins. *Pharmacological reviews* **50**:197–263.

Appleton CT, Usmani SE, Mort JS, Beier F. 2010. Rho/ROCK and MEK/ERK activation by transforming growth factor-alpha induces articular cartilage degradation. *Laboratory Investigation* **90**:20–30.

Badimon L, Vilahur G. 2012. LDL-cholesterol versus HDL-cholesterol in the atherosclerotic plaque: inflammatory resolution versus thrombotic chaos. *Annals of the New York Academy of Sciences U S A* **1254**:18–32.

Balaban NQ, Schwarz US, Riveline D, Goichberg P, Tzur G, Sabanay I, Mahalu D, Safran S, Bershadsky A, Addadi L, Geiger B. 2001. Force and focal adhesion assembly: a close relationship studied using elastic micropatterned substrates. *Nature Cell Biology* **3**:466–72.

Barry SP, Davidson SM, Townsend PA. 2008. Molecular regulation of cardiac hypertrophy. *International Journal of Biochemistry & Cell Biology* **40**:2023–39.

Basta G. 2008. Receptor for advanced glycation endproducts and atherosclerosis: From basic mechanisms to clinical implications. *Atherosclerosis* **196**:9–21.

Beningo KA, Dembo M, Kaverina I, Small JV, Wang YL. 2001. Nascent focal adhesions are responsible for the generation of strong propulsive forces in migrating fibroblasts. *Journal of Cell Biology* **153**:881–8.

Berrier AL, Yamada KM. 2007. Cell-matrix adhesion. *Journal of Cellular Physiology* **213**:565–73.

Birukova AA, Arce FT, Moldobaeva N, Dudek SM, Garcia JGN, Lal R, Birukov KG. 2009. Endothelial permeability is controlled by spatially defined cytoskeletal mechanics: atomic force microscopy force mapping of pulmonary endothelial monolayer. *Nanomedicine* **5**:30–41.

Bishop AL, Hall A. 2000. Rho GTPases and their effector proteins. *Biochemical Journal* **348 Pt 2**:241–55.

Blacher J, Asmar R, Djane S, London GM, Safar ME. 1999. Aortic pulse wave velocity as a marker of cardiovascular risk in hypertensive patients. *Hypertension* **33**:1111–7.

Boutouyrie P, Briet M, Collin C, Vermeersch S, Pannier B. 2009. Assessment of pulse wave velocity. *Artery Research* **3**:3–8.

Butcher DT, Alliston T, Weaver VM. 2009. A tense situation: forcing tumour progression. *Nature Reviews Cancer* **9**:108–122.

Butler JP, Tolić-Nørrelykke IM, Fabry B, Fredberg JJ. 2002. Traction fields, moments, and strain energy that cells exert on their surroundings. *American Journal of Physiology. Cell Physiology* **282**:C595–605.

Califano JP, Reinhart-King CA. 2010. Substrate stiffness and cell area predict cellular traction stresses in single cells and cells in contact. *Cellular and Molecular Bioengineering* **3**:68–75.

Chavez A, Smith M, Mehta D. 2011. New insights into the regulation of vascular permeability. *International Review of Cell and Molecular Biology* **290**:205–48.

Chen CS. 2008. Mechanotransduction - a field pulling together? *Journal of Cell Science* **121**:3285–92.

Chicurel ME, Chen CS, Ingber DE. 1998. Cellular control lies in the balance of forces. *Current Opinion in Cell Biology* **10**:232–9.

Chowdhury F, Na S, Li D, Poh Y-CC, Tanaka TS, Wang F, Wang N. 2010. Material properties of the cell dictate stress-induced spreading and differentiation in embryonic stem cells. *Nature Materials* **9**:82–88.

Cuerrier CM, Gagner A, Lebel R, Gobeil F, Grandbois M, Gobeil Jr. F. 2009. Effect of thrombin and bradykinin on endothelial cell mechanical properties monitored through membrane deformation. *Journal of Molecular Recognition* **22**:389–396.

Dejana E, Giampietro C. 2012. Vascular endothelial-cadherin and vascular stability. *Current Opinion in Hematology* **19**:218–23.

Dejana E, Orsenigo F, Lampugnani MG. 2008. The role of adherens junctions and VE-cadherin in the control of vascular permeability. *Journal of Cell Science* **121**:2115–2122.

Delon I, Brown NH. 2007. Integrins and the actin cytoskeleton. *Current Opinion in Cell Biology* **19**:43–50.

Dembo M, Oliver T, Ishihara A, Jacobson K. 1996. Imaging the traction stresses exerted by locomoting cells with the elastic substratum method. *Biophysical Journal* **70**:2008–2022.

Dembo M, Wang YL. 1999. Stresses at the cell-to-substrate interface during locomotion of fibroblasts. *Biophysical Journal* **76**:2307–2316.

Discher DE, Janmey P, Wang YL. 2005. Tissue cells feel and respond to the stiffness of their substrate. *Science* **310**:1139–43.

Dominguez R, Holmes KC. 2011. Actin structure and function. *Annual Review of Biophysics* **40**:169–86.

Dudek SM, Garcia JG. 2001. Cytoskeletal regulation of pulmonary vascular permeability. *Journal of Applied Physiology* **91**:1487–500.

Engler AJ, Carag-Krieger C, Johnson CP, Raab M, Tang HY, Speicher DW, Sanger JW, Sanger JM, Discher DE. 2008. Embryonic cardiomyocytes beat best on a matrix with heart-like elasticity: scar-like rigidity inhibits beating. *Journal of Cell Science* **121**:3794–3802.

Engler AJ, Sen S, Sweeney HL, Discher DE. 2006. Matrix elasticity directs stem cell lineage specification. *Cell* **126**:677–89.

Evans ND, Minelli C, Gentleman E, LaPointe V, Patankar SN, Kallivretaki M, Chen X, Roberts CJ, Stevens MM. 2009. Substrate stiffness affects early differentiation events in embryonic stem cells. *European Cells & Materials* **18**:1–4.

Frostegård J. 2005. SLE, atherosclerosis and cardiovascular disease. *Journal of Internal Medicine* **257**:485–95.

Galbraith CG, Sheetz MP. 1997. A micromachined device provides a new bend on fibroblast traction forces. *Proceedings of the National Academy of Sciences U S A* **94**:9114–9118.

Ganz A, Lambert M, Saez A, Silberzan P, Buguin A, Mège RM, Ladoux B, Mege RM. 2006. Traction forces exerted through N-cadherin contacts. *Biology of the Cell* **98**:721–730.

Gavard J. 2009. Breaking the VE-cadherin bonds. *FEBS Letters* **583**:1–6.

Georges PC, Hui JJ, Gombos Z, McCormick ME, Wang AY, Uemura M, Mick R, Janmey PA, Furth EE, Wells RG. 2007. Increased stiffness of the rat liver precedes matrix deposition: implications for fibrosis. *American Journal of Physiology. Gastrointestinal and Liver Physiology* **293**:G1147–54.

Gray DS, Liu WF, Shen CJ, Bhadriraju K, Nelson CM, Chen CS. 2008. Engineering amount of cell-cell contact demonstrates biphasic proliferative regulation through RhoA and the actin cytoskeleton. *Experimental Cell Research* **314**:2846–2854.

Greenwald SE. 2007. Ageing of the conduit arteries. *Journal of Pathology* **211**:157–72.

Grossman W, Jones D, McLaurin LP. 1975. Wall stress and patterns of hypertrophy in the human left ventricle. *Journal of Clinical Investigation* **56**:56–64.

Haga JH, Li YS, Chien S. 2007. Molecular basis of the effects of mechanical stretch on vascular smooth muscle cells. *Journal of Biomechanics* **40**:947–60.

Harris AK, Wild P, Stopak D. 1980. Silicone rubber substrata: a new wrinkle in the study of cell locomotion. *Science* **208**:177–9.

Hinz B. 2009. Tissue stiffness, latent TGF-beta1 activation, and mechanical signal transduction: implications for the pathogenesis and treatment of fibrosis. *Current Rheumatology Reports* **11**:120–126.

Hirase T, Node K. 2012. Endothelial dysfunction as a cellular mechanism for vascular failure. *American Journal of Physiology. Heart and Circulatory Physiology* **302**:H499–505.

Huang S, Ingber DE. 2005. Cell tension, matrix mechanics, and cancer development. *Cancer Cell* **8**:175–6.

Huot J, Houle F, Rousseau S, Deschesnes RG, Shah GM, Landry J. 1998. SAPK2/p38-dependent F-actin reorganization regulates early membrane blebbing during stress-induced apoptosis. *Journal of Cell Biology* **143**:1361–1373.

Huynh J, Califano JP, Reinhart-King CA. 2011. Cell-generated forces in tissue assembly and function. In: Wagoner-Johnson, AJ, Harley, BAC, editors. *Mechanobiology of Cell-Cell and Cell-Matrix Interactions*. Springer, pp. 47–74.

Ingber DE. 1997. Tensegrity: the architectural basis of cellular mechanotransduction. *Annual Review of Physiology* **59**:575–99.

Ingber DE. 2003. Tensegrity I. Cell structure and hierarchical systems biology. *Journal of Cell Science* **116**:1157–1173.

Isenberg BC, Dimilla PA, Walker M, Kim S, Wong JY. 2009. Vascular smooth muscle cell durotaxis depends on substrate stiffness gradient strength. *Biophysical Journal* **97**:1313–1322.

Jaalouk DE, Lammerding J. 2009. Mechanotransduction gone awry. *Nature Reviews. Molecular Cell Biology* **10**:63–73.

Jannat RA, Robbins GP, Ricart BG, Dembo M, Hammer DA. 2010. Neutrophil adhesion and chemotaxis depend on substrate mechanics. *Journal of Physics. Condensed Matter* **22**:194117.

Kang I, Wang Q, Eppell SJ, Marchant RE, Doerschuk CM. 2009. Effect of neutrophil adhesion on the mechanical properties of lung microvascular endothelial cells. *American Journal of Respiratory Cell and Molecular Biology* **43**:591–8.

Katsumi A, Orr AW, Tzima E, Schwartz MA. 2004. Integrins in mechanotransduction. *Journal of Biological Chemistry* **279**:12001–4.

Kim LC, Song L, Haura EB. 2009. Src kinases as therapeutic targets for cancer. *Nature reviews. Clinical Oncology* **6**:587–95.

Ko KS, Arora PD, McCulloch CA. 2001. Cadherins mediate intercellular mechanical signaling in fibroblasts by activation of stretch-sensitive calcium-permeable channels. *Journal of Biological Chemistry* **276**:35967–35977.

Kraning-Rush CM, Carey SP, Califano JP, Smith BN, Reinhart-King CA. 2011. The role of the cytoskeleton in cellular force generation in 2D and 3D environments. *Physical Biology* **8**:015009.

Krieg M, Arboleda-Estudillo Y, Puech PH, Käfer J, Graner F, Müller DJ, Heisenberg CP. 2008. Tensile forces govern germ-layer organization in zebrafish. *Nature Cell Biology* **10**:429–436.

Kris AS, Kamm RD, Sieminski AL. 2008. VASP involvement in force-mediated adherens junction strengthening. *Biochemical and Biophysical Research Communications* **375**:134–138.

Kumar S, Maxwell IZ, Heisterkamp A, Polte TR, Lele TP, Salanga M, Mazur E, Ingber DE. 2006. Viscoelastic retraction of single living stress fibers and its impact on cell shape, cytoskeletal organization, and extracellular matrix mechanics. *Biophysical Journal* **90**:3762–3773.

Ladoux B, Anon E, Lambert M, Rabodzey A, Hersen P, Buguin A, Silberzan P, Mege RM. 2010. Strength dependence of cadherin-mediated adhesions. *Biophysical Journal* **98**:534–542.

Lammerding J, Kamm RD, Lee RT. 2004. Mechanotransduction in cardiac myocytes. *Annals of the New York Academy of Sciences U S A* **1015**:53–70.

Laugesen E, Hansen KW, Knudsen ST, Erlandsen M, Ebbehøj E, Mogensen CE, Poulsen PL. 2009. Increased ambulatory arterial stiffness index and pulse pressure in microalbuminuric patients with type 1 diabetes. *American Journal of Hypertension* **22**:513–9.

Laurent S, Boutouyrie P. 2007. Recent advances in arterial stiffness and wave reflection in human hypertension. *Hypertension* **49**:1202–6.

Lee J, Leonard M, Oliver T, Ishihara A, Jacobson K. 1994. Traction forces generated by locomoting keratocytes. *Journal of Cell Biology* **127**:1957–1964.

Lemmon CA, Sniadecki NJ, Ruiz SA, Tan JL, Romer LH, Chen CS. 2005. Shear force at the cell-matrix interface: enhanced analysis for microfabricated post array detectors. *Mechanics & Chemistry of Biosystems* **2**:1–16.

Leung DW, Cachianes G, Kuang WJ, Goeddel DV, Ferrara N. 1989. Vascular endothelial growth factor is a secreted angiogenic mitogen. *Science* **246**:1306–1309.

Li B, Li F, Puskar KM, Wang JH. 2009. Spatial patterning of cell proliferation and differentiation depends on mechanical stress magnitude. *Journal of Biomechanics* **42**:1622–1627.

Li Z, Dranoff JA, Chan EP, Uemura M, Sévigny J, Wells RG, Sevigny J. 2007. Transforming growth factor-beta and substrate stiffness regulate portal fibroblast activation in culture. *Hepatology* **46**:1246–1256.

Lo CM, Wang HB, Dembo M, Wang YL. 2000. Cell movement is guided by the rigidity of the substrate. *Biophysical Journal* **79**:144–152.

Maniotis AJ, Chen CS, Ingber DE. 1997. Demonstration of mechanical connections between integrins, cytoskeletal filaments, and nucleoplasm that stabilize nuclear structure. *Proceedings of the National Academy of Sciences U S A* **94**:849–854.

Margadant C, Monsuur HN, Norman JC, Sonnenberg A. 2011. Mechanisms of integrin activation and trafficking. *Current Opinion in Cell Biology* **23**:607–14.

Marganski WA, Dembo M, Wang YL. 2003. Measurements of cell-generated deformations on flexible substrata using correlation-based optical flow. *Methods in Enzymology* **361**:197–211.

Mattace-Raso FUS, van der Cammen TJM, Hofman A, van Popele NM, Bos ML, Schalekamp M a DH, Asmar R, Reneman RS, Hoeks APG, Breteler MMB, Witteman JCM. 2006. Arterial stiffness and risk of coronary heart disease and stroke: the Rotterdam Study. *Circulation* **113**:657–63.

McBeath R, Pirone DM, Nelson CM, Bhadriraju K, Chen CS. 2004. Cell shape, cytoskeletal tension, and RhoA regulate stem cell lineage commitment. *Developmental Cell* **6**:483–495.

McEniery CM, Yasmin, Hall IR, Qasem A, Wilkinson IB, Cockcroft JR. 2005. Normal vascular aging: differential effects on wave reflection and aortic pulse wave velocity: the Anglo-Cardiff Collaborative Trial (ACCT). *Journal of the American College of Cardiology* **46**:1753–60.

Mehta D, Malik AB. 2006. Signaling mechanisms regulating endothelial permeability. *Physiological Reviews* **86**:279–367.

Midwood KS, Williams LV, Schwarzbauer JE. 2004. Tissue repair and the dynamics of the extracellular matrix. *International Journal of Biochemistry & Cell Biology* **36**:1031–7.

Moore KA, Polte T, Huang S, Shi B, Alsberg E, Sunday ME, Ingber DE. 2005. Control of basement membrane remodeling and epithelial branching morphogenesis in embryonic lung by Rho and cytoskeletal tension. *Developmental Dynamics* **232**:268–281.

Mori H, Gjorevski N, Inman JL, Bissell MJ, Nelson CM. 2009. Self-organization of engineered epithelial tubules by differential cellular motility. *Proceedings of the National Academy of Sciences U S A* **106**:14890–14895.

Narumiya S, Tanji M, Ishizaki T. 2009. Rho signaling, ROCK and mDia1, in transformation, metastasis and invasion. *Cancer Metastasis Reviews* **28**:65–76.

Nelson CM, Chen CS. 2003. VE-cadherin simultaneously stimulates and inhibits cell proliferation by altering cytoskeletal structure and tension. *Journal of Cell Science* **116**:3571–3581.

Nelson CM, Jean RP, Tan JL, Liu WF, Sniadecki NJ, Spector AA, Chen CS. 2005. Emergent patterns of growth controlled by multicellular form and mechanics. *Proceedings of the National Academy of Sciences U S A* **102**:11594–11599.

Nelson CM, Pirone DM, Tan JL, Chen CS. 2004. Vascular endothelial-cadherin regulates cytoskeletal tension, cell spreading, and focal adhesions by stimulating RhoA. *Molecular Biology of the Cell* **15**:2943–2953.

Nicosia RF. 1998. What is the role of vascular endothelial growth factor-related molecules in tumor angiogenesis? *American Journal of Pathology* **153**:11–16.

van Nieuw Amerongen GP, Koolwijk P, Versteilen A, van Hinsbergh VW. 2003. Involvement of RhoA/Rho kinase signaling in VEGF-induced endothelial cell migration and angiogenesis in vitro. *Arteriosclerosis, Thrombosis, and Vascular Biology* **23**:211–217.

Nishimura T, Takeichi M. 2009. Remodeling of the adherens junctions during morphogenesis. *Current Topics in Developmental Biology* **89**:33–54.

Noll G. 1998. Pathogenesis of atherosclerosis: a possible relation to infection. *Atherosclerosis* **140 Suppl** S3–9.

Oakes PW, Patel DC, Morin NA, Zitterbart DP, Fabry B, Reichner JS, Tang JX. 2009. Neutrophil morphology and migration are affected by substrate elasticity. *Blood* **114**:1387–1395.

Oliver T, Dembo M, Jacobson K. 1999. Separation of propulsive and adhesive traction stresses in locomoting keratocytes. *Journal of Cell Biology* **145**:589–604.

Orr AW, Helmke BP, Blackman BR, Schwartz MA. 2006. Mechanisms of mechanotransduction. *Developmental Cell* **10**:11–20.

O'Rourke MF. 2007. Arterial aging: pathophysiological principles. *Vascular Medicine* **12**:329–41.

Pajerowski JD, Dahl KN, Zhong FL, Sammak PJ, Discher DE. 2007. Physical plasticity of the nucleus in stem cell differentiation. *Proceedings of the National Academy of Sciences U S A* **104**:15619–15624.

Palecek SP, Loftus JC, Ginsberg MH, Lauffenburger DA, Horwitz AF. 1997. Integrin-ligand binding properties govern cell migration speed through cell-substratum adhesiveness. *Nature* **385**:537–540.

Paraskevas KI, Mikhailidis DP, Liapis CD. 2007. Internal carotid artery occlusion: association with atherosclerotic disease in other arterial beds and vascular risk factors. *Angiology* **58**:329–35.

Parker KK, Brock AL, Brangwynne C, Mannix RJ, Wang N, Ostuni E, Geisse NA, Adams JC, Whitesides GM, Ingber DE. 2002. Directional control of lamellipodia extension by constraining cell shape and orienting cell tractional forces. *FASEB Journal* **16**:1195–1204.

Parsons JT, Horwitz AR, Schwartz MA. 2010. Cell adhesion: integrating cytoskeletal dynamics and cellular tension. *Nature Reviews. Molecular Cell Biology* **11**:633–43.

Paszek MJ, Zahir N, Johnson KR, Lakins JN, Rozenberg GI, Gefen A, Reinhart-King CA, Margulies SS, Dembo M, Boettiger D, Hammer DA, Weaver VM. 2005. Tensional homeostasis and the malignant phenotype. *Cancer Cell* **8**:241–54.

Pellegrin S, Mellor H. 2007. Actin stress fibres. *Journal of Cell Science* **120**:3491–9.

Persad S, Dedhar S. 2003. The role of integrin-linked kinase (ILK) in cancer progression. *Cancer Metastasis Reviews* **22**:375–84.

Peyton SR, Putnam AJ. 2005. Extracellular matrix rigidity governs smooth muscle cell motility in a biphasic fashion. *Journal of Cell Physiology* **204**:198–209.

Rabodzey A, Alcaide P, Luscinskas FW, Ladoux B. 2008. Mechanical forces induced by the transendothelial migration of human neutrophils. *Biophysical Journal* **95**:1428–38.

Raines EW. 2004. PDGF and cardiovascular disease. *Cytokine & Growth Factor Reviews* **15**:237–54.

Reinhart-King CA, Dembo M, Hammer DA. 2005. The dynamics and mechanics of endothelial cell spreading. *Biophysical Journal* **89**:676–689.

Reinhart-king CA., Dembo M, Hammer DA. 2003. Endothelial cell traction forces on RGD-derivatized polyacrylamide substrata. *Langmuir* **19**:1573–1579.

Ren XD, Kiosses WB, Schwartz MA. 1999. Regulation of the small GTP-binding protein Rho by cell adhesion and the cytoskeleton. *EMBO Journal* **18**:578–585.

Roger VL, Go AS, Lloyd-Jones DM, Benjamin EJ, Berry JD, Borden WB, Bravata DM, Dai S, Ford ES, Fox CS, Fullerton HJ, Gillespie C, Hailpern SM, Heit JA, Howard VJ, Kissela BM, Kittner SJ, Lackland DT, Lichtman JH, Lisabeth LD, Makuc DM, Marcus GM, Marelli A, Matchar DB, Moy CS, Mozaffarian D,

Mussolino ME, Nichol G, Paynter NP, Soliman EZ, Sorlie PD, Sotoodehnia N, Turan TN, Virani SS, Wong ND, Woo D, Turner MB. 2012. Heart disease and stroke statistics--2012 update: a report from the American Heart Association. *Circulation* **125**:e2–e220.

de Rooij J, Kerstens A, Danuser G, Schwartz MA, Waterman-Storer CM. 2005. Integrin-dependent actomyosin contraction regulates epithelial cell scattering. *Journal of Cell Biology* **171**:153–64.

Rorth P. 2007. Collective guidance of collective cell migration. *Trends in Cell Biology* **17**:575–579.

Ross R. 1999. Atherosclerosis--an inflammatory disease. *The New England Journal of Medicine* **340**:115–26.

du Roure O, Saez A, Buguin A, Austin RH, Chavrier P, Silberzan P, Siberzan P, Ladoux B. 2005. Force mapping in epithelial cell migration. *Proceedings of the National Academy of Sciences U S A* **102**:2390–2395.

Sabass B, Gardel ML, Waterman CM, Schwarz US. 2008. High resolution traction force microscopy based on experimental and computational advances. *Biophysical Journal* **94**:207–220.

Saez A, Ghibaudo M, Buguin A, Silberzan P, Ladoux B. 2007. Rigidity-driven growth and migration of epithelial cells on microstructured anisotropic substrates. *Proceedings of the National Academy of Sciences U S A* **104**:8281–8286.

Scholey JM, Brust-Mascher I, Mogilner A. 2003. Cell division. *Nature* **422**:746–752.

Schwartz MA, DeSimone DW. 2008. Cell adhesion receptors in mechanotransduction. *Current Opinion in Cell Biology* **20**:551–556.

Shattil SJ, Kim C, Ginsberg MH. 2010. The final steps of integrin activation: the end game. *Nature Reviews. Molecular Cell Biology* **11**:288–300.

Sniadecki NJ, Anguelouch A, Yang MT, Lamb CM, Liu Z, Kirschner SB, Liu Y, Reich DH, Chen CS. 2007. Magnetic microposts as an approach to apply forces to living cells. *Proceedings of the National Academy of Sciences U S A* **104**:14553–14558.

Sniadecki NJ, Chen CS. 2007. Microfabricated silicone elastomeric post arrays for measuring traction forces of adherent cells. *Methods in Cell Biology* **83**:313–28.

Soldatos G, Cooper ME. 2006. Advanced glycation end products and vascular structure and function. *Current Hypertension Reports* **8**:472–8.

Sordella R, Jiang W, Chen GC, Curto M, Settleman J. 2003. Modulation of Rho GTPase signaling regulates a switch between adipogenesis and myogenesis. *Cell* **113**:147–158.

Stroka KM, Aranda-Espinoza H. 2009. Neutrophils display biphasic relationship between migration and substrate stiffness. *Cell Motility and the Cytoskeleton* **66**:328–341.

Sun Y, Weber KT. 2000. Infarct scar: a dynamic tissue. *Cardiovascular Research* **46**:250–256.

Sutton-Tyrrell K, Najjar SS, Boudreau RM, Venkitachalam L, Kupelian V, Simonsick EM, Havlik R, Lakatta EG, Spurgeon H, Kritchevsky S, Pahor M, Bauer D, Newman A. 2005. Elevated aortic pulse wave velocity, a marker of arterial stiffness, predicts cardiovascular events in well-functioning older adults. *Circulation* **111**:3384–3390.

Tan JL, Tien J, Pirone DM, Gray DS, Bhadriraju K, Chen CS. 2003. Cells lying on a bed of microneedles: an approach to isolate mechanical force. *Proceedings of the National Academy of Sciences U S A* **100**:1484–1489.

Trepat X, Wasserman MR, Angelini TE, Millet E, Weitz DA, Butler JP, Fredberg JJ. 2009. Physical forces during collective cell migration. *Nature Physics* **5**:426–430.

Vogel V, Sheetz M. 2006. Local force and geometry sensing regulate cell functions. *Nature Reviews. Molecular Cell Biology* **7**:265–75.

Wang N, Ostuni E, Whitesides GM, Ingber DE. 2002. Micropatterning tractional forces in living cells. *Cell Motility and the Cytoskeleton* **52**:97–106.

Wells RG. 2008. The role of matrix stiffness in regulating cell behavior. *Hepatology* **47**:1394–400.

Zhao X, Guan JL. 2011. Focal adhesion kinase and its signaling pathways in cell migration and angiogenesis. *Advanced Drug Delivery Reviews* **63**:610–5.

Zieman SJ, Melenovsky V, Kass DA. 2005. Mechanisms, pathophysiology, and therapy of arterial stiffness. *Arteriosclerosis, Thrombosis, and Vascular Biology* **25**:932–43.

Zoungas S, Asmar RP. 2007. Arterial stiffness and cardiovascular outcome. *Clinical and Experimental Pharmacology & Physiology* **34**:647–51.

CHAPTER 2

REAL-TIME PERMEABILITY MEASUREMENTS OF ENDOTHELIAL MONOLAYERS ON SOFT SUBSTRATES

Portions of this chapter were published in Science Translational Medicine (Huynh et al., 2011).

2.1 Abstract

Endothelial monolayer permeability is a hallmark of endothelial cell dysfunction and atherosclerosis. Multiple methods exist to measure monolayer permeability, but all have their limitations. Most notably, current *in vitro* methods involve placing cells on relatively stiff polycarbonate membranes which do not accurately recapitulate the mechanical environment of the endothelium *in vivo*. Here we describe a novel method to study the permeability of endothelial cells using substrates which mimic the physiological stiffness of the *in vivo* microenvironment. Using confocal microscopy, we devised a technique to monitor the movement of FITC-conjugated dextran through bovine aortic endothelial cell (BAEC) monolayers seeded on deformable polyacryalmide hydrogels made to mimic the stiffness of the endothelial basement membrane. We validated our technique by measuring the permeability of confluent BAECs after treatment with several different agonists and enhancers of permeability. Additionally, we show that permeability of BAEC monolayers is significantly enhanced when cultured on stiff substrates outside the range of physiological relevance, like those used in traditional permeability assays. These results underscore the need to measure permeability using methods that more closely mimic the *in vivo* environment. Our method is quick, experimentally easy to set up, allows for real-time

monitoring of solute flux, and accounts for substrate rigidity.

2.2 Introduction

The endothelial cell (EC) layer of the vasculature forms a semi-permeable barrier separating flowing blood from the underlying tissues and controls the passage of solutes, fluids and immune cells. Increased permeability is a hallmark of endothelial cell dysfunction and can result in pathologies including edema and chronic inflammation. Moreover, it is considered a critical first step in atherogenesis (Sima et al., 2009). Vascular permeability is regulated in part by the dynamic opening and closing of inter-endothelial cell junctions (Dejana et al., 2008). In addition to cell-cell interactions, cell-ECM interactions play a crucial role in the regulation of permeability (Mehta and Malik, 2006). Data to-date suggests that the nature of the endothelial basement membrane and the connection between cells and their matrix can alter permeability (Qiao et al., 1995). However, there are no platforms available to systematically alter both the chemical and mechanical nature of the ECM to evaluate their effects on endothelial monolayer permeability.

Currently, *in vitro* endothelial permeability is most commonly quantified by either measuring the movement of an inert fluorescently-labeled molecule across an EC monolayer or by performing transendothelial electrical resistance measurements. In the former technique, cell monolayers are grown on microporous polycarbonate filter inserts that are suspended in a culture chamber. The passage of an inert molecule, such as FITC-conjugated albumin or dextran, is detected by sampling media from the apical and basal chambers and measured using spectrophotometry. While straightforward, these studies are not without certain disadvantages—since the flux of small molecules across the membrane is due to simple diffusion into a relatively large

reservoir, experiments last several hours and coincidentally, data may not be indicative of real-time barrier function. Moreover, the technique requires that cells be seeded on filters that do not necessarily mimic the chemical or mechanical properties of the *in vivo* environment.

In transendothelial electrical resistance (TEER) measurements, electrodes are placed in the apical and basal compartments and the electrical resistance across the endothelial monolayer is monitored. TEER studies are highly sensitive and are able to resolve real-time fluctuations in permeability but are more difficult to perform experimentally. Similar to the fluorescent dye measurements described above, cells are also plated directly onto polycarbonate membranes in TEER experiments. These membranes can be coated with ECM proteins such as collagen or fibronectin; however, the Young's modulus of polycarbonate is several orders of magnitude higher than that of native blood vessels. Therefore, neither system can accurately recapitulate the *in vivo* mechanical environment.

A growing body of data suggests that substrate mechanics play an important role in governing cell function important in the vasculature, including capillary morphogenesis (Califano and Reinhart-King, 2008; Kniazeva and Putnam, 2009), neutrophil transendothelial migration (Rabodzey et al., 2008), and vascular smooth muscle cell migration (Isenberg et al., 2009). Yet, no research has been done to elucidate the role of substrate mechanics on endothelial permeability. Here, we describe a method to measure the permeability of ECs cultured on flexible hydrogel substrates which mimic the Young's modulus of native vessels. These same substrates, which were first described by Pelham and Wang (Pelham and Wang, 1997), have been widely adopted in the cell and tissue engineering community because they are easy to

fabricate, can be conjugated with a variety of ECM proteins, and are mechanically tunable. Our approach holds several key advantages over conventional permeability studies—it has simple experimental setup, is able to measure cumulative flux of solutes in real-time, permits real-time observation of cells, and most importantly, accounts for physiological substrate rigidity.

2.3 Materials and methods

Polyacrylamide gel synthesis

Polyacrylamide (PA) gels were synthesized as previously described (Califano and Reinhart-King, 2008). Briefly, glass coverslips were activated by sequential washing in 0.1 N NaOH, 3-aminopropyltrimethoxysilane, and 0.5% glutaraldehyde (Sigma-Aldrich, St. Louis, MO). 5 and 30 kiloPascal (kPa) gels were polymerized onto activated coverslips using ratios of 7.5% to 0.175% or 12% to 0.28% acrylamide to bis-acrylamide, respectively. Gel surfaces were derivatized with 0.1 mg/ml rat tail collagen type I (BD Biosciences, San Jose, CA).

Cell culture and drug treatments

Bovine aortic endothelial cells (BAECs) were maintained in Medium 199 (Invitrogen, Carlsbad, CA) supplemented with 10% FetalClone III (HyClone, Logan, UT), and 1% each of penicillin-streptomycin (Invitrogen), MEM amino acids (Invitrogen), and MEM vitamins (Mediatech, Manassas, VA). Simvastatin, BW245C, Y27632, and 40 kDa fluorescein isothiocyanate (FITC)-conjugated dextran (Sigma-Aldrich) were diluted to final concentrations of 100 μM, 1 μM, 10 μM, and 10 μM, respectively. Bovine thrombin (Calbiochem, San Diego, CA), recombinant bovine tumor necrosis factor α (TNF-α, R&D Systems, Minneapolis, MN), and recombinant human vascular endothelial growth factor (VEGF 165, R&D Systems) were used at 4 U/ml, 100 ng/ml,

and 50 ng/ml, respectively.

Immunofluorescent staining

BAECs that were two days post-confluence were fixed with 3.7% formaldehyde (VWR International, West Chester, PA) and permeabilized with 1% Triton (VWR). Gels were sequentially incubated with a 1:50 dilution of goat polyclonal VE-cadherin primary antibody (Santa Cruz Biotechnology, Santa Cruz, CA) and a 1:200 dilution of Alexa Fluor 568 donkey anti-goat secondary antibody (Invitrogen). Phase and fluorescent images were captured on a Zeiss Axio Observer.Z1m microscope equipped with a Hamamatsu ORCA-ER camera.

Measurement of endothelial permeability

BAECs were seeded onto PA gels at a density of 10,000 cells/cm^2 and allowed to grow to confluence. Two days post-confluence, BAECs were refreshed with Leibovitz's L15 media containing 10% FetalClone III (HyClone) and 1% penicillin-streptomycin (Invitrogen) and maintained at 37° C. To evaluate endothelial permeability, a 10 μM solution of 40 kDa FITC-conjugated dextran was added to the cells for 5 minutes. For simvastatin, BW245C, and Y27632 experiments, BAECs were pretreated with each agonist for 30 minutes. For barrier-disruptive agonists, BAECs were pretreated with TNF-α for 4 hours or were treated simultaneously with bovine thrombin in FITC-conjugated dextran for up to 15 minutes. Human VEGF was also administered simultaneously in FITC-conjugated dextran for 5 minutes. Confocal z-slice images (512 x 512 pixels) were obtained on a Leica TCS SP2 system equipped with a 40x dipping lens.

To quantify endothelial permeability, fluorescence intensities of the images

were measured using ImageJ software (v. 1.42q, National Institutes of Health, Bethesda, MD). A 50 x 400 pixel rectangular box was drawn directly above the cell layer and the average pixel intensity, which represents the intensity of 10 μM FITC-dextran, was recorded. A second box of width 400 pixels was then drawn directly below the cell layer and encompassed the entire height of the PA gel, which represented the average pixel intensity of FITC-dextran that had permeated through the cell monolayer into the gel. Dextran accumulation was calculated as the average pixel intensity within the gel divided by the average pixel intensity above the gel. Relative permeability values were then calculated as the dextran accumulation values of cell-seeded gels normalized to cell-free gels.

Statistical analysis

All data are reported as mean ± SEM. Student's t-test or two-way ANOVA with Bonferroni post-tests were performed for statistical analysis using GraphPad Prism (v. 5.00, GraphPad Software, Inc., La Jolla, CA). p values < 0.05 were considered significant.

2.4 Results

2.4.1 Bovine aortic endothelial cells maintain their ability to grow into confluent monolayers on polyacrylamide gels

To study the permeability of endothelial monolayers on substrates of physiological stiffness, BAECs were seeded on compliant gels and allowed to grow to confluence and form a cobblestone monolayer. Gels were fabricated with a Young's modulus of 5 kPa which corresponds to the elasticity of the arterial media as determined previously by AFM (Engler et al., 2004). As shown in Figure 2.1, on both glass and polyacrylamide, BAECs preserve their classic cobblestone morphology (Fig. 2.1A and

B) and form cell-cell junctions (Fig. 2.1C and D). While these data indicate that the monolayer morphology is similar, it is not clear if permeability remains the same.

2.4.2 Confocal microscopy can be used to measure FITC-dextran accumulation across an endothelial monolayer into a polyacrylamide gel

To quantify the permeability of BAEC monolayers on gels, we tracked the movement of fluorescently-labeled dextran through the monolayer into the gel. Cells were seeded on the gel as described in Figure 2.1, and FITC-dextran is added to the culture. Because the polyacrylamide substrates are porous, inert molecules that pass through the endothelial barrier enter the gel (Fig. 2.2A and C). Analogous to sampling media from apical and basal chambers as is performed in traditional flux assays, permeability is measured based on the fluorescent intensities above and within the gels.

Using confocal microscopy, an image of the z-plane of the cell-seeded gel immersed in FITC-dextran is taken (Fig. 2.2B). As a control, images in the absence of cells are acquired (Fig. 2.2D). The pixel intensity within the cell-seeded gel is decreased compared to the intensity within the cell-free gel at the same time interval (Fig. 2.2D), indicating as expected that the presence of the endothelial monolayer (in Fig. 2.2B) acts as a barrier to the diffusion of fluorescently-labeled dextran into the gel. To compare the differences in pixel intensities and therefore permeability characteristics of the cell-free and confluent cell conditions, the cumulative dextran accumulation was measured. The dye accumulation was defined as the fluorescent intensity within the gel divided by the intensity measured above the gel.

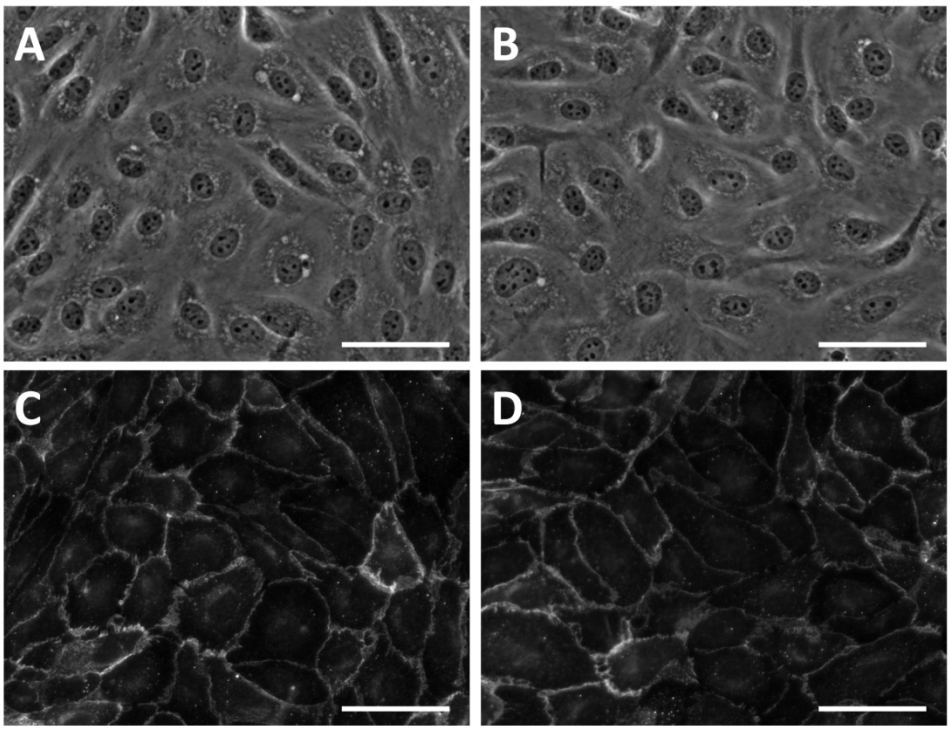

Figure 2.1. Micrographs of bovine aortic endothelial cell monolayers seeded on glass (A, C) and on 5 kPa polyacrylamide gels (B, D). (A) and (B): phase images, (C) and (D): immunofluorescent staining of VE-cadherin. Scale bars, 50 µm.

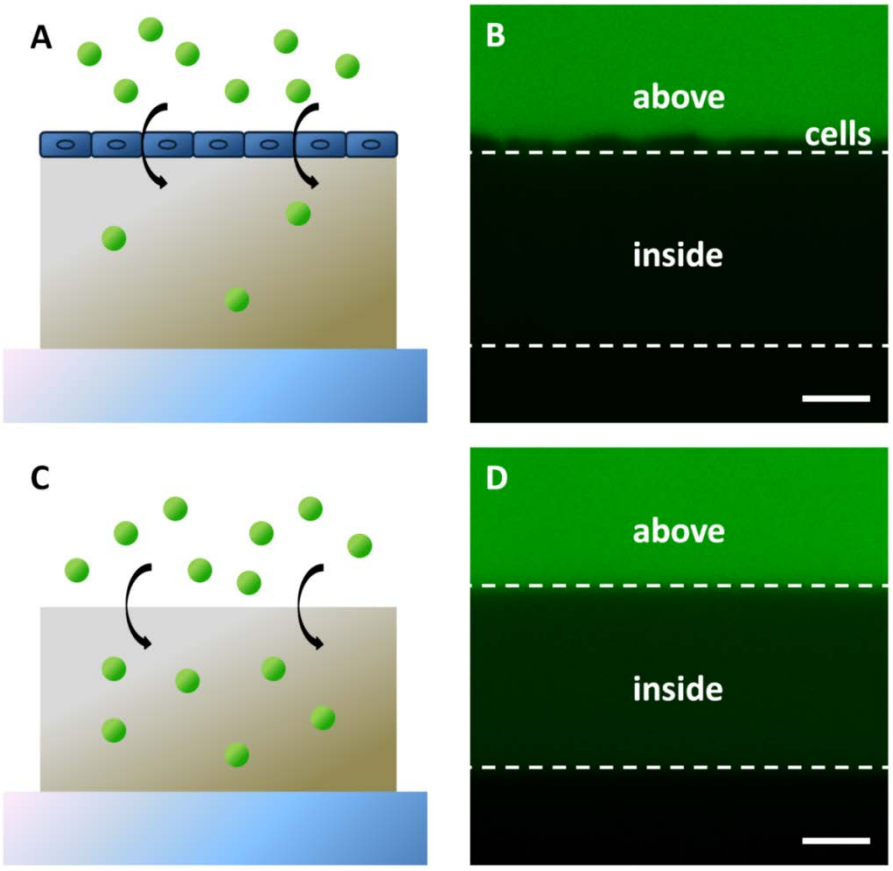

Figure 2.2. Schematic diagram of real-time permeability measurements. Cartoon schematic of dextran accumulation in gels with confluent cells (A) and without cells (C). (B) and (D) are representative confocal cross-sections of (A) and (C) after immersion in 40 kDa FITC-dextran (10 μM) for 5 minutes, depicting the method used to measure permeability. Dashed white lines represent the top and bottom edges of the gel. Permeability values of BAEC-seeded gels were calculated as the pixel intensity within the gel divided by the pixel intensity above the gel normalized to that calculated in cell-free gels. Scale bar, 20 μm.

To validate this metric, we characterized the time-dependent accumulation of dextran into gels with and without cells over 15 minutes (Fig. 2.3). As expected, cell-free gels had the highest cumulative dextran accumulation over the entire 15 minutes (Fig. 2.3A and B). Without any cell barrier impeding the diffusion of solutes, dextran accumulation plateaus at approximately t=5 min, likely due to the saturation of dextran within the gel. For this reason, all later experiments were performed with 5 minutes of dextran addition. The gels seeded with cells maintained the lowest dextran accumulation at each time point, with values of about 65% lower than that of cell-free gels (Fig. 2.3B), indicating that confluent BAECs are able to form a functional semi-permeable barrier restricting the movement of solutes into the hydrogel. To validate our method as a measure of permeability, we also tested BAEC monolayers treated with 4 U/ml thrombin, a vasoactive agent known to increase vascular permeability (Coughlin, 2000). When the endothelial barrier was perturbed by thrombin, dextran accumulation was higher at each time point throughout the length of the experiment compared to the untreated cell-seeded gels.

Because the porosity and diffusive properties of PA gels change relative to its stiffness and degree of cross-linking, the dextran accumulation within a gel of a given stiffness was normalized against the accumulation in a cell-free gel (Fig. 2.3C and 2.4). This normalized permeability metric was used to gauge the relative permeabilities of BAEC monolayers on gels in treated vs. non-treated conditions. As seen in Figure 2.3C, thrombin significantly increased endothelial barrier permeability as early as t=4 min. When comparing the permeability of thrombin-treated cells at t=1 and t=15 min, we found a 2.2-fold increase in accumulation, whereas in the untreated conditions, there was only a 1.5-fold increase in dye accumulation after 15 minutes. Additionally, our data shows that thrombin increased endothelial permeability by

about 73% (Fig. 2.4A) at t=5 min.

In addition to thrombin, we treated cells on gels with an array of known barrier-altering agonists (Fig. 2.4A). Human VEGF and recombinant bovine TNF-α, two other well-known barrier-disruptive agonists, significantly increased the relative permeability of BAEC monolayers on gels by a factor of 1.4 and 1.6, respectively. We also tested the effect of three barrier-enhancing agonists, simvastatin (van Nieuw Amerongen et al., 2000), Y27632 (Uehata et al., 1997), and BW245C (Murata et al., 2008). In all three cases, permeability as measured in our assay decreased. These data further validate our approach as a tractable method for measuring permeability.

2.4.3 Increased polyacrylamide gel stiffness induces endothelial permeability

Our lab and others (Califano and Reinhart-King, 2008; Guo et al., 2006; Ryan et al., 2001) have shown that cell-cell adhesion is increased on more compliant matrices which may lead to enhanced barrier function and decreased permeability. We tested this hypothesis by measuring the permeability of cells cultured on gels of two different stiffnesses—one that mimics the elasticity of the arterial media (5 kPa) and another that is much stiffer than physiologically relevant but less stiff than polycarbonate (30 kPa). Permeability of cells cultured on 30 kPa gels was significantly higher than on 5 kPa gels (Fig. 2.4B), similar to the increase in permeability when cells on 5 kPa gels were treated with thrombin. This suggests that substrate stiffness alone may enhance endothelial permeability similarly to drug challenges. Surprisingly, the addition of thrombin to the 30 kPa condition did not significantly increase measured permeability, indicating that a diffusion limit may exist in our system where we are unable to

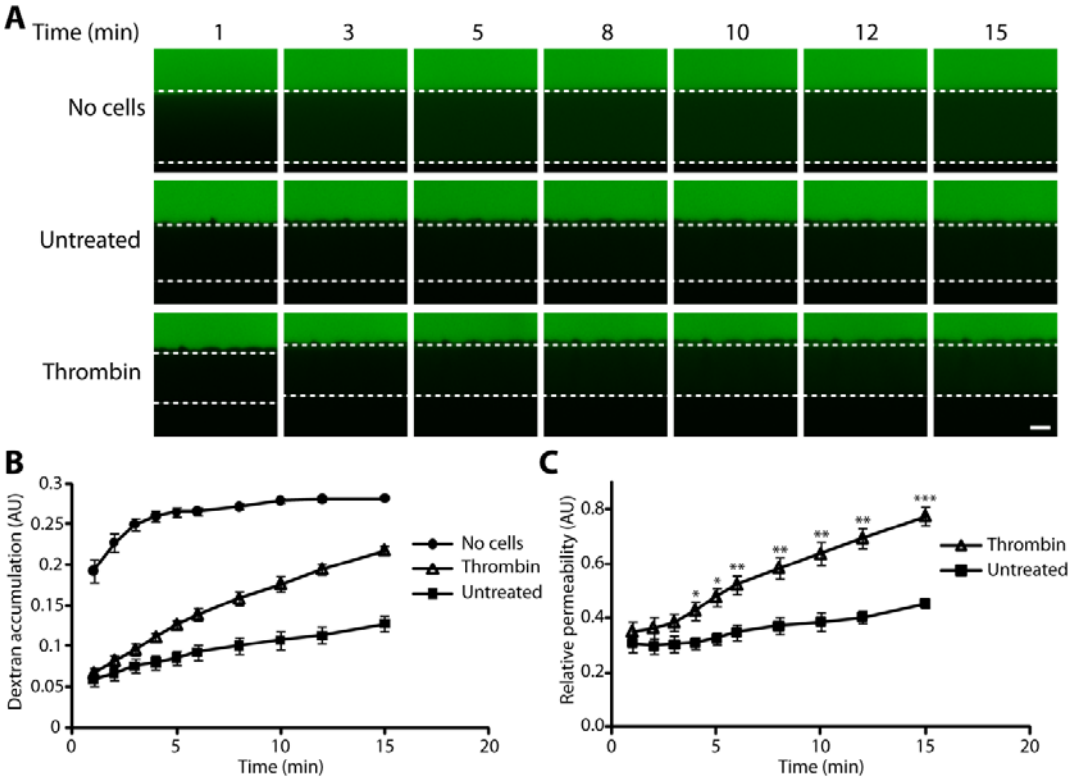

Figure 2.3. Endothelial permeability measurements. **(A)** Representative time lapse z-sections of 5 kPa polyacrylamide gels with or without bovine aortic endothelial cell monolayers, as well as cells treated with thrombin (4 U/ml), immersed in FITC-dextran. Dashed lines represent top and bottom edges of the gel. Scale bar, 20 μm. **(B)** Quantification of FITC-dextran accumulation with respect to time in 5 kPa gels without cells (solid circles), with cells treated with thrombin (open triangles), and with untreated cells (solid squares). Data are means ± SEM. **(C)** Permeability values of thrombin-treated (open triangles) or untreated (solid squares) cells cultured on 5 kPa substrates normalized by the dextran accumulation values of the gels without cells. Data are means ± SEM. $*P < 0.05$, $**P < 0.01$, $***P < 0.001$ (Student's *t* test) comparing thrombin-treated to untreated groups.

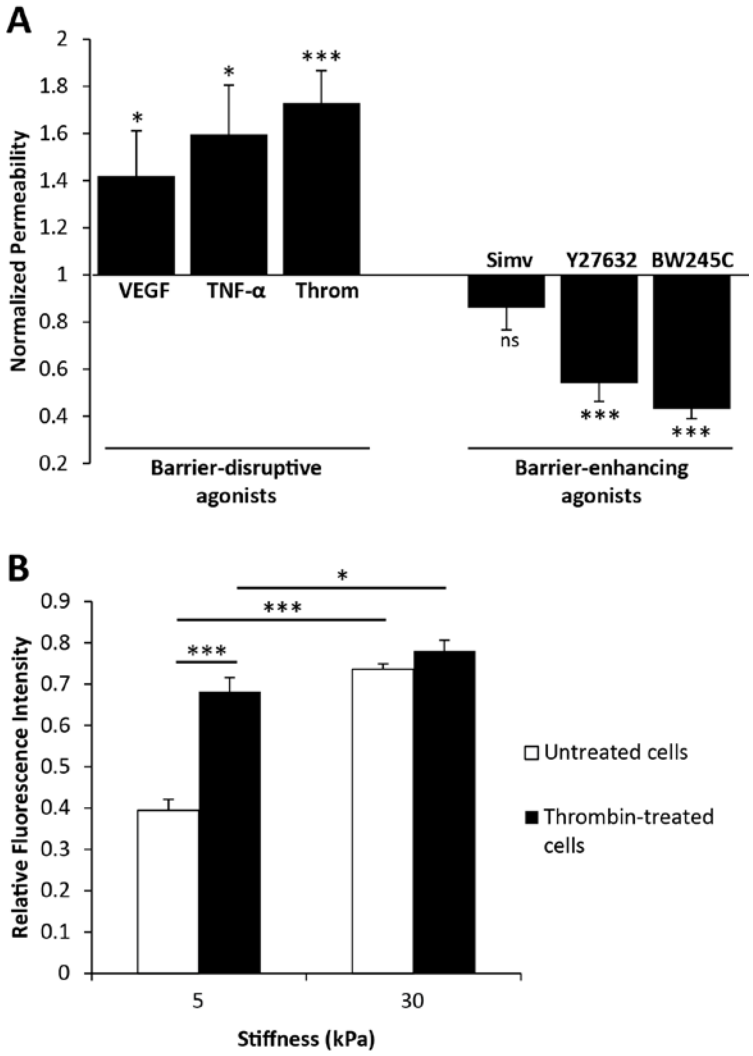

Figure 2.4. (A) Effects of known barrier-disruptive (VEGF, TNF-α, thrombin) and barrier-enhancing (simvastatin, Y27632, BW245C) agonists on the permeability of BAEC monolayers on 5 kPa polyacrylamide gels. Permeability values are normalized to that of untreated cells. Data are means ± SEM. $^{**}P < 0.01$, $^{***}P < 0.001$ (Dunnett's test) compared to untreated cells. (B) Effect of substrate stiffness (5 vs. 30 kPa) on cells treated with or without thrombin. $^{*}P < 0.05$, $^{***}P < 0.001$ (Tukey's test).

capture the full response of cells to thrombin treatment. Overall, these data underscore the importance of substrate mechanics and cell-matrix adhesions in modulating permeability which has been long overlooked in traditional permeability studies.

2.5 Discussion

Here we describe a novel method to measure the permeability of endothelial monolayers grown on soft polyacrylamide substrates that more closely mimic the stiffness of the physiological microenvironment. Using confocal microscopy, we can track the accumulation of FITC-labeled 40 kDa dextran through cell monolayers into their underlying PA gel to determine endothelial permeability. Validation of our methods was completed by measuring permeability after treatments with known barrier-disruptive and barrier-enhancing agonists. Lastly, we found that when increasing polyacrylamide stiffness from 5 to 30 kPa, endothelial permeability was enhanced, indicating that current methods to measure endothelial permeability using stiff polycarbonate substrates may not accurately capture what is occurring *in vivo*.

An interesting result elucidated in our studies was that the permeability of our monolayers was significantly lower that what others have found. Specifically, when compared to values reported by previous membrane-passage studies with BAECs, our relative permeability values were noticeably lower. In a study performed by Chang et al., BAECs stimulated with VEGF for 2 hours yielded a 4-fold increase in permeability, whereas Stockton et al. found 2.5-fold increases in permeability after 30 minutes of VEGF or TNF-α treatment (Chang et al., 2000; Stockton et al., 2004). In comparison, we found only a 1.4 and 1.6-fold increase in permeability after treatment with VEGF and TNF-α, respectively (Fig. 2.4A). Although timing of the drug treatments are different, we suspect matrix mechanics to play a role in mediating cell

susceptibility to drug treatment. Indeed, previous data suggests that cells are more sensitive to agonists on stiffer substrates (Brown et al., 2010; Paszek et al., 2005).

We also treated BAEC monolayers with several barrier-enhancing agonists, including Y27632, a specific inhibitor of Rho-associated kinase (ROCK) which is involved in cell contraction (Satoh et al., 2011; Zhou et al., 2011). In response, BAEC monolayers on 5 kPa gels exhibited a significant decrease in dextran flux (Fig. 4A), suggesting that by inhibiting cell contractility and therefore cell-matrix adhesions, cells maintain stronger cell-cell junctions and a less permeable barrier. In addition to Y27632, we tested the effect of simvastatin, a widely prescribed drug that inhibits cholesterol production (Armitage et al., 2010; Ijioma and Robinson, 2011), on endothelial permeability. Although treatment with simvastatin of cells on PA gels reduced endothelial permeability slightly, the result is not statistically different from baseline (P=0.12). Simvastatin has been found to protect endothelial monolayers from barrier-disruptive agonists (Chen et al., 2008; van Nieuw Amerongen et al., 2000), but it may not have a significant barrier-enhancing effect on non-disrupted cells. It is possible that when cultured on 5 kPa substrates that match the stiffness of healthy bovine arteries (Engler et al., 2004), BAECs may not respond to simvastatin treatment. However, based on our data showing increased permeability due to increased substrate stiffness (Fig. 2.4B), we suspect that on stiff substrates that more closely mimic a disease state, simvastatin may have a positive effect by lowering endothelial permeability. Together, these data underscore the importance of substrate mechanics and cell-matrix adhesions in modulating permeability which has been long overlooked in traditional permeability studies.

It is important to note that the porosity of polyacrylamide changes with its

stiffness. Although we did not directly measure the porosity of our substrates in this study, Williams and colleagues have done extensive work characterizing the void fraction of PA gels with respect to FITC-labeled dextran size (Williams et al., 1998). Intuitively, high percentage PA gels, which are stiffer, are less porous than their lower percentage and softer counterparts. Additionally, the fractional volume of gel available to solutes such as dextran decreases with increasing solute size. In our studies, we found that cells cultured on 30 kPa gels did not exhibit increased permeability when treated with thrombin (Fig. 2.4B). Because thrombin has been shown extensively to elicit increased endothelial permeability on even stiffer substrates, e.g. polycarbonate, we believe that our findings are not the result of endothelial cells being unresponsive to thrombin when cultured on 30 kPa gels but rather a limitation in the gel fraction available for FITC-dextran accumulation.

In summary, we have developed and validated a novel technique for measuring endothelial permeability while taking into consideration the effects of substrate mechanics. Our method is quick, easy to set up, and allows for real-time monitoring of cumulative solute flux. Moreover, it more closely mimics the *in vivo* environment which our data indicates has an important effect on permeability.

2.6 References

Armitage J, Bowman L, Wallendszus K, Bulbulia R, Rahimi K, Haynes R, Parish S, Peto R, Collins R. 2010. Intensive lowering of LDL cholesterol with 80 mg versus 20 mg simvastatin daily in 12,064 survivors of myocardial infarction: a double-blind randomised trial. *Lancet* **376**:1658-69.

Brown XQ, Bartolak-Suki E, Williams C, Walker ML, Weaver VM, Wong JY. 2010. Effect of substrate stiffness and PDGF on the behavior of vascular smooth

muscle cells: implications for atherosclerosis. *Journal of Cellular Physiology* **225**:115-22.

Califano JP, Reinhart-King CA. 2008. A balance of substrate mechanics and matrix chemistry regulates endothelial cell network assembly. *Cellular and Molecular Bioengineering* **1**:122-132.

Chang YS, Munn LL, Hillsley MV, Dull RO, Yuan J, Lakshminarayanan S, Gardner TW, Jain RK, Tarbell JM. 2000. Effect of vascular endothelial growth factor on cultured endothelial cell monolayer transport properties. *Microvascular Research* **59**:265-77.

Chen W, Pendyala S, Natarajan V, Garcia JGN, Jacobson JR. 2008. Endothelial cell barrier protection by simvastatin: GTPase regulation and NADPH oxidase inhibition. *American Journal of Physiology. Lung Cellular and Molecular Physiology* **295**:L575-83.

Coughlin SR. 2000. Thrombin signalling and protease-activated receptors. *Nature* **407**:258-64.

Dejana E, Orsenigo F, Lampugnani MG. 2008. The role of adherens junctions and VE-cadherin in the control of vascular permeability. *Journal of Cell Science* **121**:2115-22.

Engler AJ, Richert L, Wong JY, Picart C, Discher DE. 2004. Surface probe measurements of the elasticity of sectioned tissue, thin gels and polyelectrolyte multilayer films: Correlations between substrate stiffness and cell adhesion. *Surface Science* **570**:142-154.

Guo WH, Frey MT, Burnham NA, Wang YL. 2006. Substrate rigidity regulates the formation and maintenance of tissues. *Biophysical Journal* **90**:2213-20.

Huynh J, Nishimura N, Rana K, Peloquin JM, Califano JP, Montague CR, King MR, Schaffer CB, Reinhart-King CA. 2011. Age-related intimal stiffening enhances

endothelial permeability and leukocyte transmigration. *Science Translational Medicine* **3**:112ra122-112ra122.

Ijioma N, Robinson JG. 2011. Lipid-lowering effects of ezetimibe and simvastatin in combination. *Expert Review of Cardiovascular Therapy* **9**:131-45.

Isenberg BC, Dimilla PA, Walker M, Kim S, Wong JY. 2009. Vascular smooth muscle cell durotaxis depends on substrate stiffness gradient strength. *Biophysical Journal* **97**:1313-22.

Kniazeva E, Putnam AJ. 2009. Endothelial cell traction and ECM density influence both capillary morphogenesis and maintenance in 3-D. *American Journal of Physiology. Cell Physiology* **297**:C179-87.

Mehta D, Malik AB. 2006. Signaling mechanisms regulating endothelial permeability. *Physiological Reviews* **86**:279-367.

Murata T, Lin MI, Aritake K, Matsumoto S, Narumiya S, Ozaki H, Urade Y, Hori M, Sessa WC. 2008. Role of prostaglandin D2 receptor DP as a suppressor of tumor hyperpermeability and angiogenesis in vivo. *Proceedings of the National Academy of Sciences U S A* **105**:20009-14.

van Nieuw Amerongen GP, Vermeer MA, Nègre-Aminou P, Lankelma J, Emeis JJ, van Hinsbergh VW. 2000. Simvastatin improves disturbed endothelial barrier function. *Circulation* **102**:2803-9.

Paszek MJ, Zahir N, Johnson KR, Lakins JN, Rozenberg GI, Gefen A, Reinhart-King CA, Margulies SS, Dembo M, Boettiger D, Hammer DA, Weaver VM. 2005. Tensional homeostasis and the malignant phenotype. *Cancer Cell* **8**:241-54.

Pelham RJ, Wang Y l. 1997. Cell locomotion and focal adhesions are regulated by substrate flexibility. *Proceedings of the National Academy of Sciences U S A* **94**:13661-5.

Qiao RL, Yan W, Lum H, Malik AB. 1995. Arg-Gly-Asp peptide increases endothelial hydraulic conductivity: comparison with thrombin response. *American Journal of Physiology* **269**:C110-7.

Rabodzey A, Alcaide P, Luscinskas FW, Ladoux B. 2008. Mechanical forces induced by the transendothelial migration of human neutrophils. *Biophysical Journal* **95**:1428-38.

Ryan PL, Foty RA, Kohn J, Steinberg MS. 2001. Tissue spreading on implantable substrates is a competitive outcome of cell-cell vs. cell-substratum adhesivity. *Proceedings of the National Academy of Sciences U S A* **98**:4323-7.

Satoh K, Fukumoto Y, Shimokawa H. 2011. Rho-kinase: important new therapeutic target in cardiovascular diseases. *American Journal of Physiology. Heart and Circulatory Physiology* **301**:H287-96.

Sima AV, Stancu CS, Simionescu M. 2009. Vascular endothelium in atherosclerosis. *Cell and Tissue Research* **335**:191-203.

Stockton RA, Schaefer E, Schwartz MA. 2004. P21-activated kinase regulates endothelial permeability through modulation of contractility. *Journal of Biological Chemistry* **279**:46621-30.

Uehata M, Ishizaki T, Satoh H, Ono T, Kawahara T, Morishita T, Tamakawa H, Yamagami K, Inui J, Maekawa M, Narumiya S. 1997. Calcium sensitization of smooth muscle mediated by a Rho-associated protein kinase in hypertension. *Nature* **389**:990-4.

Williams JC, Mark LA, Eichholtz S. 1998. Partition and permeation of dextran in polyacrylamide gel. *Biophysical Journal* **75**:493-502.

Zhou Q, Gensch C, Liao JK. 2011. Rho-associated coiled-coil-forming kinases (ROCKs): potential targets for the treatment of atherosclerosis and vascular disease. *Trends in Pharmacological Sciences* **32**:167-73.

CHAPTER 3

AGE-RELATED INTIMAL STIFFENING ENHANCES ENDOTHELIAL PERMEABILITY AND LEUKOCYTE TRANSMIGRATION

Published in Science Translational Medicine (Huynh et al., 2011).

3.1 Abstract

Age is the most significant risk factor for atherosclerosis; however, the link between age and atherosclerosis is poorly understood. During both aging and atherosclerosis progression, the blood vessel wall stiffens owing to alterations in the extracellular matrix. Using in vitro and ex vivo models of vessel-wall stiffness and aging, we show that stiffening of extracellular matrix within the intima promotes endothelial cell permeability—a hallmark of atherogenesis. When cultured on hydrogels fabricated to match the elasticity of young and aging intima, endothelial monolayers exhibit increased permeability and disrupted cell-cell junctions on stiffer matrices. In parallel experiments, we showed a corresponding increase in cell-cell junction width with age in ex vivo aortas from young (10 weeks) and old (21 to 25 months) healthy mice. To investigate the mechanism by which matrix stiffening alters monolayer integrity, we found that cell contractility increases with increased matrix stiffness, mechanically destabilizing cell-cell junctions. This increase in endothelial permeability results in increased leukocyte extravasation, which is a critical step in atherosclerotic plaque formation. Mild inhibition of Rho-dependent cell contractility using Y-27632, an inhibitor of Rho-associated kinase, or siRNA restored monolayer integrity in vitro and in vivo. Our results suggest that extracellular matrix stiffening alone, which occurs during aging, can lead to endothelial monolayer disruption and atherosclerosis

pathogenesis. Because previous therapeutics designed to decrease vascular stiffness have been met with limited success, our findings could be the basis for the design of therapeutics that target the Rho-dependent cellular contractile response to matrix stiffening, rather than stiffness itself, to more effectively prevent atherosclerosis progression.

3.2 Introduction

Vascular stiffening accompanies a variety of cardiovascular pathologies including hypertension (Laurent and Boutouyrie, 2007) and atherosclerosis (Fernandes et al., 2008). The blood vessel wall also stiffens with age (McEniery et al., 2005). During aging, vessel stiffness increases owing to changes in the micro-scale architecture of the extracellular matrix (ECM) within the vessel wall, namely the increases in elastin fragmentation, collagen deposition, and matrix protein cross-linking (Greenwald, 2007; Zieman et al., 2005). This matrix stiffening decreases arterial distensibility and capacitance and can increase mechanical strain on the heart. Macroscopic measurements of arterial stiffness are often used for clinical diagnosis and can independently predict cardiovascular events, such as coronary heart disease and stroke (Mattace-Raso et al., 2006) and mortality in elderly patients (Sutton-Tyrrell et al., 2005). Although vascular stiffening occurs ubiquitously with age and is a predictor of cardiovascular risk, little is known about how vessel stiffness affects endothelial cells within blood vessels where arteriosclerosis initiates.

Recent evidence suggests that matrix stiffness affects cell behaviors (Discher et al., 2005), including cell spreading and adhesion (Pelham and Wang, 1997), migration (Zaman et al., 2006), and differentiation (Engler et al., 2006). It has been shown to alter vascular smooth muscle cell phenotype (Peyton and Putnam, 2005) and

promote intimal hyperplasia (Lemarié et al., 2010). Our own data suggest that changes in matrix stiffness can alter cell-cell contact (Reinhart-King et al., 2008). Because cell-cell contact is directly linked to monolayer integrity and permeability, we hypothesized that increased matrix stiffness with age may disrupt barrier function of the endothelium. Increased endothelial permeability to lipoproteins and immune cells is considered the initiating step of atherosclerosis pathogenesis, and the accumulation of debris in the intima results in the formation of atherosclerotic plaques (Lee et al., 2005; Lusis, 2000; Ross, 1999). Notably, decreasing permeability decreases plaque formation (Rozenberg et al., 2010; Sun et al., 2011). Endothelial permeability is controlled in part by the dynamic opening and closing of endothelial cell-cell junctions (Dejana et al., 2008), which are directly affected by interactions between endothelial cells and the ECM (Mehta and Malik, 2006). Although the intima stiffens during aging and atherosclerosis progression, and endothelial permeability occurs with age and is regarded as one of the first steps in atherogenesis, the relationship between age-related blood-vessel stiffening, endothelial cell function, and monolayer integrity has not been investigated in depth.

Because endothelial permeability is known as an early event in atherogenesis, we explored the effects of age-related matrix stiffness on endothelial barrier function using both in vitro and ex vivo models of intimal stiffening and aging. We found that stiffening of the matrix increased monolayer permeability. This increase in permeability was the result of upregulated cell contractility, which mechanically disrupted cell-cell junctions and promoted leukocyte transmigration—a critical step in atherosclerotic plaque formation. Pharmacological inhibition of cell contractility in vivo in mice reversed the effects of matrix stiffness on endothelial permeability by restoring tight cell-cell junctions, and also decreased leukocyte transmigration. These

findings suggest that matrix stiffening alone, which occurs during the natural aging process, can directly cause endothelial cell permeability and atherosclerosis progression.

3.3 Materials and methods

Cell culture and gel synthesis

Bovine aortic endothelial cells (BAECs) were maintained in Medium 199 (Invitrogen, Carlsbad, CA) with 10% FetalClone III (HyClone, Logan, UT) and supplements. Human umbilical vein endothelial cells (HUVECs) were maintained in Medium 200 (Invitrogen) supplemented with low serum growth supplement (Invitrogen) and 5% fetal bovine serum (Invitrogen). Polyacrylamide gels were prepared as described previously (Califano and Reinhart-King, 2008) and coated with 0.1 mg/ml rat tail collagen type I (BD Biosciences, San Jose, CA). 2.5, 5, and 10 kPa gels were made according to the ratios 5%:0.1%, 7.5%:0.175%, and 7.5%:0.35% acrylamide:bisacrylamide, respectively. All in vitro experiments were performed two days after the cells reached confluence.

Measurement of in vitro and in vivo endothelial permeability

For in vitro studies, a 10-μM solution of 40-kDa FITC-conjugated dextran (Sigma-Aldrich, St. Louis, MO) was added to BAECs for 5 min. For barrier-altering agonist experiments, BAECs were either pretreated with 1 μM BW245C (Sigma-Aldrich) for 30 min or 100 ng/ml recombinant bovine TNF-α (R&D Systems, Minneapolis, MN) for 4 h which was then washed out before being immersed in FITC-dextran for 5 min. For human VEGF (50 ng/ml, R&D Systems) or bovine thrombin (4 U/ml, Calbiochem, San Diego, CA) experiments, drugs were administered simultaneously in FITC-conjugated dextran for 5 min. For Y-27632 experiments, BAECs were

pretreated with 10 μM Y-27632 (Sigma-Aldrich) for 30 min which was then washed out before the addition of FITC-dextran. Confocal z-slices were obtained on a Leica TCS SP2 equipped with a 40× dipping lens. To calculate relative permeability, fluorescent intensities of images were measured using ImageJ software (NIH, v. 1.42q). Dextran accumulation was determined on the basis of the fluorescent intensity within the gel normalized by the fluorescent intensity above the BAEC monolayer. This value was then normalized against dextran accumulation values determined for polyacrylamide gels without cells.

All animal protocols were approved by the Cornell University Institutional Animal Care and Use Committee. For in vivo studies, endothelial permeability was measured with an Evans blue assay (Sun et al., 2011). Briefly, C57BL/6 mice were anesthetized on isoflurane, and 0.1 mg/kg Y-27632 in PBS or PBS only was administered retro-orbitally and allowed to circulate for 1 h while mice were allowed to wake. Mice were again anesthetized and 20 mg/kg Evans blue dye (Sigma-Aldrich) was administered retro-orbitally and allowed to circulate for 1 h while mice were allowed to wake. After re-anesthetizing, 10 ml PBS was perfused through the left ventricle, and the thoracic aorta was excised and cleaned of connective tissue. After drying at 80° C for 18 h, aortas were weighed. Aortas were then immersed in 150 μl formamide (Sigma-Aldrich) and incubated at 60° C for 24 h to extract Evans blue. Absorbance was read at 620 nm. The amount of dye was determined using standard curves and normalized to aorta dry weight.

Histology and atomic force microscopy indentation of mouse thoracic aortas

C57BL/6 mice were deeply anesthetized on isoflurane and euthanized. In the Y-27632 group, 0.1 mg/kg Y-27632 in PBS was administered retro-orbitally and allowed to

circulate for 1 h while mice were allowed to wake. The thoracic aorta was dissected, and individual sections were cut from the aorta, opened longitudinally, and gently scraped 10–15 times with a cotton-tipped applicator to remove the endothelium. To verify de-endothelialization, scraped and unscraped samples were fixed in 3.7% buffered formaldehyde and submitted to the university's histology service for routine hematoxylin & eosin (H&E) staining. Images were acquired using an Olympus AX70 microscope with a 40× objective and an Optronics Microfire digital camera. Scraped samples purposed for indentation testing were bonded to a glass substrate using Loctite gel adhesive (Henkel Corporation, Dusseldorf, Germany) and kept submerged in PBS.

The stiffness of the subendothelium was measured by atomic force microscopy indentation. A PicoPlus II scanning probe microscope (Agilent Technologies, Santa Clara, CA) and Au-coated SiN 0.12 N/μm cantilevers modified with 10-μm diameter polystyrene beads (Novascan, Ames, IA) were used. Photodetector sensitivity was calibrated using force curves taken in PBS on a rigid substrate. The cantilever spring constant k_c (Equation 3.1) was calibrated using Hutter's thermal noise method with corrections for cantilever tilt and optically-measured deflection (Butt and Jaschke, 1995; Hutter, 2005; Hutter and Bechhoefer, 1993).

$$k_c = 0.8174 \frac{k_B T}{\langle z^2 \rangle} \left(1 - \frac{3R}{2L} \tan \alpha \right)^{-1} \cos^2 \alpha \,, \qquad \text{(Eqn. 3.1)}$$

where k_B is Boltzmann's constant, T is temperature, $\langle z^2 \rangle$ is mean squared displacement of the primary bending mode, R is tip radius, L is cantilever length, and α is cantilever tilt angle. The calibrated spring constants were in the range of 0.10–

0.11 N/m. Indentation speed was 1 μm/s. All testing was done at room temperature and within 12 hours of animal death. In this window, we believe mechanical properties were maintained, as previous data suggests that when arteries are tested within several hours of isolation at temperatures between 22 and 37°C, there are no detectable changes in their mechanical properties (Gow et al., 1983; Schaar et al., 2002). Others have used similar transport procedures for testing of the medial layer and do not report any issue with cell viability (Engler et al., 2004; Engler et al., 2007). Additionally, other groups have used artery segments stored for longer times (>24 h) without loss of the smooth muscle cell contractile phenotype (Basha et al., 2006; Smolock et al., 2009).

Indentation force curves were analyzed using the Hertz model, which is appropriate for a spherical indenter and described in Equation 3.2:

$$F = \frac{4ER^{1/2}\delta^{3/2}}{3(1-\upsilon^2)}, \qquad \text{(Eqn. 3.2)}$$

where F is the applied force, E is the Young's modulus, R is the tip indenter radius, δ is indent depth, and v is Poisson's ratio. Incompressibility was assumed (v = 0.5). The contact point was chosen visually and the point-by-point modulus E_{pp} calculated by fitting each data point individually to E_{pp} (Equation 3.3):

$$E_{pp} = \frac{3F(1-\upsilon^2)}{4R^{1/2}\delta^{3/2}}, \qquad \text{(Eqn. 3.3)}$$

The shape of the E_{pp} vs. δ plot is sensitive to errors in the contact point (Crick and Yin, 2007). If an erroneous contact point was indicated, the contact point was corrected.

Curves in which the indenter failed to deform the tissue were discarded. A single indentation modulus value E was calculated for each indentation site by interpolating the E_{pp} vs. δ plot with a 5-point moving average, calculating an average $\underline{E_{pp}}$ vs. δ curve, and averaging E_{pp} over all δ. The resulting E is a measure of the indented site's overall stiffness.

Stiffness measurements of polyacrylamide gels

Steel balls (Abbott Ball Co., West Hartford, CT) with known density, ρ = 7,200 kg/m^3, and radius, R = 0.32 mm, were placed on polyacrylamide gels embedded with 0.5-μm fluorescent beads. A microscope was used to measure the indentation depth, δ, of the steel balls as they were magnetically removed from the gels as has previously been described (Lo et al., 2000; Reinhart-King et al., 2003). Gel stiffnesses were then calculated using the Hertz model for spherical contact. Recorded values of δ were inputted into the equation for Young's modulus, E (Equation 3.4):

$$E = \frac{3F(1-\upsilon^2)}{4R^{1/2}\delta^{3/2}}, \qquad \text{(Eqn. 3.4)}$$

where the Poisson's ratio, v, for polyacrylamide was assumed to be 0.3 (Li et al., 1993), and $F = \rho g(V - V_{cap})$, where g is 9.81 m/s^2, V is the volume of the steel ball, and V_{cap} is the indentation volume.

In vitro and ex vivo VE-cadherin junctional gap width quantification

BAECs on polyacrylamide gels were immunostained with goat polyclonal VE-cadherin primary antibody (C-19, Santa Cruz Biotechnology, Santa Cruz, CA) and Alexa Fluor 568 donkey anti-goat secondary antibody (Invitrogen). Actin was stained with FITC-conjugated phalloidin (Sigma-Aldrich) and nuclei with DAPI (Sigma-

Aldrich). Images were captured on a Zeiss Axio Observer.Z1m microscope with a Hamamatsu ORCA-ER camera.

C57BL/6 mice were anesthetized on isoflurane, and 0.1 mg/kg Y-27632 in PBS or PBS only was administered retro-orbitally and allowed to circulate for 1 h while mice were allowed to wake. The mice were then deeply anesthetized with isoflurane, overdosed on pentobarbital and intracardially perfused with cold 1% paraformaldehyde at an average flow rate of 10 ml/min, which matches the blood flow in mice to minimize artifacts from perfusion (Huo et al., 2008). Aortas were extracted and post-fixed in 1% paraformaldehyde for 1 h. Sections of the descending thoracic aorta approximately 1 mm long were stained with a biotinylated monoclonal antibody against mouse CD144 (13-1221, eBioscience, San Diego, CA). Secondary label was Texas Red streptavidin (SA-5006, Vector Laboratories, Burlingame, CA or S872, Invitrogen). Aortic sections were opened longitudinally and covered with a coverslip. Endothelial cells were imaged using a locally-built two-photon-excited fluorescence microscope using 830-nm excitation (MIRA-HP, Coherent, Santa Clara, CA) with a 63×, 1.2 NA objective (Zeiss, Germany) and 645/65-nm emission filter (Chroma Technology, Bellows Falls, VT).

Junctional gap width measurements were analyzed using ImageJ and a custom-written MATLAB algorithm. Briefly, using fluorescent images of VE-cadherin, a line was drawn perpendicular to the widest gap per junction, and the intensity profiles were recorded using ImageJ. A two-Gaussian curve was then fit to the intensity profiles in MATLAB. Gap widths were defined as the width of the two-Gaussian fit 20% above background pixel intensity.

Measurement of RhoA activity

BAEC intracellular RhoA activity was quantified using a RhoA G-LISA kit (Cytoskeleton, Denver, CO) according to the manufacturer's protocol.

Traction force microscopy

BAECs plated on polyacrylamide gels embedded with 0.5-μm diameter fluorescent beads (Invitrogen) were allowed to adhere for 24 h. Isolated cells were imaged in phase, and the fluorescent bead field beneath the cell was imaged immediately after. A second fluorescent image of the bead field was taken after cells were removed with 0.05% trypsin/EDTA (Invitrogen). Bead displacements were used to compute cellular traction vectors, *T*, and total magnitudes of force, | *F* |, using the LIBTRC analysis library developed by M. Dembo (Dembo and Wang, 1999). | *F* | (Equation 3.5) is the sum of the traction field magnitudes over the entire cell area,

$$| F | = \iint (T_x^2(x, y) + T_y^2(x, y)^{1/2}\, dxdy\,, \qquad \text{(Eqn. 3.5)}$$

where $T(x, y) = [T_x(x, y), T_y(x, y)]$ is the continuous field of cellular traction vectors defined at spatial position (*x*, *y*) over the entire cell area (Reinhart-King et al., 2005).

RNA interference

BAECs at 90% confluency on tissue culture plastic were transfected with 10 nM non-targeting (control) siRNA or siRNA targeting *ROCK1* using 2 μg/ml Lipofectamine 2000 (Invitrogen). The non-targeting sequence was 5'-AAUCAUCAAGUCUUAACCCGUACUC-3'. The sequence targeting *ROCK1* was 5'-CAGAAGUGCAGAACGUCAAACAUAA-3'. Both the control siRNA and the siRNA targeting *ROCK1* (accession number NM_001191227.1) were synthesized by

Invitrogen. *ROCK1* interference was quantified by Western blot densitometry. Primary antibodies against ROCK1 and GAPDH were purchased from Santa Cruz Biotechnology and Millipore, Billerica, MA, respectively.

Neutrophil transmigration and rolling adhesion

All human subject protocols have been approved by the Institutional Review Board for Human Participants at Cornell University. Fresh peripheral human blood was collected into vacutainer tubes containing heparin and allowed to equilibrate at room temperature. Blood was layered over 1-Step Polymorphs (Accurate Chemical, Westbury, NY) and separated by centrifugation. The neutrophil layer was collected, washed, and resuspended in flow buffer (0.5% human serum albumin (Sigma-Aldrich), 10 mM HEPES and 2 mM $CaCO_3$ in Hank's Balanced Salt Solution). HUVEC monolayers pre-treated with 0.1 ng/ml recombinant human TNF-α (R&D Systems) for 6 h were either untreated or treated with 10 μM Y-27632 for 1 h. Neutrophils (50,000 cells/cm^2) were then allowed to adhere for 5 min. Gels were gently washed twice with flow buffer to remove unattached neutrophils. HUVEC VE-cadherin was stained as described previously, and neutrophils were stained with a FITC-conjugated antibody against human CD45 (Invitrogen). Images were taken on a Zeiss LSM710 confocal microscope with a 25× objective. Transmigrated neutrophils were defined as CD45-positive cells with at least 50% of its cell body located beneath the endothelial layer.

Flow chamber assembly and leukocyte rolling experiments

Human umbilical vein endothelial cells (HUVECs) on polyacrylamide gels were stimulated with 0.1 ng/ml recombinant human TNF-α (R&D Systems) for 6 h. A rectangular parallel-plate flow chamber (GylcoTech, Gaithersburg, MD) with a gasket

of size 0.254 cm × 1 cm × 6 cm (h × w × l) was carefully assembled over polyacrylamide gels and held together by vacuum. The flow chamber assembly was secured onto the stage of an Olympus IX81 microscope equipped with a Hitachi CCD camera (KP-M1AN) connected to a DVD recorder (DVO-1000MD, Sony Electronics). A syringe pump (KDS 230, IITC Life Science, Woodland Hills, CA) was used to control the flow rate of the cell suspension. Neutrophils at a concentration of 150,000 cells/ml flow buffer (0.5% human serum albumin (HSA, Sigma-Aldrich), 10 mM HEPES and 2 mM $CaCO_3$ in Hank's Balanced Salt Solution were perfused at a wall shear stress of 2 dyn/cm^2 for a total period of 7 min. "Rolling" cells were defined as those observed to translate in the direction of flow with an average velocity less than 50% of the calculated hydrodynamic free stream velocity. During flow, 79–96 random fields of view (640 × 480 pixels, 1.52 pixel/μm) were recorded using a 20× objective (NA 0.4, Olympus).

Flow cytometry

HUVECs on gels were treated with 0.1 ng/ml TNF-α for 6 h. Gels were rinsed with PBS and inverted onto accutase (MP Biomedicals, Solon, OH). Cells were dislodged by pipetting and pelleted by centrifugation. After blocking with 1% goat serum, cells were incubated with primary antibodies against ICAM-1, VCAM-1, or E-selectin, or mouse IgG1 isotype control (R&D Systems). Secondary label was Alexa Fluor 488 anti-mouse antibody (Invitrogen). Labeled cells were resuspended and analyzed using an Accuri C6 flow cytometer.

Statistical analysis

All analyses were completed using JMP 8 (SAS Institute, Cary, NC) or GraphPad Prism 5 (GraphPad Software, Inc., La Jolla, CA). Data in Fig. 3.1B, Fig. 3.2C, Fig.

3.5A, Fig. 3.5B, and Fig. 3.8 were analyzed by parametric one-way ANOVA with post-hoc Tukey's test to compare untreated conditions. Two-way ANOVA with post-hoc Tukey's test was then used to compare Y-27632 or *ROCK1*-targeted siRNA data to its respective control. Data in Fig. 3.3D and 3.4 were analyzed by non-parametric Kruskal-Wallis ANOVA with post-hoc Dunn's test. Data in Fig. 3.5C were analyzed using Student's *t* test. All data are means ± SEM. *P* values < 0.05 were considered significant.

3.4 Results

3.4.1 Increased matrix stiffness promotes endothelial monolayer permeability by destabilizing cell-cell junctions

We first investigated the effect of substrate stiffness on the barrier function of endothelial monolayers. To mimic the stiffness of young and aged intima, synthetic hydrogel substrates (Reinhart-King, 2008) were fabricated that approximated and exceeded the Young's Modulus of 2.7 ± 1.1 kPa reported previously for the subendothelial matrix in bovine carotid arteries (Peloquin et al., 2011). Bovine aortic endothelial cells (BAECs) were seeded on polyacrylamide substrates of 2.5, 5 and 10 kPa. Endothelium permeability was measured on the basis of 40 kDa FITC-dextran movement across the monolayer (Fig. 3.1A). 40 kDa FITC-dextran was chosen as its hydrodynamic radius (~4.8 nm) approximates that of albumin (~3.6 nm) (Armstrong et al., 2004), a model protein commonly used in permeability studies (Cooper et al., 1987) and whose permeation through the endothelium is associated with cardiovascular pathologies such as diabetes (Mogensen, 1984) and atherosclerosis (Pedrinelli et al., 1998). Importantly, endothelial monolayer permeability increased as a function of matrix stiffness (Fig. 3.1B), which suggests that matrix stiffness alone,

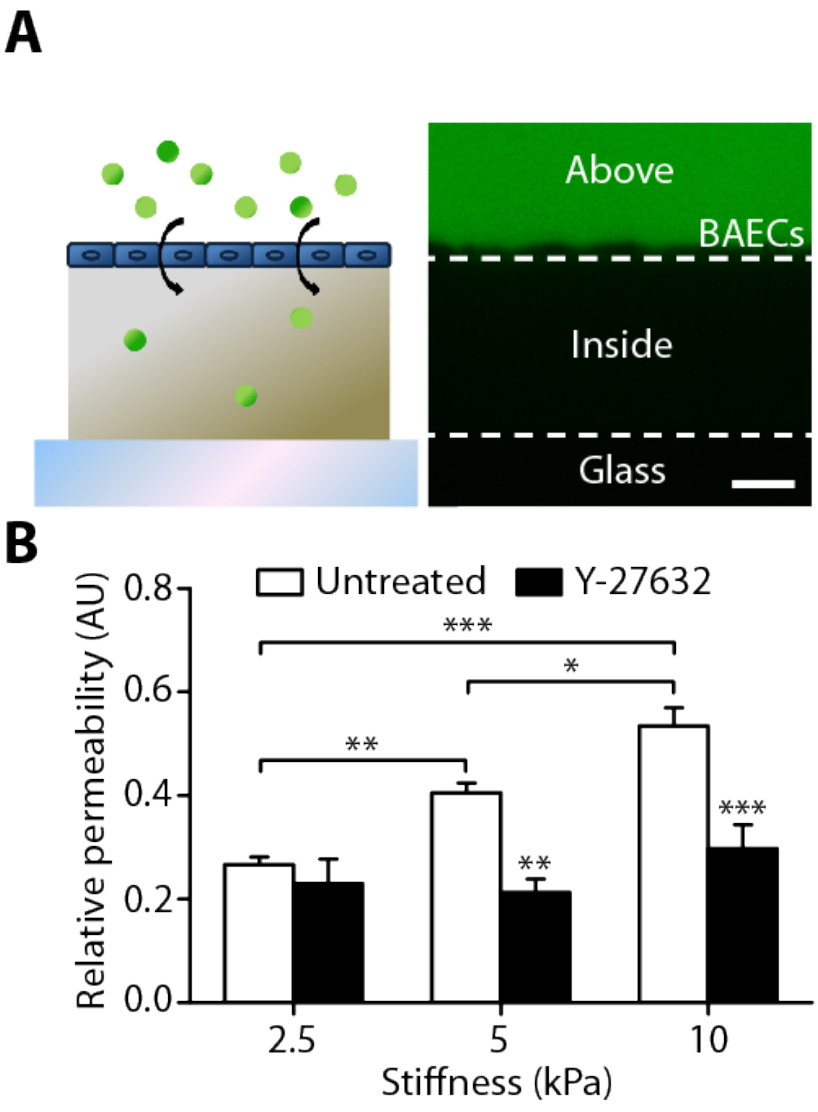
A
Above
BAECs
Inside
Glass
B
Untreated
Y-27632
Relative permeability (AU)
0.0
0.2
0.4
0.6
0.8
***
*
**
**
***
2.5
5
10
Stiffness (kPa)

Figure 3.1. Matrix stiffness increases endothelial permeability. **(A)** A cartoon shows FITC-dextran permeation through an endothelial monolayer into a polyacrylamide gel. On the right is a representative confocal cross-section of dextran capture in a 2.5-kPa polyacrylamide gel, depicting the method used to measure permeability. Dashed lines represent the top and bottom edges of the gel. Permeability values of cell (BAEC)-seeded gels were calculated as the pixel intensity within the gel divided by the pixel intensity above the gel normalized to that calculated in cell-free gels. Scale bar, 20 μm. **(B)** Relative permeability of BAECs cultured on substrates matching (2.5 kPa) and exceeding (5 and 10 kPa) the stiffness of bovine arterial intima with (n = 8 gels, three independent experiments) or without (n = 16–20 gels, ten independent experiments) Y-27632 treatment. Data are means ± SEM. *P < 0.05, **P < 0.01, ***P < 0.001 (Tukey's test) compared to respective untreated conditions unless otherwise indicated by brackets.

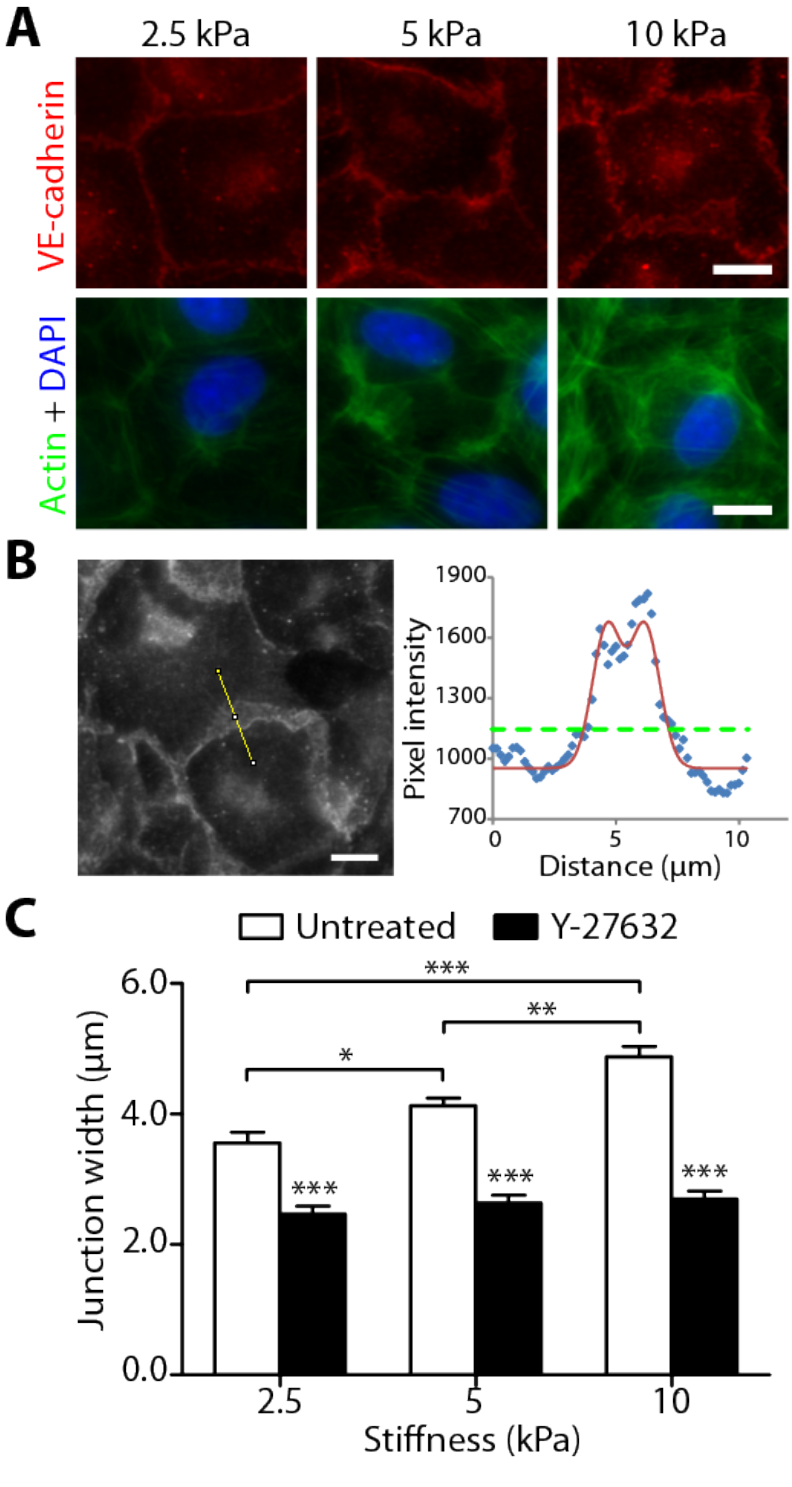
A
2.5 kPa
5 kPa
10 kPa
VE-cadherin
Actin + DAPI
B
1900
1600
1300
1000
700
Pixel intensity
0
5
10
Distance (µm)
C
Untreated
Y-27632
***
**
*
6.0
4.0
2.0
0.0
Junction width (µm)
2.5
5
10
Stiffness (kPa)

Figure 3.2. Matrix stiffness increases cell-cell junction width. **(A)** Fluorescent images showing VE-cadherin (red), actin (green), and nuclei (blue) of confluent BAECs on gels. Performed in collaboration with Joe Califano. **(B)** VE-cadherin junctional gap-width measurement. Left: VE-cadherin immunostaining of bovine aortic endothelial cells cultured on polyacrylamide gels. Scale bar, 5 μm. Right: Blue dots represent the pixel intensity profile of the yellow line drawn in the left image, whereas the red line represents a two-Gaussian fit calculated using a MATLAB program written by Mike King. The junction width was considered as the width of the fitted curve at 20% above baseline intensity, as indicated by the dashed green line. **(C)** VE-cadherin junction-width measurements of BAECs on gels with or without 30 min Y-27632 treatment (n = 60 junction measurements, two independent experiments). Scale bar, 10 μm. Data are means ± SEM. *P < 0.05, **P < 0.01, ***P < 0.001 (Tukey's test) compared to respective untreated conditions unless otherwise indicated by brackets.

without any externally added agonists, promotes increased endothelial monolayer permeability.

To investigate the mechanism by which substrate stiffness contributes to changes in permeability, we probed the integrity of the cell-cell junctions within the endothelial monolayer by fluorescently imaging vascular endothelial (VE)-cadherin (Fig. 3.2A), a cell-cell adhesion molecule that mediates endothelium stabilization (Dejana et al., 2009). Using methods similar to those that have been described previously (van Nieuw Amerongen et al., 2007) where lines were drawn perpendicularly to cell junctions to determine pixel intensities (Fig. 3.2B), we measured the separation width of intercellular junctions on polymers of varying stiffnesses (2.5 to 10 kPa). These measurements indicated that the distance between cells increased as a function of matrix stiffness (Fig. 3.2C). Together, these data suggest that increased matrix stiffness disrupts the formation of cell-cell junctions in vitro, which increases endothelial permeability.

3.4.2 Age-related intimal stiffening disrupts endothelial cell-cell junction integrity

Because blood vessel stiffness increases with age, and because our in vitro data indicated that increased matrix stiffness destabilizes cell-cell junctions (Fig. 3.2), we investigated the effects of aging and vessel stiffness on endothelial permeability and cell-cell junction integrity in a mouse model. We first characterized the intimal stiffness of de-endothelialized thoracic aortas of young (10 to 11 weeks) and old (21 to 25 months) mice using atomic force microscopy (AFM) (Fig. 3.3). To remove endothelial cells from the subendothelium, a cotton applicator was used to gently scrape away endothelial cells (Peloquin et al., 2011). H&E staining was used to ensure

endothelial cells were removed without damaging the structural integrity of the subendothelium (Fig. 3.3A). Representative Hertzian fit to AFM force-indentation data and point-by-point modulus vs. indentation depth plots are shown in Figs. 3.3B and C, respectively. Using this data, we found a significant increase in indentation modulus of the subendothelium with age (Fig. 3.3D). This measured modulus for young mice (31.9 ± 4.5 kPa, mean ± SEM) was higher than the value found for 18 to 30 month-old bovine carotid intima (2.7 ± 0.6 kPa, mean ± SEM) (Peloquin et al., 2011), presumably owing to the close proximity of the first internal elastic lamina relative to the lumen of the mouse vessel, which prevents the intima from deforming fully under indentation. The bovine carotid intima is more similar to the human carotid intima in its structure. Despite the difference between the moduli found for bovine and mouse intima, our data confirm that there is a relative increase in ECM stiffness in blood vessels with age.

Using a different set of young (10 weeks) and old (16 to 24 months) mice than those used in the stiffness measurements (Fig. 3.3D), we visualized endothelial cell-cell junctions within intact aortas based on VE-cadherin localization using two-photon microscopy (Fig. 3.4A). Intercellular distance, measured as the widest VE-cadherin separation width between two adjacent cells, was greater in aged, stiffer aortas than in younger, more compliant vessels (Fig. 3.4B), similar to the effects measured in vitro on stiffer matrices (Fig. 3.2C). In another set of young (9 weeks) and old (19 to 22 months) mice, we measured the permeability of thoracic aortas with an Evans blue dye assay and found that Evans blue deposition within the vessel wall increased with age (Fig. 3.4C). These data suggest that, with age, the intima stiffens, causing endothelial cell-cell junctions to separate and increase permeability.

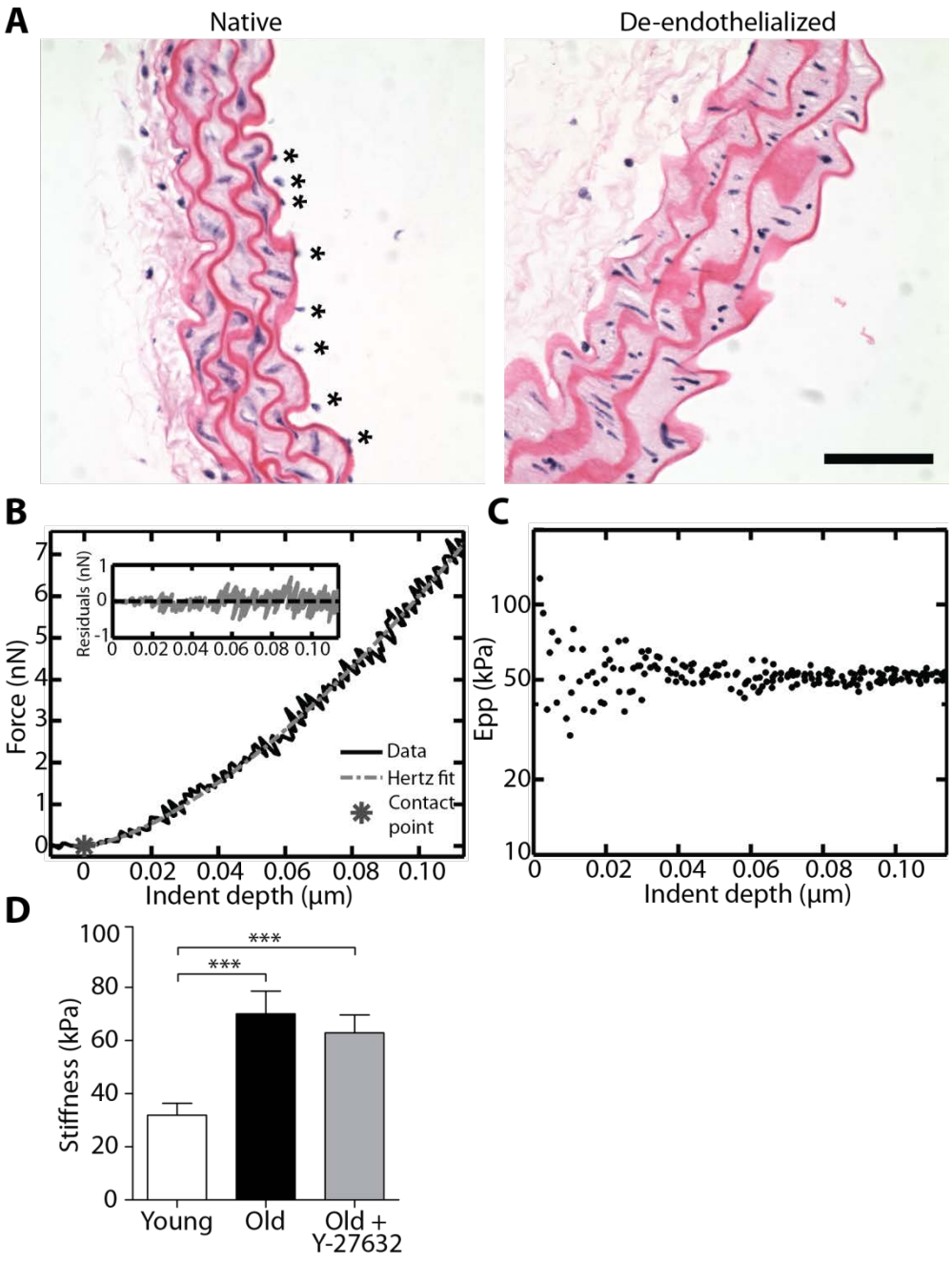
A
Native
De-endothelialized
B
Force (nN)
Indent depth (μm)
Residuals (nN)
Data
Hertz fit
Contact point
C
Epp (kPa)
Indent depth (μm)
D
Stiffness (kPa)
***
***
Young
Old
Old + Y-27632

Figure 3.3. Histology and AFM indentation of mouse thoracic aorta. **(A)** H&E staining of native and de-endothelialized aorta to show successful removal of ECs with minimal damage to underlying ECM. The section is perpendicular to the flow axis. Gentle scraping with a cotton applicator removes the ECs (asterisks) from the artery lumen, exposing the subendothelium for indentation. Scale bar, 50 μm. **(B)** Example least-squares fit of the Hertz model to AFM data, which shows the validity of the Hertz contact equation as a method to calculate the indentation modulus of mouse aortas. Insert: Residual error of the fit. **(C)** Example point-by-point modulus E_{pp} versus indentation depth plot obtained by individually fitting each data point in (B). After the initial noisy region ($\delta < 0.03$), the E_{pp} is approximately 50 kPa. **(D)** AFM indentation measurements of thoracic aorta of untreated young (10 to 11 weeks, $n = 61$ indent sites, 3 aortas) and old (20 to 25 months, $n = 55$ indent sites, 5 aortas) mice, as well as Y-27632-treated old (20 months, $n = 76$ indent sites, 4 aortas) mice. Data are means ± SEM. ***$P < 0.001$ (Dunn's test). Experiments performed in collaboration with John Peloquin.

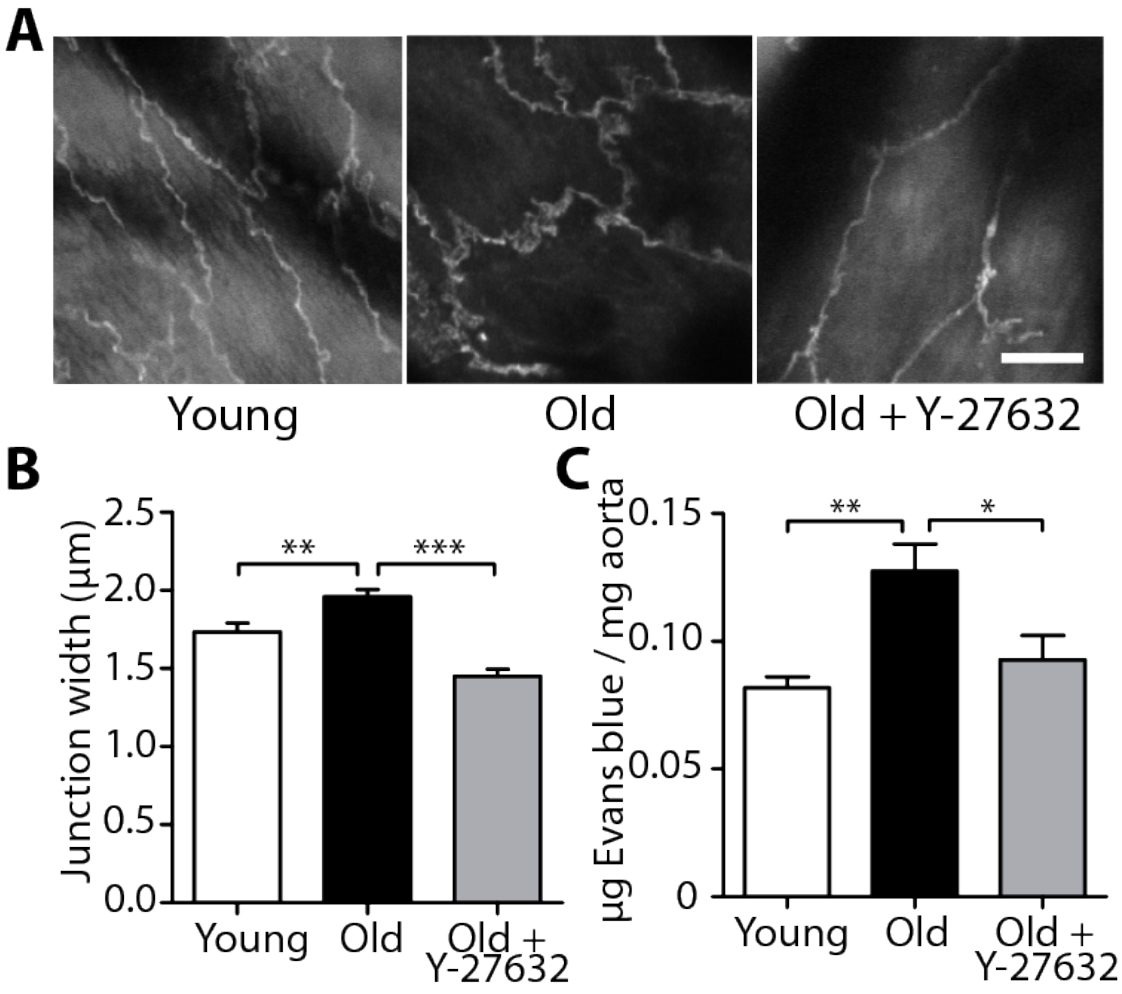
A
Young
Old
Old + Y-27632
B
Junction width (µm)
2.5
2.0
1.5
1.0
0.5
0.0
**
***
Young
Old
Old + Y-27632
C
µg Evans blue / mg aorta
0.15
0.10
0.05
0
**
*
Young
Old
Old + Y-27632

Figure 3.4. Aging increases endothelial intercellular junction separation in mice. **(B)** Permeability measurements of thoracic aorta of untreated young (9 weeks, n = 4 aortas) and old (19 to 22 months, n = 6 aortas) mice, as well as Y-27632-treated old (20 months, n = 4 aortas) mice. Data are means ± SEM. *P < 0.05, **P < 0.01 (Dunn's test). **(C)** Two-photon microscopy of VE-cadherin immunofluorescent staining in endothelial cells of intact, untreated young (10 week) and old (16 month) thoracic mouse aortas, as well as Y-27632-treated old (24 month) thoracic aortas. Scale bar, 10 μm. **(D)** VE-cadherin junction width measurements of thoracic aortic endothelial cells from untreated young (10 weeks, n = 240 width measurements, 4 aortas) and old (16 to 24 months, n = 390 width measurements, 7 aortas) mice, as well as Y-27632-treated old (21 to 24 months, n = 156 width measurements, 3 aortas) mice. Data are means ± SEM. **P < 0.01, ***P < 0.001 (Dunn's test). Experiments performed in collaboration with Nozomi Nishimura and Chris Schaffer.

3.4.3 Endothelial permeability and cell-cell junctions are regulated by cell contractility

Previous work suggests that endothelial permeability is regulated in part by the cellular cytoskeleton and cell contractility (Birukova et al., 2009). The Rho signaling pathway is a well-established mediator of the sustained contraction of the cytoskeleton (Mehta and Malik, 2006; Shyy, 2002). Evidence in other cell types suggests that matrix stiffness induces changes in Rho activation (Huang and Ingber, 2005; Paszek et al., 2005). When activated, Rho and its downstream effector Rho-associated kinase (ROCK) stimulate cell contractility by modulating actomyosin contraction and cell-matrix adhesion. To explore the intracellular mechanisms by which the mechanical properties of the matrix affect monolayer permeability, we hypothesized that stiffer substrates induce Rho activation, leading to increased cell contractility, the physical separation of cell-cell junctions, and increased permeability. Using a commercially available Rho detection kit, we found increased Rho activity in endothelial cells on 10 kPa substrates compared to those on 2.5 kPa substrates (Fig. 3.5A). To ensure that Rho activation was not altered by the concentration of acrylamide within the hydrogel substrates but rather by stiffness, we made two formulations of gels with different acrylamide concentrations that were both approximately 2.5 kPa in stiffness (Fig. 3.5B). Rho activity was unchanged (Fig. 3.5C), suggesting that polymer composition does not activate Rho independently of stiffness. To determine if increased Rho activity resulted in increased cell contractility, we used traction force microscopy to quantify the forces exerted by endothelial cells as a function of matrix stiffness. Endothelial cells exerted stronger traction forces on 10 kPa substrates than on 2.5 kPa substrates (Fig. 3.6A), and the total magnitude of cellular force increased as a function of matrix stiffness (Fig. 3.6B).

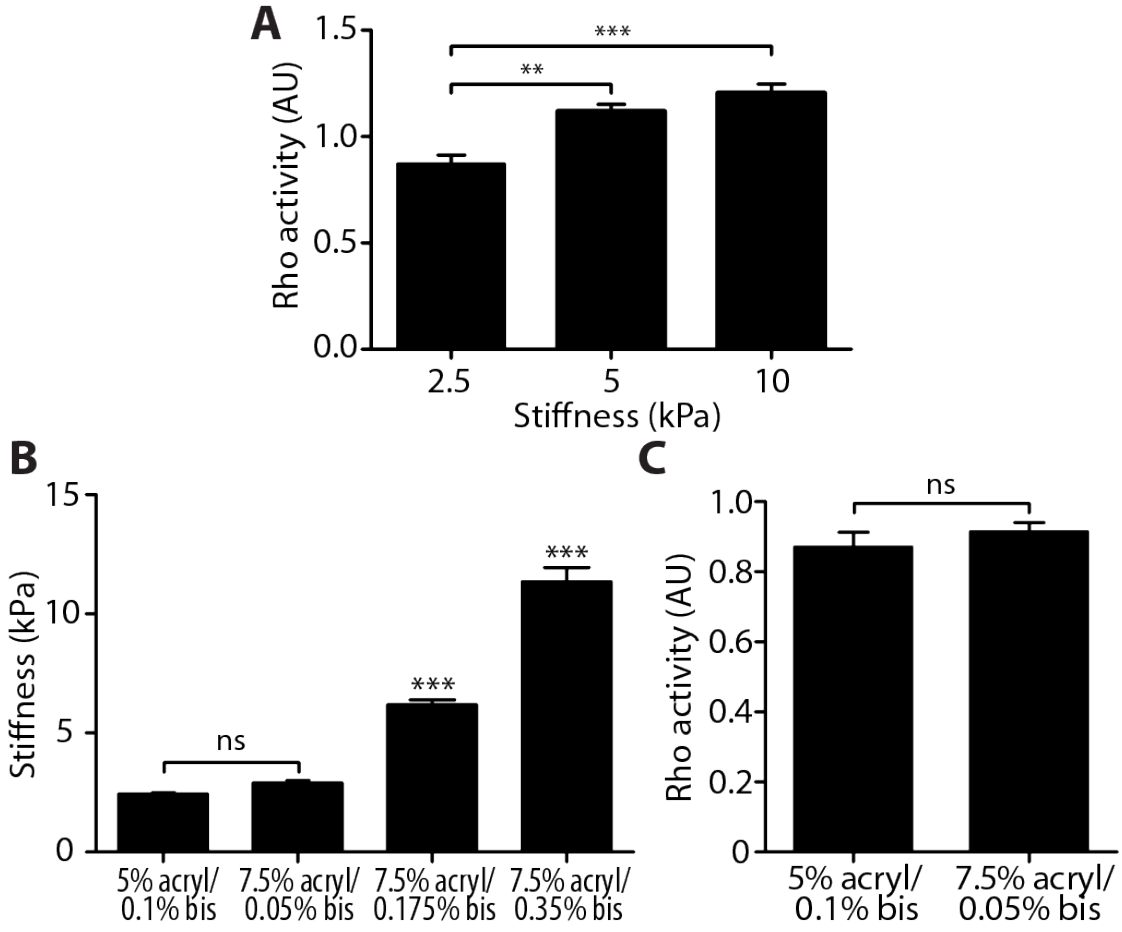
A
Rho activity (AU)
1.5
1.0
0.5
0.0
***
**
2.5
5
10
Stiffness (kPa)
B
Stiffness (kPa)
15
10
5
0
ns
***
***
5% acryl/ 0.1% bis
7.5% acryl/ 0.05% bis
7.5% acryl/ 0.175% bis
7.5% acryl/ 0.35% bis
C
Rho activity (AU)
1.0
0.8
0.6
0.4
0.2
0
ns
5% acryl/ 0.1% bis
7.5% acryl/ 0.05% bis

Figure 3.5. Rho activity increases due to matrix stiffening. **(A)** Rho activity of BAECs cultured on polyacrylamide gels of different stiffness (three independent experiments, each performed in duplicate). Data are means ± SEM. $^{**}P < 0.01$, $^{***}P < 0.001$ (Tukey's test). **(B** and **C)** Gels made from different acrylamide concentrations that are similar in stiffness elicit similar levels of Rho activation. Experiments performed in collaboration with Joe Califano. **(B)** Stiffness measurements of polyacrylamide gels of varying percentages of acrylamide and bisacrylamide. Data are means ± SEM (n = 7–8 measurements, 2 gels per group). $^{***}P < 0.001$, ns (not significant), (Tukey's test) compared to 5% acrylamide/0.1% bisacrylamide. **(C)** Intracellular Rho activity of bovine aortic endothelial cells seeded on polyacrylamide gels of similar stiffness. Data for the 5% acrylamide/0.1% bisacrylamide is re-plotted from the 2.5 kPa group of **(A)**. Data are means ± SEM (n = 3 independent experiments, each performed in duplicate). ns, not significant (Student's t test).

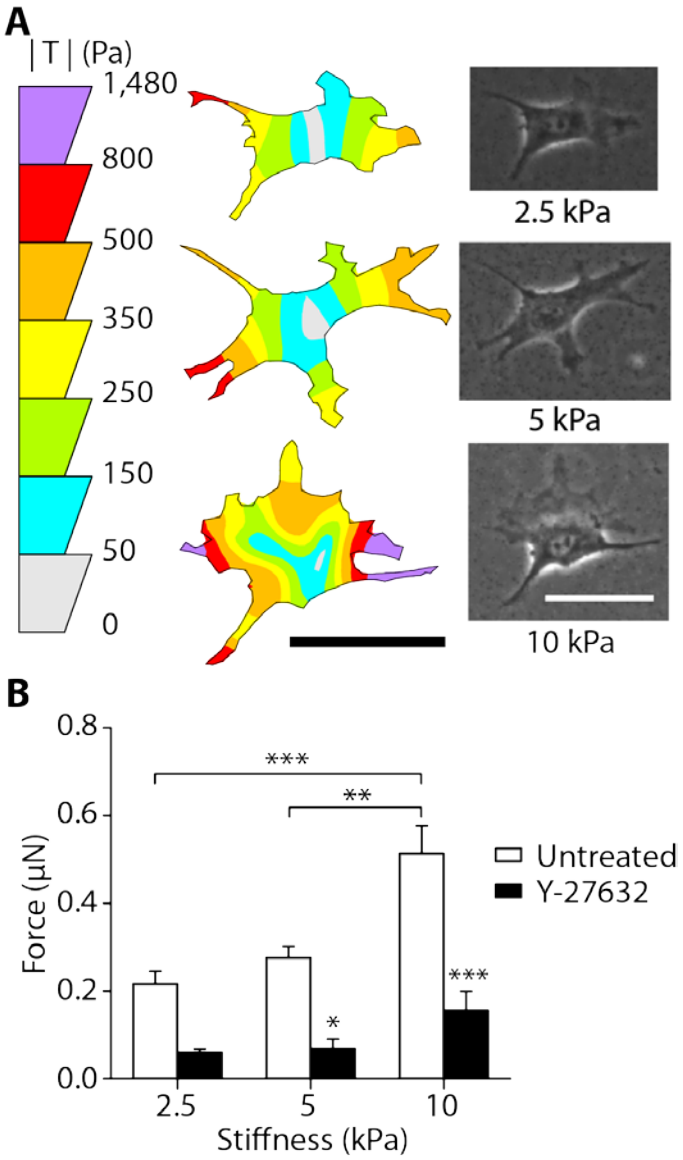

Figure 3.6. Matrix stiffness increases cell contractility, and inhibition of cell contractility restores barrier integrity. **(A)** Representative traction force distribution maps and phase images of BAECs on gels. Scale bars, 50 μm. **(B)** Traction force microscopy measurements of cell contractility with (n = 9–12 cells) or without (n = 19–34 cells) Y-27632 treatment. Data are means ± SEM. *P < 0.05, **P < 0.01, ***P < 0.001 (Tukey's test) compared to respective untreated conditions, unless otherwise indicated by brackets.

To further investigate the role of the Rho pathway in regulating increased cellular contractility and monolayer permeability in response to matrix stiffness, we inhibited ROCK, a downstream target of Rho, using the pharmacological inhibitor Y-27632. When ROCK was inhibited by exposing cells to Y-27632 for 30 min, cellular force decreased to a similar level across all matrices (Fig. 3.6B). Furthermore, endothelial permeability on 5 and 10 kPa substrates decreased to levels found on 2.5 kPa substrates (Fig. 3.1B). Similarly, endothelial permeability decreased with addition of siRNA targeting *ROCK1* (Fig. 3.7). In our mouse model, Y-27632 treatment of old (20 months) mice also decreased the permeability of the thoracic aorta endothelium to Evans blue dye compared to untreated old mice (Fig. 3.4C). These data indicate that age-related stiffness-induced permeability is mediated by increased contractility and that decreasing contractility restores monolayer integrity.

Measurements of cell-cell junction separation width in Y-27632-treated cells demonstrated that decreasing ROCK activity decreases the average cell-cell separation distance to about 2 μm (Fig. 3.2C). Likewise, cell-cell separation decreased significantly in Y-27632-treated old (21 to 24 months) mice compared to untreated old mice (Fig. 3.4C). Y-27632 treatment did not change intimal stiffness (Fig. 3.3D), suggesting that Y-27632 acts intracellularly to inhibit contractility, but does not cause local matrix rearrangement and stiffness changes. Taken together, these data indicate that increased endothelial monolayer permeability in response to matrix stiffness is the result of greater cell contractility, which destabilizes and widens intercellular junctions. Importantly, our data suggest that the adverse effect of age-related matrix stiffening can be reversed in vivo by inhibiting Rho pathway–mediated cell contractility.

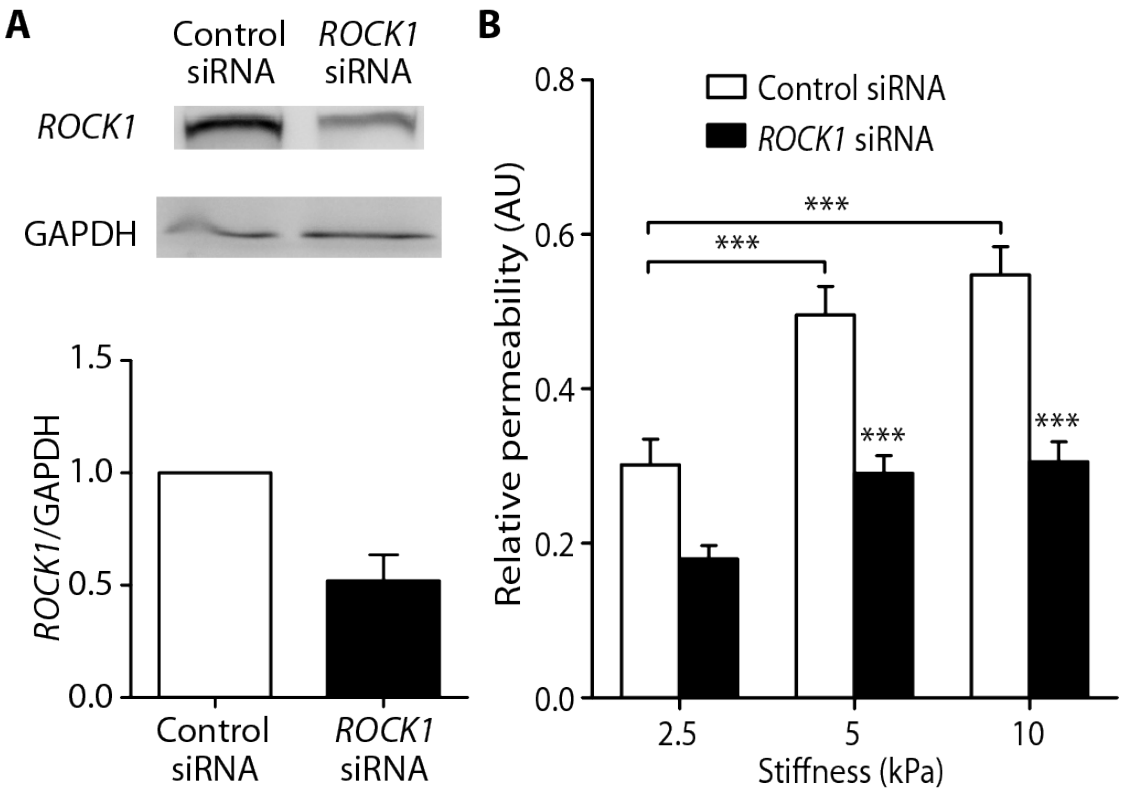

Figure 3.7. RNAi of *ROCK1* decreases stiffness-induced endothelial permeability. **(A)** (Top) Western blot analysis and (bottom) densitometry quantification of RNAi of *ROCK1* (*n* = 2). **(B)** Relative permeability of BAECs cultured on gels of varying stiffnesses with (*n* = 13–15 gels) or without (*n* = 13 gels) siRNA knockdown of *ROCK1*. Data are means ± SEM. **P* < 0.05, ***P* < 0.01, ****P* < 0.001 (Tukey's test) compared to respective control siRNA, unless otherwise indicated by brackets.

3.4.4 Increased matrix stiffness promotes leukocyte transmigration

Because VE-cadherin rearrangement and monolayer permeability are known to regulate leukocyte transmigration into the vessel wall (Alcaide et al., 2008; Turowski et al., 2008), we asked whether stiffer substrates and the subsequent widening of junctions promote increased transmigration of leukocytes, a crucial step in the formation of atherosclerotic plaques. Primary human leukocytes were seeded on top of TNF-α–stimulated endothelial cells that were first seeded on polyacrylamide matrices. Leukocytes that had transmigrated were defined as those in which at least 50% of their cell body appeared beneath the endothelial monolayer (Fig. 3.8A). Notably, the number of transmigrated leukocytes increased as a function of matrix stiffness (Fig. 3.8B), and Y-27632 treatment of endothelial monolayers decreased transmigration (Fig. 3.8B), which suggests that decreased cell-cell separation inhibits leukocyte transmigration. Of the cells that transmigrated, between 87 and 98% migrated through the monolayer at cell-cell junctions (Fig. 3.8C), indicating that paracellular transmigration dominated over transcellular transmigration.

To determine if increased transmigration may also be due to differential expression of endothelial inflammatory molecules associated with leukocyte adhesion and transmigration, we also investigated the number of captured leukocytes under shear (to mimic blood flow) and the relative expression levels of intercellular adhesion molecule-1 (ICAM-1), vascular cell adhesion molecule-1 (VCAM-1), and E-selectin—three endothelial cell inflammatory markers responsible for mediating leukocyte adhesion to the endothelium. Our data revealed no differences in leukocyte attachment to TNF-α–stimulated endothelial cells as a function of matrix stiffness (Fig. 3.9). Additionally, the expression levels of ICAM-1 (Fig. 3.10A), VCAM-1 (Fig. 3.10B), and E-selectin (Fig. 3.10C) in TNF-α-treated endothelial cells did not change

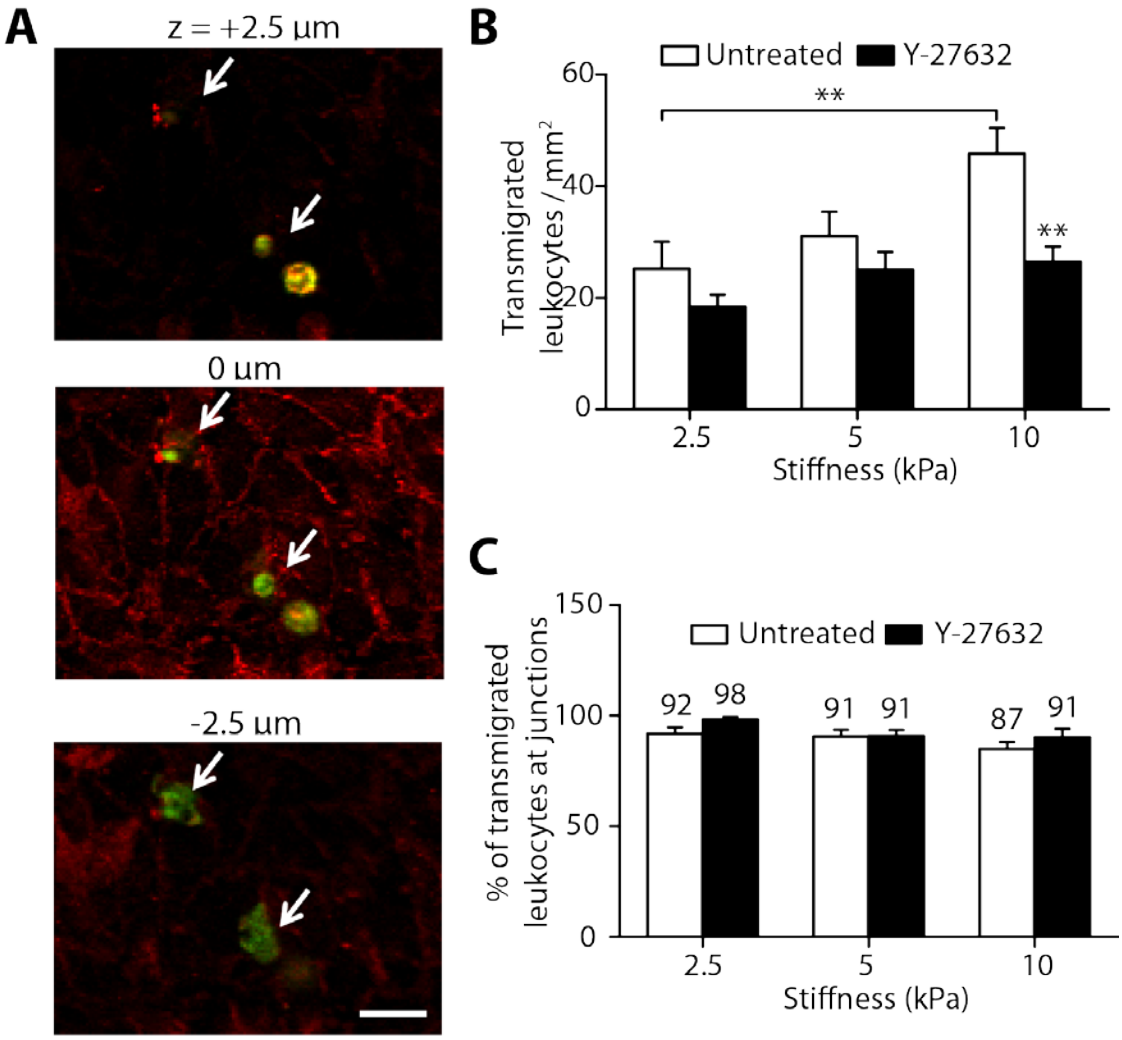
A
z = +2.5 µm
0 µm
-2.5 µm
B
Untreated
Y-27632
**
**
Transmigrated leukocytes / mm²
60
40
20
0
2.5
5
10
Stiffness (kPa)
C
Untreated
Y-27632
% of transmigrated leukocytes at junctions
150
100
50
0
92
98
91
91
87
91
2.5
5
10
Stiffness (kPa)

Figure 3.8. Matrix stiffness enhances leukocyte transmigration. **(A)** Representative fluorescent images of leukocytes (green) transmigrating through an endothelial monolayer (VE-cadherin, red). Experiments performed in collaboration with Kuldeep Rana and Mike King. Images were taken at focal planes above the monolayer (+2.5 µm), at the monolayer (0 µm), and below the monolayer (–2.5 µm). Arrows indicate transmigrated cells. Scale bar, 20 µm. **(B)** Histogram showing the effect of matrix stiffness on the number of transmigrated leukocytes. Endothelial cells were either untreated (n = 19 fields of view, three independent experiments) or pre-treated with Y-27632 (n = 17–18 fields of view). Data are means ± SEM. $^{**}P < 0.01$ (Tukey's test) compared to respective untreated condition, unless otherwise indicated by brackets. **(C)** Percentage of leukocytes that transmigrated through intercellular junctions. Numbers above bars indicate the nominal values. Data are means ± SEM.

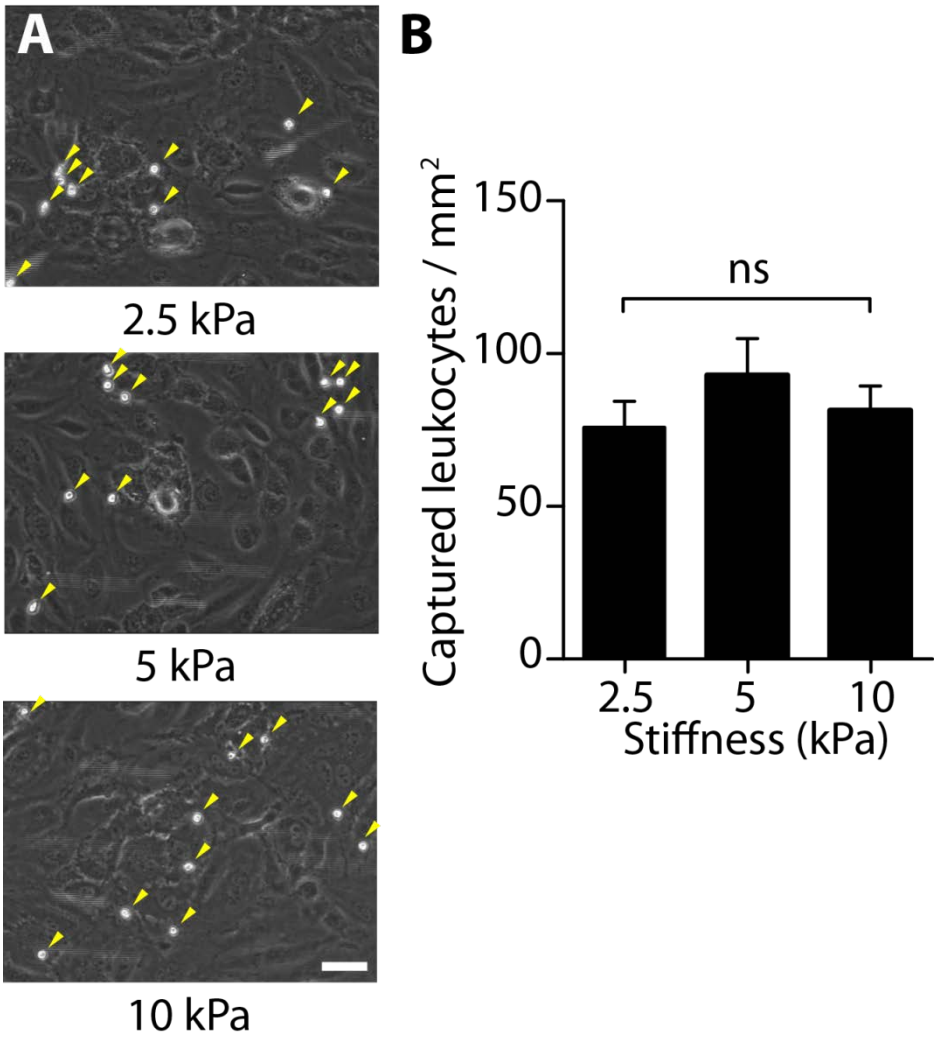

Figure 3.9. Leukocytes captured on HUVEC monolayers on polyacrylamide gels under flow. **(A)** Representative micrographs of captured leukocytes. Yellow arrowheads indicate attached leukocytes. Leukocytes were rolled for 7 min in a parallel-plate flow chamber at 2 dyn/cm^2. Scale bar, 50 µm. **(B)** The effect of substrate stiffness on the number of captured leukocytes. Data are means ± SEM (*n* = 79 to 96 fields of view per stiffness). ns, not significant (Tukey's test). Experiments performed in collaboration with Kuldeep Rana and Mike King.

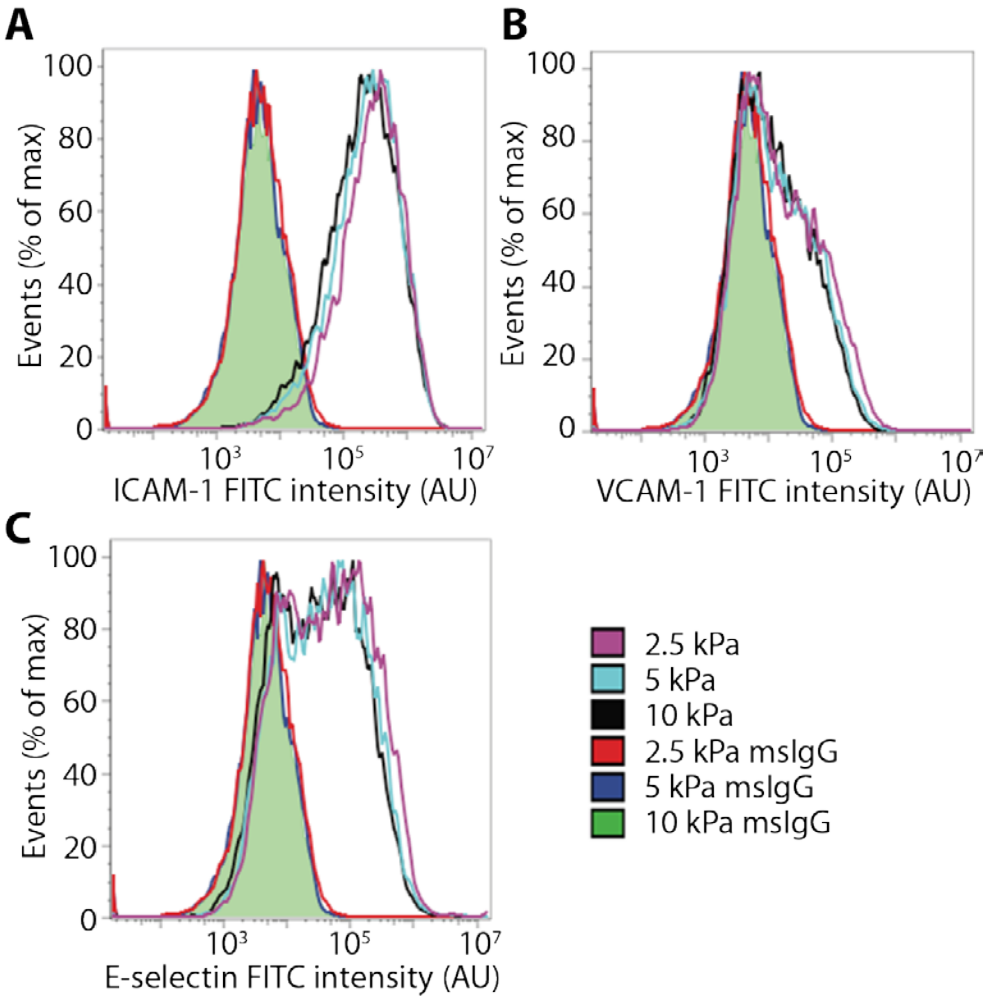

Figure 3.10. Flow cytometry analysis of HUVEC expression of **(A)** ICAM-1, **(B)** VCAM-1, and **(C)** E-selectin on gels after a 6-h treatment with TNF-α. Shaded green curves represent overlapping mouse IgG isotype controls (msIgG) for each of the three matrices. Three independent experiments were performed. No statistically significant differences (Tukey's test) were found between the three stiffnesses for all three adhesion molecules. Experiments performed in collaboration with Christine Montague.

as a function of matrix stiffness. Mouse IgG isotype controls were used to ensure non-specific binding of antibodies was not different between stiffnesses. These results suggest that the increase in transmigration on stiffer matrices is probably not from a differential upregulation of inflammatory molecules associated with leukocyte attachment, but rather an increase in cell-cell junction separation, which promotes transmigration.

3.5 Discussion

Vessel stiffening accompanies the progression of both aging and atherosclerosis and is used to predict risk of cardiovascular diseases (Mattace-Raso et al., 2006; Sutton-Tyrrell et al., 2005); yet, the relationship between age-related changes in ECM mechanical properties that result in blood vessel stiffening and endothelial cell permeability is relatively unknown. In the present study, we demonstrate that increased vessel stiffness promotes disruption of endothelial barrier integrity, a hallmark of atherogenesis. Moreover, we demonstrate that by inhibiting endothelial cellular contractility via the Rho/ROCK pathway, we can prevent increased permeability with age. Because increased permeability of the endothelium permits cholesterol uptake in the vessel wall (Lusis, 2000), these results demonstrate one possible therapeutic approach to preventing cholesterol accumulation within the vessel wall is to inhibit increased endothelial cell contractility.

Recently, others have also shown that endothelial cell contractile pathways modulate permeability (Krishnan et al., 2011) and leukocyte transmigration (Stroka and Aranda-Espinoza, 2011; Sun et al., 2011). Krishnan *et al.* (Krishnan et al., 2011) showed that human umbilical vein endothelial cells (HUVECs) generated strong traction forces on stiff substrates (11 kPa) and formed intercellular gaps when treated

with permeability-inducing agent thrombin; whereas cells on more compliant substrates (1.2 kPa) were less contractile and did not form gaps in response to thrombin. Sun *et al*. (Sun et al., 2011) showed that non-muscle myosin light-chain kinase deficiency, which reduces endothelial contractility, attenuates endothelial permeability and monocyte transmigration in an atherosclerotic mouse model. Importantly, we reversed the negative effects of matrix stiffening in both our mouse and in in vitro models by pharmacologically inhibiting Rho-dependent cell contraction (Fig. 3.6B). In addition to matrix stiffening, ROCK inhibition has also been shown to inhibit the negative effects of barrier-disruptive agonists that increase cell contractility, such as thrombin (van Nieuw Amerongen et al., 2000) and TNF-α (Nwariaku et al., 2003). These data collectively indicate that inhibiting increased endothelial cell contractility may inhibit the progression of atherosclerosis.

To assess cardiovascular risk clinically, non-invasive techniques, such as pulse wave velocity tests, have been implemented to indirectly measure patient arterial stiffness (Blacher et al., 1999). Because stiffness is known to correlate with the risk of cardiovascular disease, there is now substantial interest in the discovery or design of therapeutics that target vessel stiffening to prevent and treat cardiovascular disease. Thus far, several drugs have been identified, including angiotensin-converting enzyme inhibitors and calcium channel blockers (Oliver and Webb, 2003). However, their mechanisms of action within the endothelium are poorly understood and often confounded owing to their actions on other aspects of the cardiovascular system, like blood pressure and heart rate (Hope and Hughes, 2007). More recently, alagebrium, a drug that disrupts advanced glycation end-product (AGE) crosslinks that stiffen vessel walls, has shown mild success in treating patients with chronic (Willemsen et al., 2010) or diastolic heart failure (Little et al., 2005) and improving endothelial flow-

mediated dilation in patients with systolic hypertension (Zieman et al., 2007). Therefore, there is evidence clinically that decreasing vessel stiffness can improve patient health.

Here, we present another approach to mitigate the deleterious effects of vessel stiffening on cardiovascular health. Rather than exclusively targeting vessel stiffness, we propose that also targeting the endothelial cells' response to vessel stiffening may also prevent or slow atherogenesis. In some cases, directly targeting the stiffening within vessel walls is beneficial because decreasing vessel stiffness decreases the load on the heart and can decrease risk of heart failure. However, in the case of atherosclerosis, a therapy which also targets the endothelium may have certain advantages over using "de-stiffening" agents alone. ROCK inhibitors, as were used here, work quickly through intracellular signaling pathways rather than on the matrix within the vessel wall, which may require long-term treatment before significant changes occur. Because decreasing cellular contractility decreases permeability, which is one of the first steps in atherogenesis, ROCK-inhibition therapy may be more suitable for patients who are at-risk or in the very early stages of arteriosclerosis. In those patients with advanced atherosclerosis, inhibiting endothelial contractility may slow the growth of atherosclerotic lesions by preventing additional cholesterol uptake and inflammatory cell transmigration, but may not directly reduce the size of lesions that are already present. Therefore, ROCK-inhibition therapy will likely be best used as a preventative treatment for atherosclerosis and should be used in conjunction with additional therapies for the treatment of other cardiovascular complications, like heart failure, that are also due in part to vessel stiffening.

Currently, fasudil is the only ROCK inhibitor approved for clinical use (Dong et al., 2010). Originally used to treat cerebral vasospasm, fasudil has shown promise in treating a variety of cardiovascular diseases, including pulmonary hypertension (Fukumoto et al., 2005), atherosclerosis (Nohria et al., 2006), and aortic stiffness (Noma et al., 2007). Ongoing phase II clinical trials using fasudil are being performed to understand the relationship between Rho-dependent cell signaling and carotid atherosclerosis (ClinicalTrials.gov Identifier: NCT00670202). There is also some evidence that statins, which include the widely marketed Crestor and Lipitor brands, decrease Rho/ROCK activity through pleiotropic effects (Dong et al., 2010). As such, statins, in addition to their known ability to lower cholesterol levels in the blood, may also be effective in lowering cholesterol accumulation in the vessel wall by restoring barrier integrity. Overall, our data indicate that pharmacological ROCK inhibition may prevent atherosclerosis progression by preventing increased endothelial monolayer permeability and leukocyte transmigration due to vessel wall stiffening.

3.6 References

Alcaide P, Newton G, Auerbach S, Sehrawat S, Mayadas TN, Golan DE, Yacono P, Vincent P, Kowalczyk A, Luscinskas FW. 2008. p120-Catenin regulates leukocyte transmigration through an effect on VE-cadherin phosphorylation. *Blood* **112**:2770–2779.

Armstrong JK, Wenby RB, Meiselman HJ, Fisher TC. 2004. The hydrodynamic radii of macromolecules and their effect on red blood cell aggregation. *Biophysical Journal* **87**:4259–70.

Basha M, Chang S, Smolock EM, Moreland RS, Wein AJ, Chacko S. 2006. Regional differences in myosin heavy chain isoform expression and maximal shortening

velocity of the rat vaginal wall smooth muscle. *American Journal of Physiology. Regulatory, Integrative and Comparative Physiology* **291**:R1076–84.

Birukova AA, Arce FT, Moldobaeva N, Dudek SM, Garcia JGN, Lal R, Birukov KG. 2009. Endothelial permeability is controlled by spatially defined cytoskeletal mechanics: atomic force microscopy force mapping of pulmonary endothelial monolayer. *Nanomedicine* **5**:30–41.

Blacher J, Asmar R, Djane S, London GM, Safar ME. 1999. Aortic pulse wave velocity as a marker of cardiovascular risk in hypertensive patients. *Hypertension* **33**:1111–7.

Butt H-J, Jaschke M. 1995. Calculation of thermal noise in atomic force microscopy. *Nanotechnology* **6**:1–7.

Califano JP, Reinhart-King CA. 2008. A balance of substrate mechanics and matrix chemistry regulates endothelial cell network assembly. *Cellular and Molecular Bioengineering* **1**:122–132.

Cooper JA, Del Vecchio PJ, Minnear FL, Burhop KE, Selig WM, Garcia JG, Malik a B. 1987. Measurement of albumin permeability across endothelial monolayers in vitro. *Journal of Applied Physiology* **62**:1076–83.

Crick SL, Yin FCP. 2007. Assessing micromechanical properties of cells with atomic force microscopy: importance of the contact point. *Biomechanics and Modeling in Mechanobiology* **6**:199–210.

Dejana E, Orsenigo F, Lampugnani MG. 2008. The role of adherens junctions and VE-cadherin in the control of vascular permeability. *Journal of Cell Science* **121**:2115–22.

Dejana E, Tournier-Lasserve E, Weinstein BM. 2009. The control of vascular integrity by endothelial cell junctions: molecular basis and pathological implications. *Developmental Cell* **16**:209–21.

Dembo M, Wang YL. 1999. Stresses at the cell-to-substrate interface during locomotion of fibroblasts. *Biophysical Journal* **76**:2307–16.

Discher DE, Janmey P, Wang YL. 2005. Tissue cells feel and respond to the stiffness of their substrate. *Science* **310**:1139–43.

Dong M, Yan BP, Liao JK, Lam YY, Yip GWK, Yu CM. 2010. Rho-kinase inhibition: a novel therapeutic target for the treatment of cardiovascular diseases. *Drug Discovery Today* **15**:622–9.

Engler AJ, Rehfeldt F, Sen S, Discher DE. 2007. Microtissue elasticity: measurements by atomic force microscopy and its influence on cell differentiation. *Methods in Cell Biology* **83**:521–45.

Engler AJ, Sen S, Sweeney HL, Discher DE. 2006. Matrix elasticity directs stem cell lineage specification. *Cell* **126**:677–89.

Engler AJ, Richert L, Wong JY, Picart C, Discher DE. 2004. Surface probe measurements of the elasticity of sectioned tissue, thin gels and polyelectrolyte multilayer films: Correlations between substrate stiffness and cell adhesion. *Surface Science* **570**:142–154.

Fernandes VRS, Polak JF, Cheng S, Rosen BD, Carvalho B, Nasir K, McClelland R, Hundley G, Pearson G, O'Leary DH, Bluemke DA, Lima JAC. 2008. Arterial stiffness is associated with regional ventricular systolic and diastolic dysfunction: the Multi-Ethnic Study of Atherosclerosis. *Arteriosclerosis, Thrombosis, and Vascular Biology* **28**:194–201.

Fukumoto Y, Matoba T, Ito A, Tanaka H, Kishi T, Hayashidani S, Abe K, Takeshita A, Shimokawa H. 2005. Acute vasodilator effects of a Rho-kinase inhibitor, fasudil, in patients with severe pulmonary hypertension. *Heart* **91**:391–2.

Gow BS, Castle WD, Legg MJ. 1983. An improved microindentation technique to measure changes in properties of arterial intima during atherogenesis. *Journal of Biomechanics* **16**:451–8.

Greenwald SE. 2007. Ageing of the conduit arteries. *The Journal of Pathology* **211**:157–72.

Hope SA, Hughes AD. 2007. Drug effects on the mechanical properties of large arteries in humans. *Clinical and Experimental Pharmacology & Physiology* **34**:688–93.

Huang S, Ingber DE. 2005. Cell tension, matrix mechanics, and cancer development. *Cancer Cell* **8**:175–6.

Huo Y, Guo X, Kassab GS. 2008. The flow field along the entire length of mouse aorta and primary branches. *Annals of Biomedical Engineering* **36**:685–99.

Hutter JL. 2005. Comment on tilt of atomic force microscope cantilevers: effect on spring constant and adhesion measurements. *Langmuir* **21**:2630–2.

Hutter JL, Bechhoefer J. 1993. Calibration of atomic-force microscope tips. *Review of Scientific Instruments* **64**:1868.

Huynh J, Nishimura N, Rana K, Peloquin JM, Califano JP, Montague CR, King MR, Schaffer CB, Reinhart-King CA. 2011. Age-related intimal stiffening enhances endothelial permeability and leukocyte transmigration. *Science Translational Medicine* **3**:112ra122–112ra122.

Krishnan R, Klumpers DD, Park CY, Rajendran K, Trepat X, van Bezu J, van Hinsbergh VWM, Carman CV, Brain JD, Fredberg JJ, Butler JP, van Nieuw Amerongen GP. 2011. Substrate stiffening promotes endothelial monolayer disruption through enhanced physical forces. *American Journal of Physiology. Cell Physiology* **300**:C146–54.

Laurent S, Boutouyrie P. 2007. Recent advances in arterial stiffness and wave reflection in human hypertension. *Hypertension* **49**:1202–6.

Lee K, Forudi F, Saidel GM, Penn MS. 2005. Alterations in internal elastic lamina permeability as a function of age and anatomical site precede lesion development in apolipoprotein E-null mice. *Circulation Research* **97**:450–6.

Lemarié CA, Tharaux PL, Lehoux S. 2010. Extracellular matrix alterations in hypertensive vascular remodeling. *Journal of Molecular and Cellular Cardiology* **48**:433–9.

Li Y, Hu Z, Li C. 1993. New method for measuring poisson's ratio in polymer gels. *Journal of Applied Polymer Science* **50**:1107–1111.

Little WC, Zile MR, Kitzman DW, Hundley WG, O'Brien TX, Degroof RC. 2005. The effect of alagebrium chloride (ALT-711), a novel glucose cross-link breaker, in the treatment of elderly patients with diastolic heart failure. *Journal of Cardiac Failure* **11**:191–5.

Lo CM, Wang HB, Dembo M, Wang YL. 2000. Cell movement is guided by the rigidity of the substrate. *Biophysical Journal* **79**:144–52.

Lusis AJ. 2000. Atherosclerosis. *Nature* **407**:233–41.

Mattace-Raso FUS, van der Cammen TJM, Hofman A, van Popele NM, Bos ML, Schalekamp MADH, Asmar R, Reneman RS, Hoeks APG, Breteler MMB, Witteman JCM. 2006. Arterial stiffness and risk of coronary heart disease and stroke: the Rotterdam Study. *Circulation* **113**:657–63.

McEniery CM, Yasmin, Hall IR, Qasem A, Wilkinson IB, Cockcroft JR. 2005. Normal vascular aging: differential effects on wave reflection and aortic pulse wave velocity: the Anglo-Cardiff Collaborative Trial (ACCT). *Journal of the American College of Cardiology* **46**:1753–60.

Mehta D, Malik AB. 2006. Signaling mechanisms regulating endothelial permeability. *Physiological Reviews* **86**:279–367.

Mogensen CE. 1984. Microalbuminuria predicts clinical proteinuria and early mortality in maturity-onset diabetes. *The New England Journal of Medicine* **310**:356–60.

van Nieuw Amerongen GP, Beckers CML, Achekar ID, Zeeman S, Musters RJP, van Hinsbergh VWM. 2007. Involvement of Rho kinase in endothelial barrier maintenance. *Arteriosclerosis, Thrombosis, and Vascular Biology* **27**:2332–9.

van Nieuw Amerongen GP, van Delft S, Vermeer MA, Collard JG, van Hinsbergh VW. 2000. Activation of RhoA by thrombin in endothelial hyperpermeability: role of Rho kinase and protein tyrosine kinases. *Circulation Research* **87**:335–40.

Nohria A, Grunert ME, Rikitake Y, Noma K, Prsic A, Ganz P, Liao JK, Creager MA. 2006. Rho kinase inhibition improves endothelial function in human subjects with coronary artery disease. *Circulation Research* **99**:1426–32.

Noma K, Goto C, Nishioka K, Jitsuiki D, Umemura T, Ueda K, Kimura M, Nakagawa K, Oshima T, Chayama K, Yoshizumi M, Liao JK, Higashi Y. 2007. Roles of rho-associated kinase and oxidative stress in the pathogenesis of aortic stiffness. *Journal of the American College of Cardiology* **49**:698–705.

Nwariaku FE, Rothenbach P, Liu Z, Zhu X, Turnage RH, Terada LS. 2003. Rho inhibition decreases TNF-induced endothelial MAPK activation and monolayer permeability. *Journal of Applied Physiology* **95**:1889–95.

Oliver JJ, Webb DJ. 2003. Noninvasive assessment of arterial stiffness and risk of atherosclerotic events. *Arteriosclerosis, Thrombosis, and Vascular Biology* **23**:554–66.

Paszek MJ, Zahir N, Johnson KR, Lakins JN, Rozenberg GI, Gefen A, Reinhart-King CA, Margulies SS, Dembo M, Boettiger D, Hammer DA, Weaver VM. 2005. Tensional homeostasis and the malignant phenotype. *Cancer Cell* **8**:241–54.

Pedrinelli R, Penno G, Dell'Omo G, Bandinelli S, Giorgi D, Di Bello V, Nannipieri M, Navalesi R, Mariani M. 1998. Transvascular and urinary leakage of albumin in atherosclerotic and hypertensive men. *Hypertension* **32**:318–23.

Pelham RJ, Wang YL. 1997. Cell locomotion and focal adhesions are regulated by substrate flexibility. *Proceedings of the National Academy of Sciences U S A* **94**:13661–5.

Peloquin J, Huynh J, Williams RM, Reinhart-King CA. 2011. Indentation measurements of the subendothelial matrix in bovine carotid arteries. *Journal of Biomechanics* **44**:815–21.

Peyton SR, Putnam AJ. 2005. Extracellular matrix rigidity governs smooth muscle cell motility in a biphasic fashion. *Journal of Cellular Physiology* **204**:198–209.

Reinhart-King CA, Dembo M, Hammer DA. 2005. The dynamics and mechanics of endothelial cell spreading. *Biophysical Journal* **89**:676–89.

Reinhart-King CA. 2008. Endothelial cell adhesion and migration. *Methods in Enzymology* **443**:45–64.

Reinhart-King CA, Dembo M, Hammer DA. 2008. Cell-cell mechanical communication through compliant substrates. *Biophysical Journal* **95**:6044–51.

Reinhart-King CA, Dembo M, Hammer DA. 2003. Endothelial cell traction forces on RGD-derivatized polyacrylamide Substrata. *Langmuir* **19**:1573–1579.

Ross R. 1999. Atherosclerosis--an inflammatory disease. *The New England Journal of Medicine* **340**:115–26.

Rozenberg I, Sluka SHM, Rohrer L, Hofmann J, Becher B, Akhmedov A, Soliz J, Mocharla P, Borén J, Johansen P, Steffel J, Watanabe T, Lüscher TF, Tanner FC.

2010. Histamine H1 receptor promotes atherosclerotic lesion formation by increasing vascular permeability for low-density lipoproteins. *Arteriosclerosis, Thrombosis, and Vascular Biology* **30**:923–30.

Schaar JA, de Korte CL, Mastik F, van der Steen AFW. 2002. Effect of temperature increase and freezing on intravascular elastography. *Ultrasonics* **40**:879–81.

Shyy JYJ. 2002. Role of integrins in endothelial mechanosensing of shear stress. *Circulation Research* **91**:769–775.

Smolock EM, Trappanese DM, Chang S, Wang T, Titchenell P, Moreland RS. 2009. siRNA-mediated knockdown of h-caldesmon in vascular smooth muscle. *American Journal of Physiology. Heart and Circulatory Physiology* **297**:H1930–9.

Stroka KM, Aranda-Espinoza H. 2011. Endothelial cell substrate stiffness influences neutrophil transmigration via myosin light chain kinase-dependent cell contraction. *Blood* **118**:1632–40.

Sun C, Wu MH, Yuan SY. 2011. Nonmuscle myosin light-chain kinase deficiency attenuates atherosclerosis in apolipoprotein E-deficient mice via reduced endothelial barrier dysfunction and monocyte migration. *Circulation* **124**:48–57.

Sutton-Tyrrell K, Najjar SS, Boudreau RM, Venkitachalam L, Kupelian V, Simonsick EM, Havlik R, Lakatta EG, Spurgeon H, Kritchevsky S, Pahor M, Bauer D, Newman A. 2005. Elevated aortic pulse wave velocity, a marker of arterial stiffness, predicts cardiovascular events in well-functioning older adults. *Circulation* **111**:3384–90.

Turowski P, Martinelli R, Crawford R, Wateridge D, Papageorgiou AP, Lampugnani MG, Gamp AC, Vestweber D, Adamson P, Dejana E, Greenwood J. 2008. Phosphorylation of vascular endothelial cadherin controls lymphocyte emigration. *Journal of Cell Science* **121**:29–37.

Willemsen S, Hartog JWL, Hummel YM, Posma JL, van Wijk LM, van Veldhuisen DJ, Voors AA. 2010. Effects of alagebrium, an advanced glycation end-product breaker, in patients with chronic heart failure: study design and baseline characteristics of the BENEFICIAL trial. *European Journal of Heart Failure* **12**:294–300.

Zaman MH, Trapani LM, Sieminski AL, Siemeski A, Mackellar D, Gong H, Kamm RD, Wells A, Lauffenburger DA, Matsudaira P. 2006. Migration of tumor cells in 3D matrices is governed by matrix stiffness along with cell-matrix adhesion and proteolysis. *Proceedings of the National Academy of Sciences U S A* **103**:10889–94.

Zieman SJ, Melenovsky V, Clattenburg L, Corretti MC, Capriotti A, Gerstenblith G, Kass DA. 2007. Advanced glycation endproduct crosslink breaker (alagebrium) improves endothelial function in patients with isolated systolic hypertension. *Journal of Hypertension* **25**:577–83.

Zieman SJ, Melenovsky V, Kass DA. 2005. Mechanisms, pathophysiology, and therapy of arterial stiffness. *Arteriosclerosis, Thrombosis, and Vascular Biology* **25**:932–43.

CHAPTER 4

SUBSTRATE STIFFNESS PROMOTES CIRCULAR DORSAL RUFFLE FORMATION IN VASCULAR SMOOTH MUSCLE CELLS

4.1 Abstract

As atherosclerosis progresses, vascular smooth muscle cells (VSMCs) invade from the medial layer into the intimal layer and proliferate, contributing to atherosclerotic plaque formation. This migration is stimulated in part by platelet-derived growth factor (PDGF) released by endothelial cells or inflammatory cells trapped in the vessel microenvironment, and also vessel stiffening, which occurs with age and atherosclerosis progression. PDGF induces the formation of circular dorsal ruffles (CDRs), actin-based structured associated with increased cell motility. Here we show that mechanical changes in vessel stiffness enhance the formation of CDRs in VSMCs in response to PDGF stimulation. Our data indicate that matrix stiffness increases cellular contractility, and that intracellular pre-stress is necessary for robust CDR formation. When treated with agonists that promote contractility, cells increase CDR formation, whereas agonists that inhibit contractility lead to decreased CDR formation. Substrate stiffness promotes CDR formation in response to PDGF by upregulating myosin light chain kinase and Src activity. Together, these data indicate that vessel stiffening accompanying atherogenesis may exacerbate VSMC migration by increasing CDR formation in response to PDGF.

4.2 Introduction

During atherosclerosis, the vessel wall stiffens due to excess extracellular matrix (ECM) deposition, matrix crosslinking, and elastin fragmentation (Greenwald, 2007;

Zieman et al., 2007). Vascular smooth muscle cells, which populate the arterial media, convert from a quiescent phenotype to exhibit abnormal ECM deposition and migration into the vascular intima (Beamish et al., 2010; Davis-Dusenbery et al., 2011), leading to fibrotic plaque formation and blood vessel occlusion (Lusis, 2000; Ross, 1999). Matrix stiffness has been shown to modulate VSMC migration (Isenberg et al., 2009; Peyton and Putnam, 2005) and proliferation (Brown et al., 2010; McDaniel et al., 2007), cell behaviors that occur with atherosclerotic plaque generation. Thus, arterial stiffening may be a contributing factor for the progression of atherosclerosis.

Circular dorsal ruffles (CDRs) are thought to play a role in directed vascular smooth muscle migration (Gu et al., 2011; Huang et al., 2011). They are transient actin-based structures that form in VSMCs in response to platelet-derived growth factor (PDGF) signaling. In this signaling cascade, PDGF binding to its receptor results in Src phosphorylation. Phosphorylated Src activates and modulates a number of downstream effector proteins, including F-actin, the Arp2/3 complex, WAVE-1/2, neuronal Wiskott-Aldrich Syndrome protein (N-WASP), and cortactin (Buccione et al., 2004). These proteins act in concert to reorganize actin into CDRs.

It is believed that wide-scale actin cytoskeletal rearrangements induced by CDRs allows cells to become polarized and motile (Ballestrem et al., 1998). Quiescent contractile VSMCs typically exhibit robust stress fibers and cell-matrix attachments that inhibit cell migration. When stimulated with growth factors, actin stress fibers dissasemble and are reorganized into CDRs, leaving a meshwork of disassembled cortical actin to be used for lamellipodia extension and cell migration (Krueger et al., 2003). Additionally, CDRs may also function to release matrix metalloproteinases

(MMPs) which degrade ECM and facilitate cell invasion (Suetsugu et al., 2003).

Because CDRs are actin-based structures and because actin is known to form more robust stress fibers in response to matrix stiffness (Assoian and Klein, 2008; Discher et al., 2005), we hypothesized that CDR formation in VSMCs is modulated by the mechanical properties of the extracellular microenvironment. Our data indicate that substrate stiffness enhances F-actin organization and cellular contractility priming cells for robust PDGF-stimulated CDR formation. Given that CDRs are thought to enable migration, these data indicate that blood vessel stiffening during atherosclerosis may promote intimal hyperplasia and VSMC migration by inducing CDR formation.

4.3 Materials and methods

Cell culture and gel synthesis

A7R5 rat aortic VSMCs obtained from American Type Culture Collection (ATCC) were maintained in Dulbecco's modified Eagle's medium (DMEM) (Invitrogen, Carlsbad, CA) with 10% fetal bovine serum (Invitrogen) and 1% penicillin/streptavidin (Invitrogen). Polyacrylamide (PA) gels were prepared as described previously (Huynh et al., 2011) and coated with 0.002 to 0.2 μg/ml rat tail collagen type I (BD Biosciences, San Jose, CA). Briefly, 22 × 22 mm or 48 × 65 coverslips (VWR International, Radnor, PA) were activated by subsequent washing in 0.1 N sodium hydroxide (VWR), 3-aminopropyltrimethoxysilane (VWR), and 0.5% glutaraldehyde (Sigma-Aldrich, St. Louis, MO). 1, 2.5, 5, 10, and 30 kiloPascal (kPa) gels were polymerized onto activated coverslips according to the ratios 3%:0.1%, 5%:0.1%, 7.5%:0.175%, 7.5%:0.35%, and 12%:0.28% acrylamide:bisacrylamide (Bio-Rad, Hercules, CA), respectively. Cells were seeded onto PA gels and incubated overnight prior to further experimentation.

Drug treatments

To induce circular dorsal ruffle formation, VSMCs were treated with 10 ng/ml platelet-derived growth factor (PDGF-BB) (R&D Systems, Minneapolis, MN) for 5 min. In some studies, cells were pre-treated with 10 nM calyculin A for 5 min (Sigma-Aldrich) or 10 μM ML-7 for 30 min (Sigma-Aldrich).

Immunofluorescent staining

A7R5s on PA gels were fixed in 3.7% formaldehyde and subsequently washed in 1% Triton X-100 (Mallinckrodt Baker, Phillipsburg, NJ), 0.2% Tween (Mallinckrodt Baker), and blocked with 3% bovine serum albumin (Sigma-Aldrich). Cells were then immunostained with a 1:200 dilution of mouse monoclonal α-actinin (Sigma-Aldrich) or rabbit polyclonal cortactin primary antibody (Santa Cruz Biotechnology, Santa Cruz, CA). Secondary antibodies were Alexa Fluor 568 donkey anti-mouse or anti-rabbit (Invitrogen). Actin was stained with Alexa Fluor 488 phalloidin (Invitrogen) and nuclei with 4',6-diamidino-2-phenylindole (DAPI) (Sigma-Aldrich). Images were captured on a Zeiss Axio Observer.Z1m microscope with a Hamamatsu ORCA-ER camera.

Western blotting

A7R5 cells cultured on 48 × 65 mm PA gels were lysed with a modified radio-immunoprecipitation assay (RIPA) buffer (150 mM sodium chloride, 50 mM Tris-hydrochloride, 0.5% sodium deoxycholate, 0.1% sodium dodecyl sulfate, 1% Nonidet P40, 25 mM sodium fluoride, 1 mM sodium orthovanadate, 1:500 dilution of protease inhibitor cocktail (Sigma-Aldrich)). Cell lysate was cleared by centrifugation at 14,000 x g and the supernatant was separated by sodium dodecyl sulfate

polyacrylamide gel electrophoresis (SDS-PAGE). After protein transfer onto nitrocellulose, blots were probed using antibodies against phosphorylated myosin light chain at threonine-18 and serine-19 (pMLC) (Cell Signaling Technology, Beverly, MA), total myosin light chain (MLC) (Cell Signaling Technology), phosphorylated Src at Tyr-416 (pSrc) (Cell Signaling Technology), and total Src (Cell Signaling Technology). Anti-rabbit horseradish peroxidase (HRP) conjugated secondary antibodies were obtained from Cell Signaling Technology or Santa Cruz Biotechnology. After incubation in SuperSignal West Pico Chemiluminescent Substrate (Thermo Scientific, Rockford, IL), blots were exposed and imaged using a FujiFilm ImageQuant LAS-4000. Protein densitometry was performed using ImageJ software (v. 1.46, National Institutes of Health, Bethesda, MD)

Traction force microscopy

A7R5 cells were cultured overnight on PA gels embedded with 0.5 μm diameter fluorescent beads (Invitrogen). Individual cells and the stressed fluorescent bead field beneath the cell were imaged. After cell removal with 0.05% trypsin-EDTA (Invitrogen), a second fluorescent image of the unstressed bead field was imaged. Bead displacements were calculated from the stressed and unstressed images and used to compute cellular traction vectors and total magnitudes of force using the LIBTRC analysis library developed by Dr. Micah Dembo (Department of Biomedical Engineering, Boston University).

Statistical analysis

Statistical analyses were performed using JMP 8 (SAS Institute, Cary, NC), GraphPad Prism 5 (GraphPad Software, Inc.), or Excel 2010 (Microsoft, Corporation, Redmond, WA). Parametric one-way or two-way ANOVA with post-hoc Tukey’s honest

significance test were performed where appropriate. P values < 0.05 were considered statistically significant.

Data in Fig. 4.2B were fit to a dose-response curve (Poch and Pancheva, 1995) described by Equation 4.1:

$$Y = E_{min} + \frac{E_{max} - E_{min}}{1 + (\frac{x}{ED_{50}})^h}, \qquad \text{(Eqn. 4.1)}$$

where Y is the response (in this case, percentage of cells exhibiting CDRs), E_{min} is the minimum response, E_{max} is the maximum response, x is the dose (in this case, stiffness), h is the Hill slope, and ED_{50} is the effective dose that elicits a half-maximal response. The values for E_{min}, E_{max}, and h were constrained to stay constant between collagen densities.

4.4 Results

4.4.1 Matrix stiffening, but not increased collagen density, promotes circular dorsal ruffle formation

Using PA gels varying in stiffness from 1 to 30 kPa, we first observed A7R5 VSMCs actin organization with respect to substrate stiffness. With increasing stiffness, VSMCs better organize their actin cytoskeleton into F-actin-rich stress fibers (Fig. 4.1A). On soft substrates (1 and 2.5 kPa gels) cells spread less and do not form many stress fibers; however, on stiff substrates (10 kPa and above) cells are much more well-spread and exhibit robust stress fibers that extend the length of the cell. After inducing circular dorsal ruffle formation in VSMCs with PDGF, cells were fixed and stained for actin and either α-actinin or cortactin, markers of CDRs. The colocalization of these proteins was used to determine the formation of CDRs with respect to matrix

stiffness (Fig. 4.1B). Quantification of the percentage of cells that exhibit CDRs reveals that a larger percentage of cells cultured on stiff substrates formed CDRs compared to those cultured on more compliant substrates (Fig. 4.2A).

Because protein density has been shown to alter VSMC spreading and migration speeds (Peyton and Putnam, 2005), we tested whether the collagen density conjugated to the PA gels affects the formation of CDRs. We modeled the percentage of cells that exhibit CDRs versus substrate stiffness and collagen density as a pharmacokinetic dose-response curve, where stiffness was modeled as the dose. Compared to 0.002 or 0.02 mg/ml collagen, 0.2 mg/ml collagen shifted the stiffness-response curve to the left, indicating that on substrates conjugated with 0.2 mg/ml collagen, a higher percentage of cells formed CDRs on lower stiffness (Fig. 4.2B). Additionally, the effective dose that elicits a half-maximal response, or ED_{50}, decreased from ~12 kPa on 0.002 and 0.02 mg/ml collagen-conjugated gels to ~7 kPa on 0.2 mg/ml collagen-conjugated gels. Together, our data suggest that stiffer substrates and higher collagen densities promote the formation of CDRs.

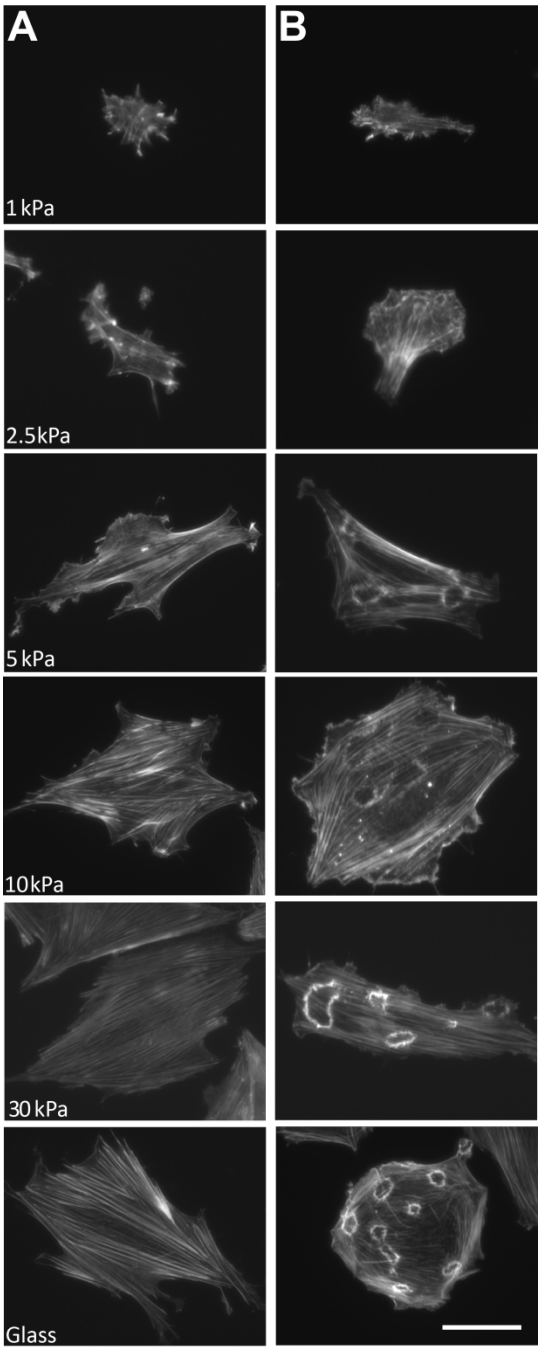

Figure 4.1. Representative images of A7R5 vascular smooth muscle cell actin organization cultured on polyacrylamide gels varying in stiffness from 1 to 30 kPa without **(A)** and with **(B)** 5 min PDGF-induced circular dorsal ruffles. Cells were stained for F-actin using Alexa Fluor 488 phalloidin. Scale bar, 50 μm.

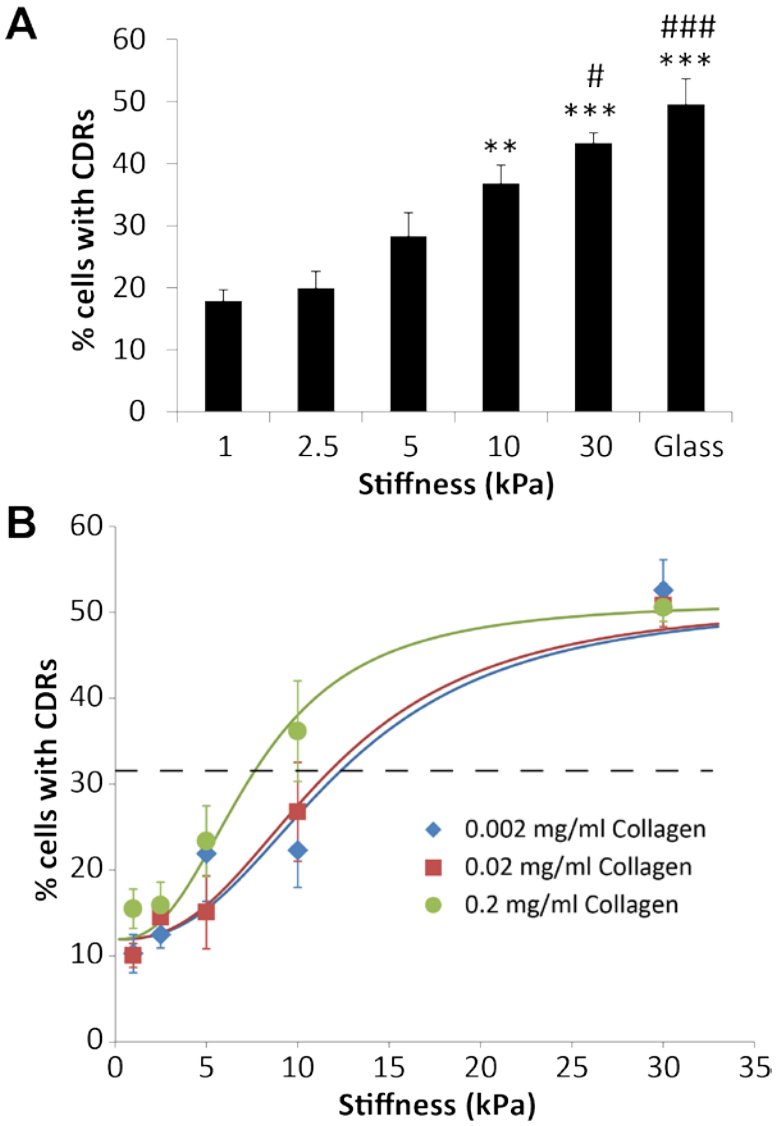

Figure 4.2. Increased substrate stiffness, but not collagen density, promotes circular dorsal ruffle formation. **(A)** The percentage of cells exhibiting PDGF-induced CDR formation on polyacrylamide gels derivatized with 0.2 mg/ml rat tail type I collagen (*n* = 6 independent experiments). Data are means ± SEM. ***P* < 0.01 vs. 1 or 2.5 kPa, ****P* < 0.001 vs. 1 or 2.5 kPa, #*P* < 0.05 vs. 5 kPa, ###*P* < 0.001 vs. 5 kPa (Tukey's test). **(B)** The percentage of cells forming CDRs on gels derivatized with 0.2, 0.02, and 0.002 mg/ml collagen (*n* = 3 independent experiments). The dashed black line represents the half-maximal response. Data are means ± SEM.

4.4.2 Cell force is required for circular dorsal ruffle formation

Recent data indicates that CDRs formation may be related to cell contractility (Zeng et al., 2011), and because our data showed that increased substrate stiffness promotes robust stress fiber formation, we asked whether stress fiber organization resulted in higher cell contraction and whether these forces are required for the formation of CDRs. Traction force microscopy was performed to quantify cell traction forces of VSMCs cultured on 2.5, 5, 10, and 30 kPa substrates (Figure 4.3A). Cells exhibited higher traction forces when cultured on stiffer substrates (Fig. 4.3B).

Our data indicate that cells that generate higher traction forces also exhibit more CDRs. As such, we sought to determine whether force is a prerequisite for CDR formation. To upregulate or downregulate cell force, cells were treated with either calyculin A, an inhibitor of myosin light chain phosphatase, or ML-7, an inhibitor of myosin light chain kinase, respectively. Regardless of stiffness, cells treated with calyculin A increased their traction force generation significantly (Fig. 4.4A, green bars). Cells cultured on stiffer substrates that were treated with ML-7 exhibited lower traction forces compared to their respective untreated controls (Fig. 4.4A, blue bars). Notably, a higher percentage of cells pretreated with calyculin A formed CDRs in response to PDGF treatment compared to cells not treated with contractility-altering drugs. Conversely, significantly fewer cells formed CDRs when pretreated with ML-7, indicating that myosin light chain regulated cell contractility is necessary for robust CDR formation.

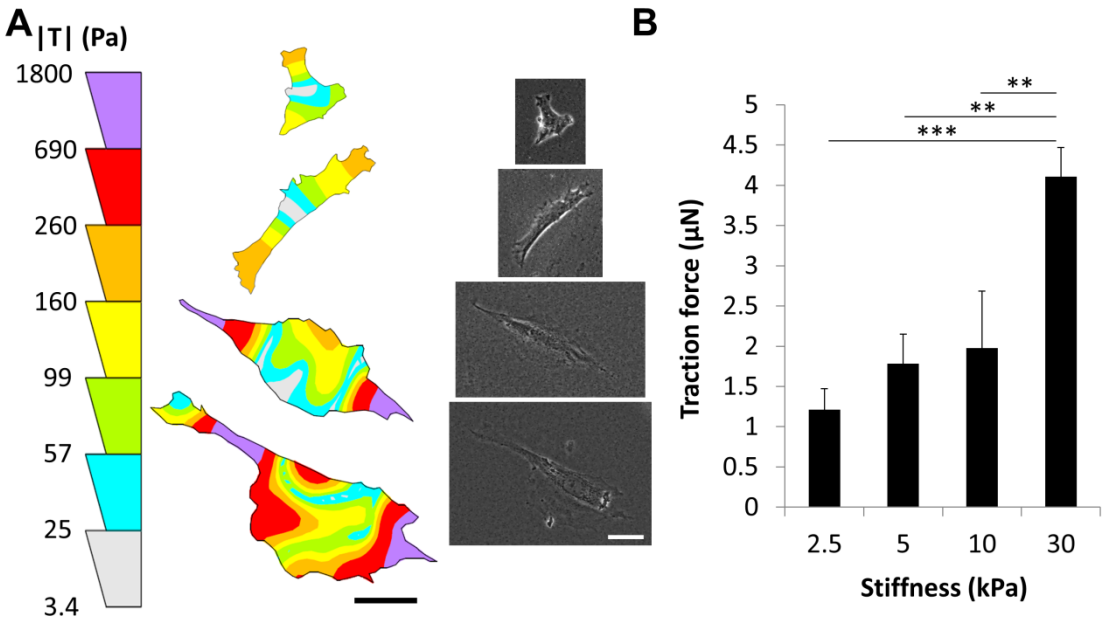

Figure 4.3. Substrate stiffness regulates intracellular pre-stress. **(A)** Representative traction force maps and phase images of A7R5 VSMCs on polyacrylamide gels. Scale bars, 50 μm. **(B)** The total magnitudes of cell traction force measurements with respect to substrate stiffness (n = 12-26 cells, 3 independent experiments). Data are means ± SEM. $^{**}P < 0.01$, $^{***}P < 0.001$ (Tukey's test).

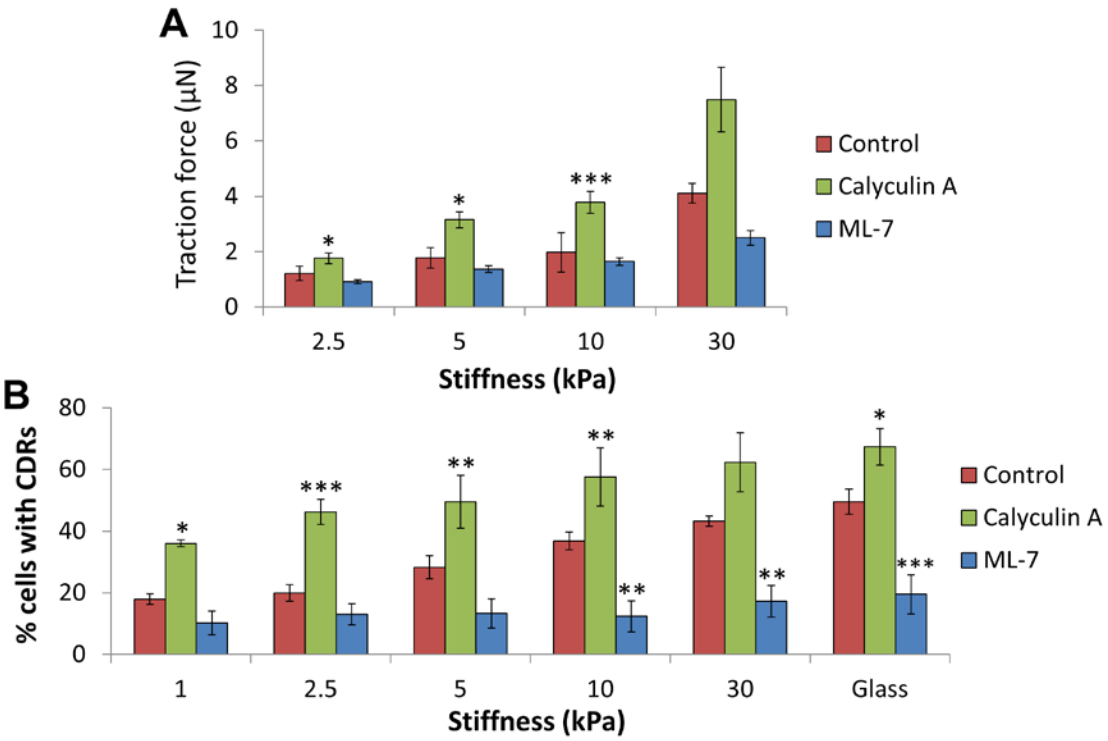

Figure 4.4. Pharmacological control of cell force modulates CDR formation. **(A)** Traction force measurements of untreated (red bars, n = 12-26), calyculin A treated (green bars, n = 46-60), and ML-7 treated (blue bars, n = 37-51) cells. Data are means ± SEM. *P < 0.05 compared to respective untreated controls (Tukey's test). (B) The percentage of cells cultured on gels that exhibit CDRs (n = 3 independent experiments). Data are means ± SEM. *P < 0.05, **P < 0.01, ***P < 0.001 compared to respective untreated controls (Tukey's test).

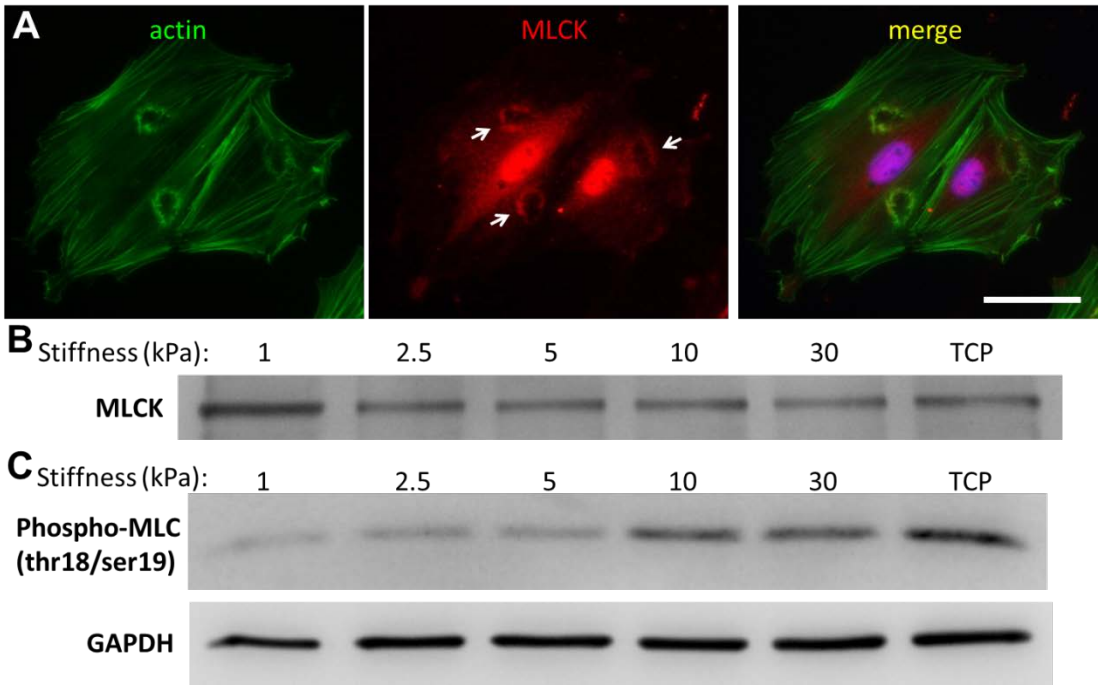

Figure 4.5. Substrate stiffness upregulates MLCK activity to prime cells for robust CDR formation. **(A)** Representative immunofluorescent images of F-actin (green) and MLCK (red). White arrows indicate the localization of MLCK at CDRs. Scale bar, 50 μm. **(B)** Representative immunoblot of Src and MLCK co-immunoprecipitation. **(C)** Representative immunoblots of phosphorylated MLC at residues threonine-18 and serine-19 and GAPDH with respect to substrate stiffness.

4.4.3 Substrate stiffness acts through myosin light chain to prime cells for circular dorsal ruffle formation

It is widely accepted that substrate stiffness regulates cellular contractility, in part, through the myosin light chain (MLC) signaling pathway (Clark et al., 2007). In this pathway, myosin light chain kinase (MLCK) phosphorylates MLC, which enables actin-myosin mediated contraction. Interestingly, MLCK is also known to complex with Src (Barfod et al., 2011), a tyrosine kinase that mediates PDGF-induced CDR formation. Because of its dual role in both the cellular contraction signaling cascade and in complexing with Src, we hypothesized that MLCK modulates PDGF-dependent CDR formation in response to increased substrate stiffness. Immunofluorescent staining indicates that MLCK colocalizes with CDRs (Fig. 4.5A). Additionally, MLCK and Src complex in A7R5 VSMCs, as evidenced by co-immunoprecipitation studies (Fig. 4.5B). However the amount of MLCK that complexes with Src does not change with stiffness. MLCK phosphorylates MLC at residues threonine-18 and serine-19 (Ikebe and Hartshorne, 1985), and as such, we asked whether substrate stiffness induces differential MLC phosphorylation through MLCK activity. Our results indicate that MLC phosphorylation at threonine-18 and serine-19 increases with substrate stiffness (Fig. 4.5C), indicating that MLCK activity is upregulated by stiffness. Together, our data indicate that substrate stiffness regulates cell contractility through modulating MLCK activity, resulting in increased MLC phosphorylation. When treated with PDGF, activated MLCK readily complexes with Src to form more CDRs on stiff substrates.

4.4.4 Substrate stiffness increases PDGF-induced Src activity

It has been shown previously that mechanically-induced Src activation is dependent on substrate stiffness and F-actin integrity (Na et al., 2008). Additionally, others have

found that an intact actin cytoskeleton is required for proper Src activation (Sandilands et al., 2004). Because our data and others have determined that substrate stiffness regulates actin cytoskeletal organization (Fig. 4.1A) (Zeng et al., 2011) and PDGF is known to induce CDR formation through a Src-dependent signaling cascade, we sought to determine whether substrate stiffness may regulate PDGF-induced Src activity. Lysates from PDGF-treated cells cultured on gels of varying stiffness were probed for Src phosphorylation at residue tyrosine 416, a marker for activated Src. Phosphorylation increases with substrate stiffness (Fig. 4.6), suggesting that PDGF-induced Src activation is mediated by substrate stiffness. When Src was inhibited with pharmacological inhibitor PP1, VSMCs were unable to form CDRs regardless of substrate stiffness (data not shown).

4.5 Discussion

The migration of VSMCs from the medial layer into the intima contributes to the formation of plaques in atherosclerosis (Gerthoffer, 2007). This migration is thought to be stimulated by the release of growth factors, particularly PDGF, from endothelial cells (Evanko et al., 1998) or macrophages once they infiltrate into the vessel wall (Raines, 2004; Ross et al., 1990). Vascular stiffening accompanies atherosclerosis and is measured by clinicians to determine cardiovascular risk (Mattace-Raso et al., 2006; Sutton-Tyrrell et al., 2005). Research from our lab and others showed that vascular stiffening may promote endothelial permeability (Huynh et al., 2011; Krishnan et al., 2011) and leukocyte transmigration (Stroka and Aranda-Espinoza, 2011; Sun et al., 2011), hallmarks of atherogenesis. Here, we present data that implicate vascular stiffening to promote the formation of VSMC CDRs, structures believed to play a large role in initiating cell motility.

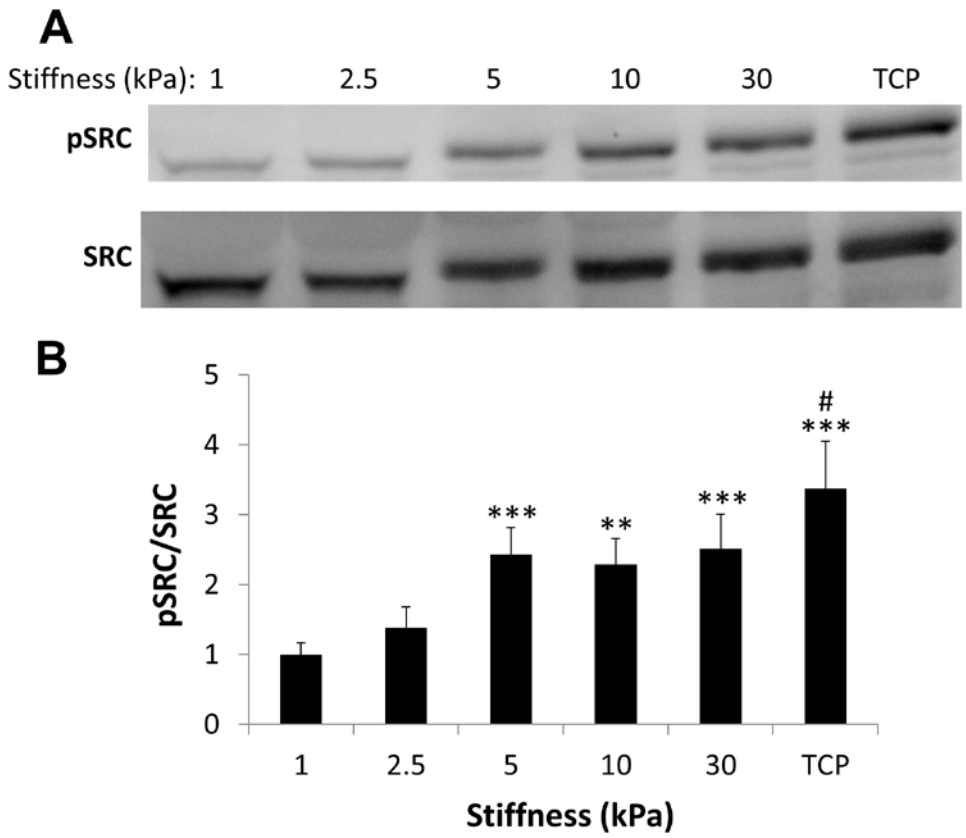

Figure 4.6. Src activity increases with substrate stiffness. **(A)** Representative immunoblots of phosphorylated Src (pSrc) and total Src. **(B)** The ratio of pSrc to total Src in cells cultured on gels of varying stiffness (n = 6 independent experiments). Data are means ± SEM. **P < 0.01 vs. 1 or 2.5 kPa, ***P < 0.001 vs. 1 or 2.5 kPa, #P < 0.05 vs. 5, 10, or 30 kPa (Tukey's test).

Our results indicated that CDR formation in VSMCs is dependent on substrate stiffness and collagen density. On more compliant substrates, cells displayed fewer CDRs compared to cells cultured on stiffer substrates (Fig. 4.2). Moreover, our data indicate that cell contractility is a prerequisite for CDR formation, and upregulation of cell force results in increased CDR formation (Fig. 4.4). Although the total magnitude of cell force increases with substrate stiffness, it remains to be seen whether local forces, particularly at sites of CDR formation, regulate actin dynamics to form CDRs. Substrate stiffness likely promotes the formation of CDRs through upregulation of MLC-dependent cell contractility. Interestingly, substrate stiffness also upregulated Src phosphorylation (Fig. 4.6), and inhibition of Src with PP1 prevented the formation of CDRs (data not shown).

It is widely accepted that, during atherosclerosis progression, VSMCs switch from a quiescent “contractile” phenotype to a migratory “synthetic” phenotype, where they are able to degrade their matrix and invade into the intima (Owens et al., 2004). Previous data suggests that PDGF signaling, which is both a potent migratory signal and initiator of CDRs, is a major contributing factor to the VSMC phenotypic switch (Raines et al., 2000). Our data suggests that the matrix stiffening that occurs concomitant with atherosclerosis progression may exacerbate phenotypic switching by increasing the percentage of cells that exhibit CDR formation in response to PDGF signaling. This is likely due to heightened MLCK activity of cells in stiffer microenvironments, as evidenced by our data showing MLCK colocalization with CDRs and increased MLC phosphorylation at resides threonine-18 and serine-19 (Fig. 4.5). Several upstream activators may also directly contribute to CDR formation, particularly RhoGTPase and Rho-associated kinase (ROCK). RhoGTPase activity, which has been shown to increase with substrate stiffness (Huang and Ingber, 2005;

Huynh et al., 2011), activates ROCK, which also phosphorylates MLC at serine-19 to regulate stress fiber formation (Totsukawa et al., 2000). ROCK also functions to prevent myosin light chain phosphatase from deactivating MLC (Wang et al., 2009). Hence, it is likely that upstream RhoGTPase and ROCK are contributing to the generation of intracellular pre-stress priming cells for strong CDR formation. When treated with Y-27632, a ROCK inhibitor, VSMCs were unable to form robust CDRs (data not shown), similar to our results using ML-7 to inhibit MLCK and consequently CDR formation. Therefore, there is significant evidence that cell contractility is an important regulator of CDR formation.

Previous data suggests that substrate rigidity enhances PDGF receptor phosphorylation intensity and length (Brown et al., 2010). Here we show that downstream of PDGF receptor phosphorylation, Src activity also increases with substrate stiffness (Fig. 4.6), resulting in increased CDR formation. Although the mechanisms behind Src phosphorylation leading to the formation of CDRs are not entirely understood, we and others found that Src localization is necessary for CDR formation (Azimifar et al., 2012). Recent studies by Azimifar and colleagues show that Src phosphorylation in response to growth factor stimulation is not sufficient for fibroblasts to form CDRs but that Src localization to focal adhesions by associating with integrin-linked kinase (ILK) is necessary for CDR formation. Because focal adhesions are also known to be regulated by matrix stiffness, this is consistent with our results where substrate stiffness regulates the activity of the Src-MLCK complex in forming CDRs in VSMCs (Fig. 4.5). It is not surprising then that Src, MLCK, and focal adhesion kinase (FAK) have been found to associate with one another to control adhesion turnover at the leading edge, resulting in lamellapodia protrusions and cell migration (Webb et al., 2004).

In addition to VSMC migration, our data also have implications in cancer, where stiffening of the tumor microenvironment has been shown to promote cancer cell migration and metastasis (Kumar and Weaver, 2009; Paszek et al., 2005; Wolf and Friedl, 2011). Invasive cancer cells form actin-based structures that are similar to CDRs in their protein makeup called invadopodia. Like CDRs, invadopodia are hypothesized to enhance cell migration (Ridley, 2011); however, they play a more significant role in cell invasion by releasing MMPs to degrade their surrounding extracellular matrix (Linder et al., 2011; Poincloux et al., 2009). Because invadopodia formation is also dependent on Src activity (Murphy and Courtneidge, 2011), our data suggests that substrate stiffness may also regulate invadopodia formation. Indeed, recent findings by Alexander and coworkers showed that breast carcinoma cells formed more invadopodia and degraded more of their matrix when cultured on stiffer substrates (Alexander et al., 2008). Although MMP2 has been shown to colocalize with CDRs (Suetsugu et al., 2003), the ability of CDRs to actively promote ECM degradation similarly to invadopodia has not yet been shown. To better understand the matrix degradation capacity of CDRs, it may be necessary to perform these experiments in 3D scaffolds since CDRs form on the dorsal side of cells.

Here we provide evidence that vessel stiffening regulates the formation of CDRs in VSMCs. These structures likely contribute to the migration of VSMCs, possibly by phenotypically switching quiescent “contractile” VSMCs into more migratory “synthetic” cells through wide-scale actin rearrangement. Intracellular pre-stress, which is modulated by matrix stiffness, primes cells for robust CDR formation. Collectively, our data suggests that the changes in vessel stiffness that accompany atherosclerosis enhance CDR formation and therefore contributes to the advancement

of disease.

4.6 References

Alexander NR, Branch KM, Parekh A, Clark ES, Iwueke IC, Guelcher SA, Weaver AM. 2008. Extracellular matrix rigidity promotes invadopodia activity. *Current Biology* **18**:1295–9.

Assoian RK, Klein EA. 2008. Growth control by intracellular tension and extracellular stiffness. *Trends in Cell Biology* **18**:347–52.

Azimifar SB, Böttcher RT, Zanivan S, Grashoff C, Krüger M, Legate KR, Mann M, Fässler R. 2012. Induction of membrane circular dorsal ruffles requires co-signalling of integrin-ILK-complex and EGF receptor. *Journal of Cell Science* **125**:435–48.

Ballestrem C, Wehrle-Haller B, Imhof BA. 1998. Actin dynamics in living mammalian cells. *Journal of Cell Science* **111 (Pt 1**:1649–58.

Barfod ET, Moore AL, Van de Graaf BG, Lidofsky SD. 2011. Myosin light chain kinase and Src control membrane dynamics in volume recovery from cell swelling. *Molecular Biology of the Cell* **22**:634–50.

Beamish JA, He P, Kottke-Marchant K, Marchant RE. 2010. Molecular regulation of contractile smooth muscle cell phenotype: implications for vascular tissue engineering. *Tissue Engineering. Part B, Reviews* **16**:467–91.

Brown XQ, Bartolak-Suki E, Williams C, Walker ML, Weaver VM, Wong JY. 2010. Effect of substrate stiffness and PDGF on the behavior of vascular smooth muscle cells: implications for atherosclerosis. *Journal of Cellular Physiology* **225**:115–22.

Buccione R, Orth JD, McNiven MA. 2004. Foot and mouth: podosomes, invadopodia and circular dorsal ruffles. *Nature Reviews. Molecular Cell Biology* **5**:647–57.

Clark K, Langeslag M, Figdor CG, van Leeuwen FN. 2007. Myosin II and mechanotransduction: a balancing act. *Trends in Cell Biology* **17**:178–86.

Davis-Dusenbery BN, Wu C, Hata A. 2011. Micromanaging vascular smooth muscle cell differentiation and phenotypic modulation. *Arteriosclerosis, Thrombosis, and Vascular Biology* **31**:2370–7.

Discher DE, Janmey P, Wang YL. 2005. Tissue cells feel and respond to the stiffness of their substrate. *Science* **310**:1139–43.

Evanko SP, Raines EW, Ross R, Gold LI, Wight TN. 1998. Proteoglycan distribution in lesions of atherosclerosis depends on lesion severity, structural characteristics, and the proximity of platelet-derived growth factor and transforming growth factor-beta. *American Journal of Pathology* **152**:533–46.

Gerthoffer WT. 2007. Mechanisms of vascular smooth muscle cell migration. *Circulation Research* **100**:607–21.

Greenwald SE. 2007. Ageing of the conduit arteries. *Journal of Pathology* **211**:157–72.

Gu Z, Noss EH, Hsu VW, Brenner MB. 2011. Integrins traffic rapidly via circular dorsal ruffles and macropinocytosis during stimulated cell migration. *Journal of Cell Biology* **193**:61–70.

Huang M, Satchell L, Duhadaway JB, Prendergast GC, Laury-Kleintop LD. 2011. RhoB links PDGF signaling to cell migration by coordinating activation and localization of Cdc42 and Rac. *Journal of Cellular Biochemistry* **112**:1572–84.

Huang S, Ingber DE. 2005. Cell tension, matrix mechanics, and cancer development. *Cancer Cell* **8**:175–6.

Huynh J, Nishimura N, Rana K, Peloquin JM, Califano JP, Montague CR, King MR, Schaffer CB, Reinhart-King CA. 2011. Age-related intimal stiffening enhances

endothelial permeability and leukocyte transmigration. *Science Translational Medicine* **3**:112ra122–112ra122.

Ikebe M, Hartshorne DJ. 1985. Phosphorylation of smooth muscle myosin at two distinct sites by myosin light chain kinase. *Journal of Biological Chemistry* **260**:10027–31.

Isenberg BC, Dimilla PA, Walker M, Kim S, Wong JY. 2009. Vascular smooth muscle cell durotaxis depends on substrate stiffness gradient strength. *Biophysical Journal* **97**:1313–1322.

Krishnan R, Klumpers DD, Park CY, Rajendran K, Trepat X, van Bezu J, van Hinsbergh VWM, Carman CV, Brain JD, Fredberg JJ, Butler JP, van Nieuw Amerongen GP. 2011. Substrate stiffening promotes endothelial monolayer disruption through enhanced physical forces. *American Journal of Physiology. Cell Physiology* **300**:C146–54.

Krueger EW, Orth JD, Cao H, McNiven MA. 2003. A dynamin-cortactin-Arp2/3 complex mediates actin reorganization in growth factor-stimulated cells. *Molecular Biology of the Cell* **14**:1085–96.

Kumar S, Weaver VM. 2009. Mechanics, malignancy, and metastasis: the force journey of a tumor cell. *Cancer Metastasis Reviews* **28**:113–27.

Linder S, Wiesner C, Himmel M. 2011. Degrading devices: invadosomes in proteolytic cell invasion. *Annual Review of Cell and Developmental Biology* **27**:185–211.

Lusis AJ. 2000. Atherosclerosis. *Nature* **407**:233–41.

Mattace-Raso FUS, van der Cammen TJM, Hofman A, van Popele NM, Bos ML, Schalekamp MADH, Asmar R, Reneman RS, Hoeks APG, Breteler MMB, Witteman JCM. 2006. Arterial stiffness and risk of coronary heart disease and stroke: the Rotterdam Study. *Circulation* **113**:657–63.

McDaniel DP, Shaw GA, Elliott JT, Bhadriraju K, Meuse C, Chung KH, Plant AL. 2007. The stiffness of collagen fibrils influences vascular smooth muscle cell phenotype. *Biophysical Journal* **92**:1759–69.

Murphy DA, Courtneidge SA. 2011. The “ins” and “outs” of podosomes and invadopodia: characteristics, formation and function. *Nature Reviews Molecular Cell Biology* **12**:413–426.

Na S, Collin O, Chowdhury F, Tay B, Ouyang M, Wang Y, Wang N. 2008. Rapid signal transduction in living cells is a unique feature of mechanotransduction. *Proceedings of the National Academy of Sciences U S A* **105**:6626–31.

Owens GK, Kumar MS, Wamhoff BR. 2004. Molecular regulation of vascular smooth muscle cell differentiation in development and disease. *Physiological Reviews* **84**:767–801.

Paszek MJ, Zahir N, Johnson KR, Lakins JN, Rozenberg GI, Gefen A, Reinhart-King CA, Margulies SS, Dembo M, Boettiger D, Hammer DA, Weaver VM. 2005. Tensional homeostasis and the malignant phenotype. *Cancer Cell* **8**:241–54.

Peyton SR, Putnam AJ. 2005. Extracellular matrix rigidity governs smooth muscle cell motility in a biphasic fashion. *Journal of Cell Physiology* **204**:198–209.

Poch G, Pancheva SN. 1995. Calculating slope and ED50 of additive dose-response curves, and application of these tabulated parameter values. *Journal of Pharmacological and Toxicological Methods* **33**:137–145.

Poincloux R, Lizárraga F, Chavrier P. 2009. Matrix invasion by tumour cells: a focus on MT1-MMP trafficking to invadopodia. *Journal of Cell Science* **122**:3015–24.

Raines EW, Koyama H, Carragher NO. 2000. The extracellular matrix dynamically regulates smooth muscle cell responsiveness to PDGF. *Annals of the New York Academy of Sciences* **902**:39–51; discussion 51–2.

Raines EW. 2004. PDGF and cardiovascular disease. *Cytokine & Growth Factor Reviews* **15**:237–54.

Ridley AJ. 2011. Life at the leading edge. *Cell* **145**:1012–22.

Ross R. 1999. Atherosclerosis--an inflammatory disease. *The New England Journal of Medicine* **340**:115–26.

Ross R, Masuda J, Raines EW, Gown AM, Katsuda S, Sasahara M, Malden LT, Masuko H, Sato H. 1990. Localization of PDGF-B protein in macrophages in all phases of atherogenesis. *Science* **248**:1009–12.

Sandilands E, Cans C, Fincham VJ, Brunton VG, Mellor H, Prendergast GC, Norman JC, Superti-Furga G, Frame MC. 2004. RhoB and actin polymerization coordinate Src activation with endosome-mediated delivery to the membrane. *Developmental Cell* **7**:855–69.

Stroka KM, Aranda-Espinoza H. 2011. Endothelial cell substrate stiffness influences neutrophil transmigration via myosin light chain kinase-dependent cell contraction. *Blood* **118**:1632–40.

Suetsugu S, Yamazaki D, Kurisu S, Takenawa T. 2003. Differential roles of WAVE1 and WAVE2 in dorsal and peripheral ruffle formation for fibroblast cell migration. *Developmental Cell* **5**:595–609.

Sun C, Wu MH, Yuan SY. 2011. Nonmuscle myosin light-chain kinase deficiency attenuates atherosclerosis in apolipoprotein E-deficient mice via reduced endothelial barrier dysfunction and monocyte migration. *Circulation* **124**:48–57.

Sutton-Tyrrell K, Najjar SS, Boudreau RM, Venkitachalam L, Kupelian V, Simonsick EM, Havlik R, Lakatta EG, Spurgeon H, Kritchevsky S, Pahor M, Bauer D, Newman A. 2005. Elevated aortic pulse wave velocity, a marker of arterial stiffness, predicts cardiovascular events in well-functioning older adults. *Circulation* **111**:3384–3390.

Totsukawa G, Yamakita Y, Yamashiro S, Hartshorne DJ, Sasaki Y, Matsumura F. 2000. Distinct roles of ROCK (Rho-kinase) and MLCK in spatial regulation of MLC phosphorylation for assembly of stress fibers and focal adhesions in 3T3 fibroblasts. *Journal of Cell Biology* **150**:797–806.

Wang Y, Zheng XR, Riddick N, Bryden M, Baur W, Zhang X, Surks HK. 2009. ROCK isoform regulation of myosin phosphatase and contractility in vascular smooth muscle cells. *Circulation Research* **104**:531–40.

Webb DJ, Donais K, Whitmore LA, Thomas SM, Turner CE, Parsons JT, Horwitz AF. 2004. FAK-Src signalling through paxillin, ERK and MLCK regulates adhesion disassembly. *Nature Cell Biology* **6**:154–61.

Wolf K, Friedl P. 2011. Extracellular matrix determinants of proteolytic and non-proteolytic cell migration. *Trends in Cell Biology* **21**:736–44.

Zeng Y, Lai T, Koh CG, LeDuc PR, Chiam KH. 2011. Investigating circular dorsal ruffles through varying substrate stiffness and mathematical modeling. *Biophysical Journal* **101**:2122–30.

Zieman SJ, Melenovsky V, Clattenburg L, Corretti MC, Capriotti A, Gerstenblith G, Kass DA. 2007. Advanced glycation endproduct crosslink breaker (alagebrium) improves endothelial function in patients with isolated systolic hypertension. *Journal of Hypertension* **25**:577–83.

CHAPTER 5

EXPLORING BIOMECHANICS IN THE CLASSROOM

5.1 Abstract

In June 2009, I was selected to be a fellow in the Cornell's National Science Foundation Graduate STEM Fellows in K-12 Education (NSF GK-12) program. As part of this year-long fellowship, I had the pleasure and honor of working with Ms. Stacey Coston from Waverly High School to develop and give several lectures over a broad range of biomedical topics to students in 6^{th} to 12^{th} grade. Additionally, I developed two science labs that bring polymer science and cardiovascular biomechanics into the classroom. To introduce concepts of polymer science, students made "silly putty" from borax and glue. To introduce cardiovascular biomechanics, students built a model blood vessel out of rubber tubing to understand how vessel stiffness affects blood flow. This chapter chronicles my time as a GK-12 Fellow and overviews the teachings accomplished in Ms. Coston's classroom. The language in this chapter diverges from the rest of the thesis as I describe the process of developing inquiry-based learning modules and the results and impacts of these modules on student learning.

5.2 Introduction

As part of the NSF GK-12 Fellowship, I was paired with Stacey Coston, a teacher from Waverly High School who teaches taught Anatomy and Physiology and Forensic Science. We started our collaboration in the summer of 2009 by familiarizing her with several protocols in the Reinhart-King lab, including cell culture, immunofluorescent staining, and microscopy. Outside of the lab, we attended

meetings held by Dr. Chris Schaffer, Dr. Shivaun Archer, and Nev Singhota on the values and implementation of inquiry-based learning.

Inquiry-based learning (IBL) is a pedagogical philosophy that is gaining traction in science education (Bell et al., 2010). In IBL, rather than learning through rote memorization of scientific facts, students are tasked with developing and analyzing experiments and critically thinking about their results, skills that translate especially well to careers in science and research. Although the benefits of IBL over traditional learning methods are debated (Hmelo-Silver et al., 2007; Kirschner et al., 2006), the goals of IBL are in line with the goals of the NSF GK-12 program, which are to better engage high school students in science and to develop problem solving skills.

5.3 Results from Stacey's summer research

To give Stacey a better understanding of how research is conducted in an academic setting, I supervised Stacey on a project that was related to vascular smooth muscle cell (VSMC) migration. The goal of her project was to understand how vascular stiffness and treatment with phorbol 12,13-dibutyrate (PDBu) affected cell migration. After learning cell culture, polyacrylamide gel synthesis, immunofluorescent staining, and time-lapse microscopy, Stacey performed experiments to analyze migration speeds of VSMCs with respect to substrate stiffness and PDBu treatment.

Below are figures Stacey created for a poster which represents the culmination of her summer research. In summary, Stacey found that VSMCs treated with PDBu formed podosomes, actin-rich adhesion structures that degrade extracellular matrix

(Gimona et al., 2008), potentially aiding VSMC migration and invasion (Fig. 5.1). These podosomes form and disassemble within minutes and may organize into ring-shaped clusters (Fig. 5.2). By tracking cell movement over time and calculating mean-squared displacements (Fig. 5.3), Stacey found that cells migrate slightly faster on stiffer substrates, and PDBu treatment further increased cell migration speeds (Fig. 5.4). Persistence times, the time cells spend before significantly change migratory directions (Harms et al., 2005), decreased with PDBu treatment.

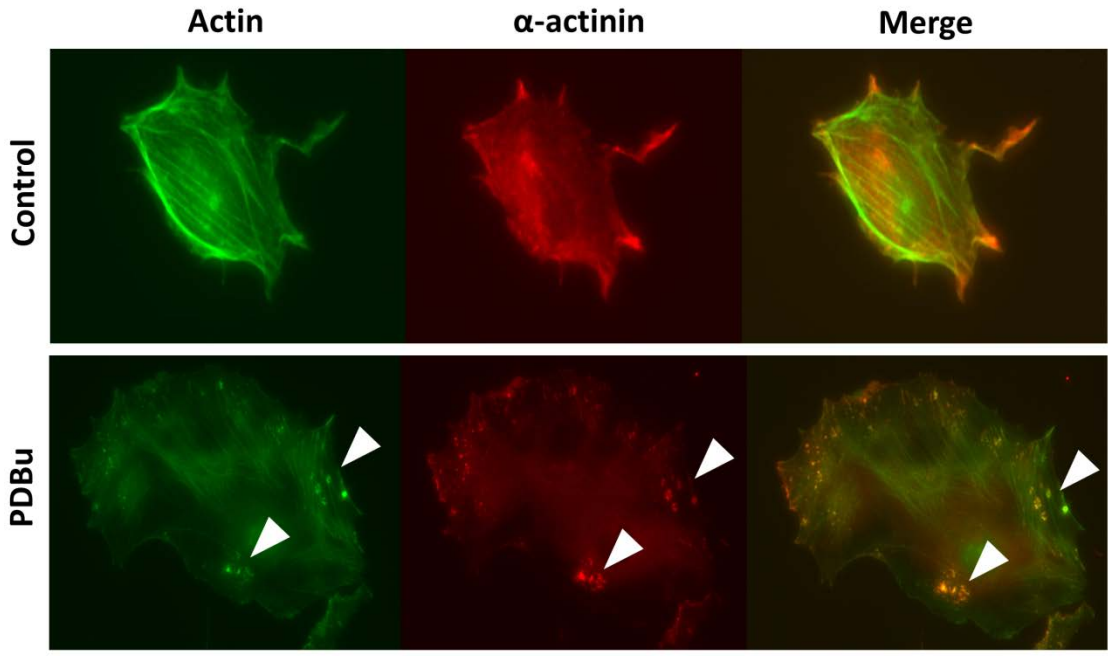

Figure 5.1. Representative immunofluorescent images of VSMCs on 10,000 Pa polyacrylamide gels stained for actin and α-actinin. Podosomes are evident in the untreated cells whereas form as clusters of dots (marked by white arrowheards) in PDBu-treated cells. Podosomes appear as dynamic structures when cells migrate and are often found on the leading edge of cell movement.

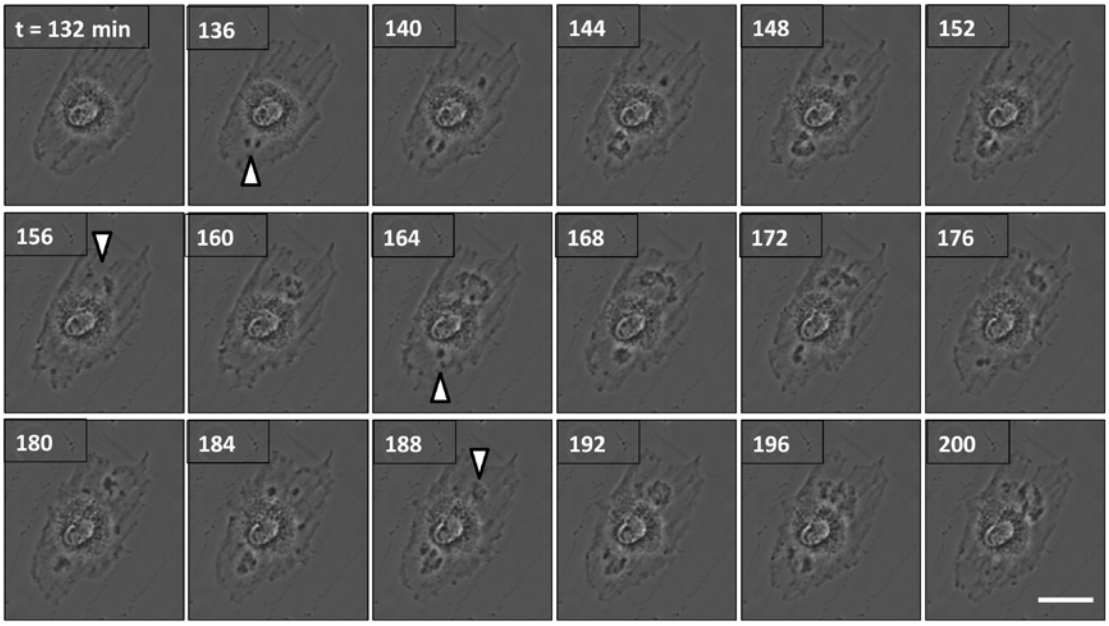

Figure 5.2. Time-lapse images of podosome formation in a VSMC on a 2,500 Pa polyacrylamide gel. The time indicated represents minutes elapsed after PDBu stimulation. As shown above, podosomes are dynamic structures that form and disassemble on the order of minutes. Arrowheads indicate the initial stages of podosome formation.

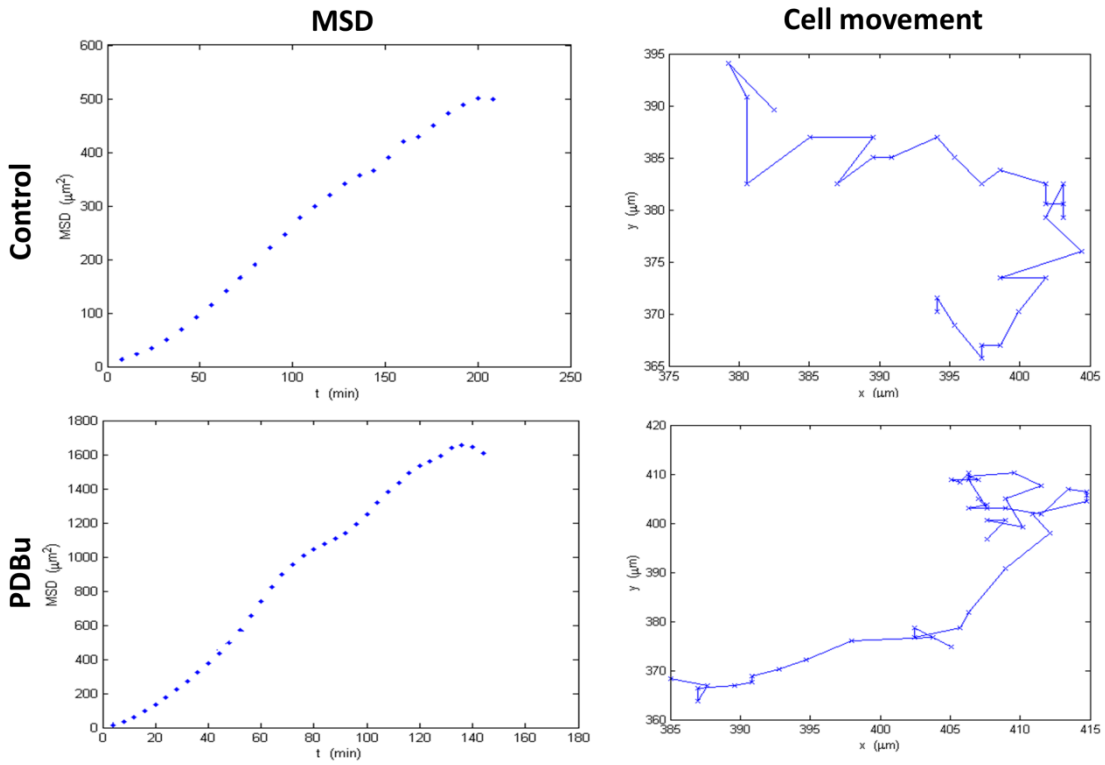

Figure 5.3. Representative mean-squared displacement data and cell movement plots of VSMCs without or with PDBu treatment.

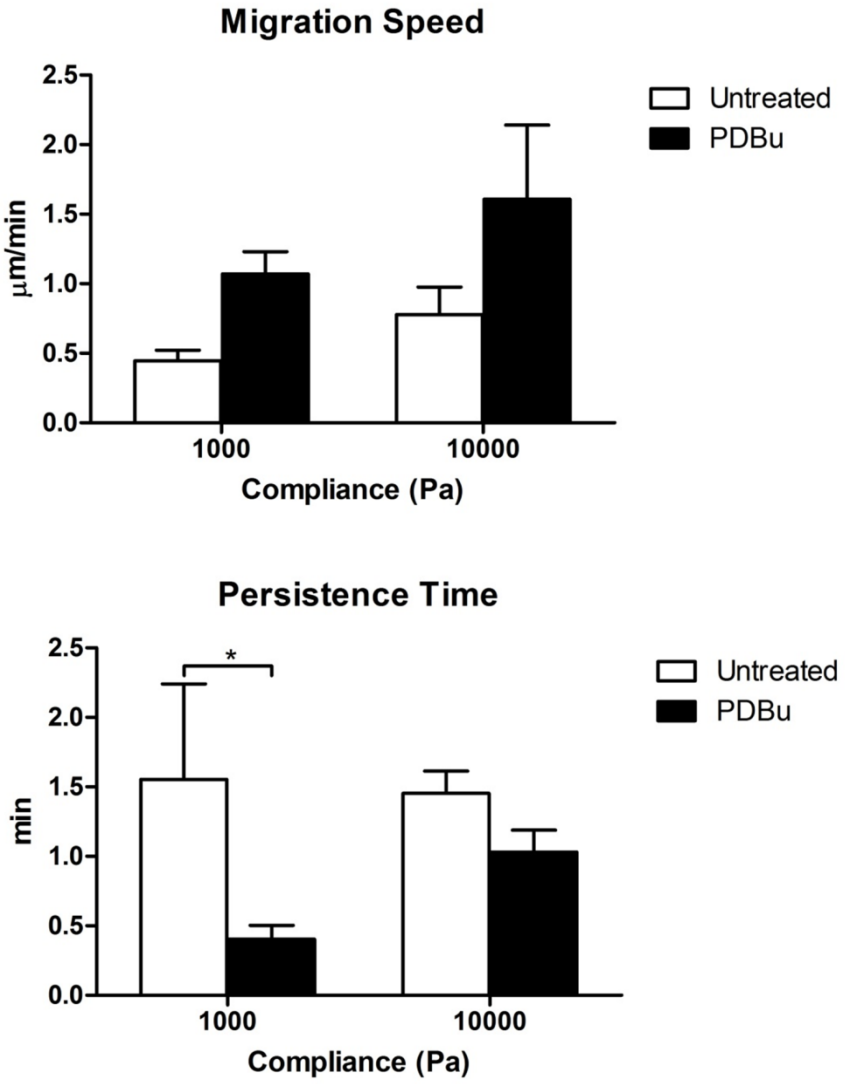

Figure 5.4. VMSC migration speed increased slightly with stiffness and the addition of PDBu. PDBu has been found to upregulate stress fiber and focal adhesion disassembly and actin polymerization. Persistence time decreases with addition of PDBu. This may occur because PDBu causes VMSC to actively undergo cytoskeletal rearrangement.

5.4 Development of curricular materials

In addition to performing research, Stacey worked with me to develop new curriculums that would educate her students about cutting edge research. I had a different role than most other NSF GK-12 Fellows in that I was a "Guest Lecturer" in addition to being a "Resident Scientist" who helped with lab activities. One of our goals was to translate some of the research she performed while in our lab into engaging material for her students. One concept that is universally understood is that a single cell is the smallest unit of life; however, the majority of students at the high school level fail to realize that cells are capable of sensing and responding to their environment, much like whole organisms. To teach this to students, I developed a lecture that explained the concepts of cell-cell communications. The advent of Youtube is particularly helpful in communicating science to students. In this lecture, which can be found in Appendix E.2., I liken cell signaling cascades to a Rube-Goldberg machine where a series of processes must occur correctly for cells to respond to their environment. To show cell sensing and environmental response, I used a particularly engaging video captured by the late David Rogers of Vanderbilt University that shows a neutrophil tracking down and killing bacteria.

In addition to lecturing about cell communications, I created several other lectures that introduce biomedical concepts to Stacey's students. Some of the lectures, like those on bioterrorism and cancer, were created in response to a student survey that gauged their scientific interests. Other lectures focused on the applications and potential of nanotechnology, tissue engineering, and prosthetic heart valves. Due to the generosity of Jonathan Butcher's lab, I used sample heart valves as props in one lecture. All of these lectures have been included in Appendix E.

During my time at Waverly High School, I also served as a mentor who provided career advice to rising juniors and seniors. Because I am closer to the

students in age and obtained my undergraduate degree more recently, Stacey thought that I would be an invaluable source of information for students who were considering higher education. We developed a lunch seminar where interested students were encouraged to ask any questions they wanted. Some questions that stood out were about deciding on an undergraduate major, dorm life and social activities, graduate education, careers and opportunities in science, and the undergraduate experience in general.

5.5 Inquiry-based labs

I developed two labs aimed to teach students the importance of stiffness in the progression of cardiovascular diseases. In the first lab, titled "Elasticity of blood vessels," the students explored the role of blood vessel elasticity on the flow of blood using plastic tubing to model the circulatory system. In the second lab, titled "Polymer chemistry: physical properties of gels," students were asked to make silly putty and design an experiment to characterize the stiffness of their silly putty, which varied based on the amount of polymer and crosslinker they used.

The blood vessel elasticity lab was more straightforward and less inquiry-based. In this lab, students attached several pieces of plastic tubing between a basketball pump and a beaker full of water (Appendix E.1.3). When pumped, the flow of air through the tubes resulted in bubbles that arise from the beaker, representing the flow of blood. The students were then made to change type of tubing to see how that changed the severity of the bubbling. They were given two different stiffnesses of latex, one colored pink which was thin and very compliant, the other colored amber which was thicker and stiffer. When students used these tubes to make their model blood vessel, they found that the pink elastic latex resulted in much less violent bubble formation in the beaker. This model mimics a more elastic vessel in the body, whereby

vessel expansion slows the rate of blood flow and allows for more continuous blood flow. Inelastic vessels do not expand and increased blood flow is found. The students also modeled the occurrence of an aneurysm by plugging the tubes such that air flow does not move through. In this case, the pink latex balloons outward, thinning and stiffening.

The polymer science lab was much less structured than the vessel elasticity lab and could be considered a guided-inquiry lab. In the beginning of the lab, students in groups of 3-4 were instructed to mix a 4-to-1 ratio of glue-to-borax to obtain silly putty. After qualitatively characterizing some of its properties, such as viscoelasticity and stiffness, the students were allowed to make silly putty from whatever ratios of glue-to-borax they wanted. The addition of food coloring gave students another level of freedom and creativity, and the students highly enjoyed making and playing with various polymers.

The defining moment of the lab was when students started running experiments to quantitatively characterize the stiffness of their various ratios. I provided rulers and stopwatches so students could take time and distance measurements, but I did not give them any hints as to how to compare their gels with one another. I was very pleased when students developed several different experiments to characterize their gels. Because silly putty is viscoelastic, it “flows” in response to gravity. Using this concept, one group measured the distance their gels lengthened when held in the air for 10 seconds, while another group record the time it took for gels to lengthen 12 inches. Other students shaped the gel into a sphere, placed the ball on the table, and measured the time it took to flatten to a certain diameter. Another group dropped balls of silly putty from a certain height and measured the rebounding height, using that to characterize their polymer’s stiffness.

Following the collection of data, groups presented their findings. Interestingly,

some groups found that some ratios did not form polymers, while some groups found conflicting results even though they used the same ratios as other groups. We ended the activity with a summary of results from the students and an explanation for the discrepancies in results between groups. We discussed the concept of experimental controls and consistency between experiment runs. For example, many groups did not control for initial gel size, either by measuring the mass or perhaps the circumference of the sphere before it started to deform. The students learned that a different approach to quantifying their data would be to calculate a percent change from their initial measurements.

5.6 Results from the lab exercises

To gauge whether students learned from the labs, I administered a 10 question quiz (Appendix E.1.5) immediately before and approximately 4 weeks after the labs. The results are shown in Fig. 5.5A. In the post-test, the students improved about 3.5 points in their scores, indicating that they still remembered what they learned from the labs. Fig. 5.5B summarizes the performance of students with respect to the question number. The students improved drastically in 8 of the 10 questions.

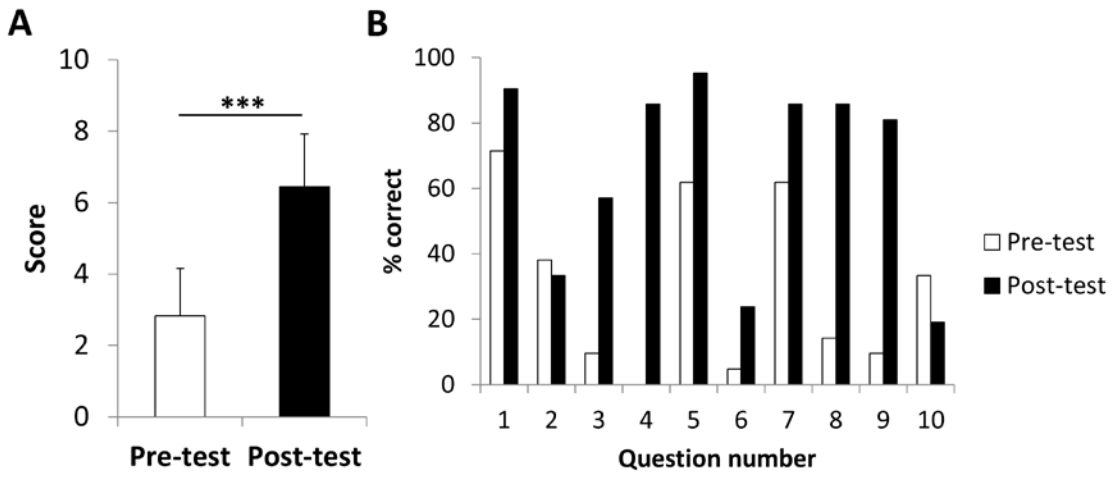

Figure 5.5. Pre- and post-test results of the atherosclerosis quiz. **(A)** Post-test scores were significantly higher than pre-test scores. Data are means ± SD (n = 21 students). ***P < 0.001 (Student's t-test) **(B)** The percentage of students that answered each question correctly is plotted pre- and post-test.

5.7 Conclusions

My goal was to engage Stacey's high school students in science and technology. I believe that through the various lectures and inquiry-based labs that we administered, the students were able to expand their knowledge of science, understand possible applications of science, and get an idea of how to design and conduct experiments. My appointment as an NSF GK-12 Fellow was an invaluable experience that taught me how to communicate science more effectively and grow as a mentor. The questions I received from students during my experience taught me to think quickly to explain difficult or confusing concepts using analogies to reach a wider audience. I also learned to use inquiry-based learning to teach, engage, and challenge students.

5.8 References

Bell T, Urhahne D, Schanze S, Ploetzner R. 2010. Collaborative inquiry learning: Models, tools, and challenges. *International Journal of Science Education* **32**:349–377.

Gimona M, Buccione R, Courtneidge SA, Linder S. 2008. Assembly and biological role of podosomes and invadopodia. *Current Opinion in Cell Biology* **20**:235–41.

Harms BD, Bassi GM, Horwitz AR, Lauffenburger DA. 2005. Directional persistence of EGF-induced cell migration is associated with stabilization of lamellipodial protrusions. *Biophysical Journal* **88**:1479–88.

Hmelo-Silver CE, Duncan RG, Chinn CA. 2007. Scaffolding and achievement in problem-based and inquiry learning: A response to Kirschner, Sweller, and Clark (2006). *Educational Psychologist* **42**:99–107.

Kirschner PA, Sweller J, Clark RE. 2006. Why minimal guidance during instruction does not work: An analysis of the failure of constructivist, discovery, problem-

based, experiential, and inquiry-based teaching. *Educational Psychologist* **41**:75–86.

CHAPTER 6

CONCLUSIONS AND FUTURE DIRECTIONS

6.1 Conclusions

As our knowledge of atherosclerosis continues to expand, particularly of its origins and pathogenesis, so too will our ability to develop therapeutics to prevent or reverse the progression of atherosclerosis. This thesis contributes to the knowledge of atherogenesis by identifying age-related vascular stiffening as a potent inducer of endothelial permeability, an initiating step of atherosclerosis, and also of vascular smooth muscle cell migration, which occurs in the later stages of atherosclerosis. Using tunable matrices that mimic the stiffness of healthy and aged vessels, this work demonstrates that endothelial and vascular smooth muscle cells cultured on stiffer matrices exhibit atherosclerotic phenotypes. Additionally, the pharmacological inhibition of stiffness-induced cell contractility may potentially mitigate the progression of atherosclerosis.

In Chapter 2, we developed a novel method for assaying the permeability of tracer molecules through an endothelial monolayer cultured on soft, porous substrates. Because the stiffness of porous membranes used in traditional permeability studies are orders of magnitude higher than that of native blood vessels, the development of a new permeability assay that matches physiological stiffness was required. Using confocal microscopy, our technique detects the amount of FITC-conjugated dextran that permeates through an endothelial layer and accumulates within the underlying polyacrylamide gel. By measuring the fluorescent intensity of the entrapped molecules, the relative permeability of the endothelial cells can be determined as they

are subjected to varying stiffnesses or drug treatments.

This method is has some advantages over traditional Transwell membrane assays because in those assays, the membranes are stiff plastics that do not represent physiological stiffness. Additionally, transmembrane studies generally take hours for tracer molecules to move a detectable amount through the membrane. Increased data variability is also a concern because of repeated sampling from the Transwell to be used in spectrophotometric absorbance measurements. Our permeability measurement method holds advantages in that the movement of tracer molecules can be detected within minutes and is real-time with confocal scanning.

Although our method has clear advantages, it is not without limitations. On very stiff substrates where the void fraction of the gel is small, only a certain amount of tracer molecules will be able to accumulate within the gel before the gel is saturated. In our studies, cells cultured on 30 kPa gels did not show increased permeability in response to thrombin, possibly indicating that 30 kPa gels are saturated by FITC-dextran within 5 minutes. A possible way to overcome this limitation is to perform shorter experiments on the order of 1 to 2 minutes of dextran diffusion, which may allow for the detection of endothelial permeability before the gel becomes saturated. Additionally, it may be possible to polymerize 30 kPa gels that have a larger void fraction by optimizing the total acrylamide and crosslinker amount (Charest et al., 2012; Rüchel et al., 1978). Taken together, the work described in Chapter 2 expands upon traditional permeability assays to account for substrate stiffness.

Using our newly developed permeability assay, we explored the effects of substrate stiffness on endothelial permeability, a hallmark of atherosclerosis, in

Chapter 3. The work presented in this chapter is the first to directly measure endothelial permeability in response to substrate stiffness. Our data indicated that increased substrate stiffness results in increased endothelial permeability, widening of endothelial cell-cell junctions, and increased leukocyte transmigration through endothelial cell monolayers. One of the most impactful findings of this study was that pharmacological inhibition of stiffness-induced ROCK-dependent endothelial cell contractility reversed all three of the aforementioned events. In addition to reversing hallmarks of atherosclerosis *in vitro*, inhibition of ROCK reduced cell-cell junction widths and vessel permeability *in vivo* using a mouse model. Therefore, pharmacological inhibition of endothelial cell contractility may be a potential treatment to slow or prevent the progression of atherosclerosis.

Although the work described in this thesis suggests that ROCK inhibition may potentially slow or prevent atherosclerosis, dosage remains a significant concern. In our experiments, cells *in vitro* were treated with Y-27632 for 30 minutes. In comparison, van Nieuw Amerongen and colleagues found that prolonged Y-27632 treatment of endothelial cells for 24 hours or more resulted in less VE-cadherin accumulation at cell-cell junctions and increased permeability (van Nieuw Amerongen et al., 2007), indicating possible negative effects of prolonged ROCK inhibition. Additionally, because ROCK is present in many other cell types including leukocytes and smooth muscle cells, off-target effects of ROCK inhibition should be characterized and minimized to ensure drug safety. However, once the safety and dosage of ROCK inhibition is elucidated, targeting endothelial cell contractility to prevent permeability and leukocyte extravasation remains an attractive therapeutic approach to slowing atherosclerosis.

Other potential therapeutic targets include integrin and focal adhesion kinase (FAK) signaling, which are upstream of RhoGTPase and ROCK activity and are utilized in mechanosensing. By reducing integrin or FAK activity, it may be possible to elicit similar decreases in cell contractility as ROCK inhibition to reverse hallmarks of atherosclerosis. Likewise, inhibition of myosin light chain downstream of Rho/ROCK may induce comparable responses. Alternatively, inhibiting the expression of endothelial adhesion molecules may be an attractive approach to decreasing leukocyte attachment and transmigration phenotypic of atherosclerosis.

In Chapter 4, the effects of vessel stiffening on vascular smooth muscle cell circular dorsal ruffle formation were investigated. Our data indicated that increased substrate stiffness promotes CDR formation. Because CDRs are recognized to provide wide-scale cytoskeletal rearrangements that promote cell motility, stiffness-induced CDR formation may encourage VSMC migration in the later stages of atherosclerosis. We determined that increased VSMC contractility due to substrate stiffness promotes CDR formation. Interestingly, pharmacological inhibition of cell-generated forces prevents CDR formation. This result is not unlike our results using endothelial cells, where inhibition of cell contractility reversed hallmarks of atherosclerosis. Together with the results from previous chapters, this work indicates that cell contractility inhibitors have therapeutic potential in preventing several hallmarks of atherosclerosis, namely endothelial permeability, leukocyte transmigration, and VSMC migration and invasion.

The findings presented in this dissertation not only help us understand the role of matrix stiffness in atherosclerosis, but also the complex relationship between cell-ECM and cell-cell interactions. The knowledge gained through these experiments

could be used in the design of tissue engineered scaffolds that better control cell phenotypes, or therapeutics that block cell-ECM interactions, thereby slowing the pathogeneses of stiffness-related diseases such as atherosclerosis and cancer metastasis.

6.2 Future directions

Although the work described in this dissertation contributed to our knowledge of atherosclerosis, additional work is required to fully understand the role of mechanical stimuli in dictating the progression of atherosclerosis.

One advantage of the polyacrylamide gel system that was not explored in this study is the ability to coat the surface with various ECM proteins. During the progression of atherosclerosis, fibronectin is deposited at atheroprone sites and contributes to endothelial dysfunction (Feaver et al., 2010; Sottile and Hocking, 2002). Our system is well adapted to study the effects of different ECM proteins, such as fibronectin, on endothelial permeability and traction generation. Preliminary data indicates that endothelial cells exhibit increased permeability when cultured on fibronectin-derivatized gels compared to collagen-derivatized gels (Fig. 6.1).

In addition to endothelial permeability, future work should elucidate the role of substrate stiffness on endothelial dysfunction. Our own work showed that the expression of adhesion molecules ICAM-1, VCAM-1, and E-selectin was not dependent on substrate stiffness. However, there are many other markers of endothelial dysfunction, including reactive oxygen species (ROS) generation (Hulsmans and Holvoet, 2010; Kondo et al., 2009) and decreased nitric oxide (NO) production (Lubos et al., 2008; Thomas et al., 2008), which are also hallmarks of

atherosclerosis. The study of these events with respect to substrate stiffness may further tie age-related vessel stiffening with atherosclerosis.

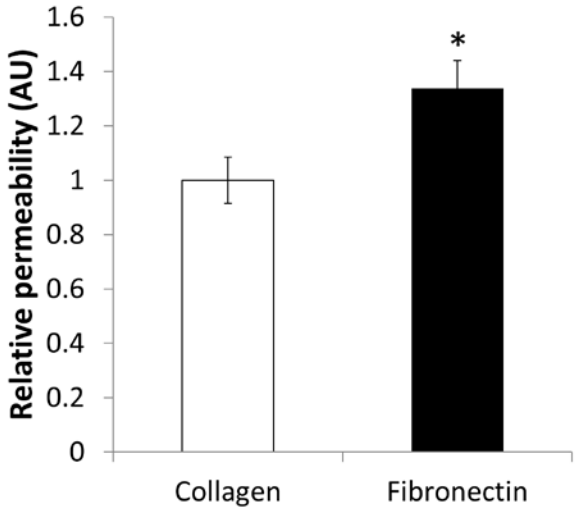

Figure 6.1. Effect of extracellular matrix type on endothelial permeability. Data are means ± SEM. *$P < 0.05$ (Student's t-test).

Future work should also investigate other mechanical stimuli, such as flow-mediated shear stress, in combination with substrate stiffness. Within the vasculature, atherosclerotic plaques tend to develop in specific regions where flow is disturbed (VanderLaan et al., 2004). Shear stress plays a crucial role in the localization of atherogenesis and dictates endothelial phenotype (Hahn and Schwartz, 2009). Steady, laminar, atheroprotective flow maintains endothelial alignment and integrity, whereas disturbed, atheroprone flow promotes permeability (Ogunrinade et al., 2002) and junctional reorganization (Melchior and Frangos, 2010) and separation (Malek et al., 1999). Interestingly, many of the signaling pathways utilized in response to substrate sensing and flow sensing overlap (Shyy and Chien, 1997). The study of both substrate stiffness and shear stress in combination would greatly expand our knowledge of the contributions of mechanical stimuli in disease progression.

In addition to shear stress, advanced glycation end-products (AGEs) are thought to contribute to endothelial dysfunction and atherosclerosis. AGEs are produced by the nonenzymatic reaction between proteins and reducing sugars (Zieman and Kass, 2004) and interact directly with endothelial cells through the receptor for advanced glycation end products (RAGE), causing impaired endothelial function (Lin et al., 2009; Yan et al., 2007). The accumulation of AGEs with age also leads to the crosslinking of vessel matrix and increased stiffening (Greenwald, 2007). It would be interesting to study the relationship between substrate stiffness, AGE-signaling, and endothelial function. Recent work has already implicated AGE-signaling to induce endothelial permeability by activating cell contractility (Hirose et al., 2010).

Much of the work presented in this dissertation describes the measurement of traction forces generated by cells in response to their matrix. However, the study of

forces generated between cells at their junctions may also help to explain the maintenance of endothelial barriers. The work described by Maruthamuthu and co-workers sough to understand the relationship between cell-ECM forces and cell-cell forces (Maruthamuthu et al., 2011). Future work in endothelial cell-cell force measurements may provide insights into the ability of cells to create tension through VE-cadherin bonds to regulate endothelial permeability.

Although the work presented in Chapter 4 of this thesis indicates that ROCK inhibition decreases endothelial permeability in mice, it would be worthwhile to study the therapeutic potential of ROCK inhibition in mice that develop atherosclerosis. An established mouse model of atherosclerosis is the apolipoprotein E-deficient (apoE-/-) mouse, which exhibits lipid abnormalities (Buzello et al., 2003), elevated serum plasma cholesterol, and impaired clearance of plasma lipoproteins (Imaizumi, 2011). These experiments may provide insights as to whether ROCK therapy can prevent the permeation and deposition of lipoproteins in younger mice that presumably have more compliant vessels, but readily develop atherosclerosis. More long-term studies should elucidate the therapeutic potential of ROCK inhibition by characterizing the number and size of atherosclerotic lesions that form within apoE-/- mice. Kaplan-Meier survival plots may provide an additional understanding of the benefits of ROCK inhibition in extending life.

Our work implicated substrate stiffness as an inducer of circular dorsal ruffle formation in vascular smooth muscle cells. As the mechanisms and machinery behind CDR formation are elucidated, future work with CDRs should focus on understanding its formation in 3D matrices for two reasons. First, three-dimensional scaffolds better mimic the physiological environment in which VSMCs are found. Second, CDRs

form on the dorsal side of cells, requiring the use of 3D matrices to fully understand their behaviors and functions. Because our work indicates that force generation regulates CDR formation on 2D substrates, traction force measurements of cells in 3D may provide insights to the role of cell contractility in inducing CDR formation in 3D. Studies performed by Legant and colleagues show the feasibility of measuring traction forces in 3D (Legant et al., 2010). Lastly, MMP2 has been shown to localize at CDRs (Suetsugu et al., 2003), indicating that CDRs may potentially have a role in matrix degradation and cell invasion. Future work should explore MMP secretion and ECM degradation at CDR sites within 3D matrices to better understand the function of CDRs.

Ultimately, future directions of this work will provide additional insights into the role of vessel stiffening in endothelial dysfunction and VSMC migration typical of atherosclerosis, as well as potential therapies and biomaterial designs for preventing or treating atherosclerosis.

6.3 References

Buzello M, Törnig J, Faulhaber J, Ehmke H, Ritz E, Amann K. 2003. The apolipoprotein e knockout mouse: a model documenting accelerated atherogenesis in uremia. *Journal of the American Society of Nephrology* **14**:311–6.

Charest JM, Califano JP, Carey SP, Reinhart-King CA. 2012. Fabrication of substrates with defined mechanical properties and topographical features for the study of cell migration. *Macromolecular Bioscience* **12**:12–20.

Feaver RE, Gelfand BD, Wang C, Schwartz MA, Blackman BR. 2010. Atheroprone hemodynamics regulate fibronectin deposition to create positive feedback that sustains endothelial inflammation. *Circulation Research* **106**:1703–11.

Greenwald SE. 2007. Ageing of the conduit arteries. *Journal of Pathology* **211**:157–72.

Hahn C, Schwartz MA. 2009. Mechanotransduction in vascular physiology and atherogenesis. *Nature Reviews. Molecular Cell Biology* **10**:53–62.

Hirose A, Tanikawa T, Mori H, Okada Y, Tanaka Y. 2010. Advanced glycation end products increase endothelial permeability through the RAGE/Rho signaling pathway. *FEBS Letters* **584**:61–66.

Hulsmans M, Holvoet P. 2010. The vicious circle between oxidative stress and inflammation in atherosclerosis. *Journal of Cellular and Molecular Medicine* **14**:70–8.

Imaizumi K. 2011. Diet and atherosclerosis in apolipoprotein E-deficient mice. *Bioscience, Biotechnology, and Biochemistry* **75**:1023–35.

Kondo T, Hirose M, Kageyama K. 2009. Roles of oxidative stress and redox regulation in atherosclerosis. *Journal of Atherosclerosis and Thrombosis* **16**:532–8.

Legant WR, Miller JS, Blakely BL, Cohen DM, Genin GM, Chen CS. 2010. Measurement of mechanical tractions exerted by cells in three-dimensional matrices. *Nature Methods* **7**:969–71.

Lin L, Park S, Lakatta EG. 2009. RAGE signaling in inflammation and arterial aging. *Frontiers in Bioscience* **14**:1403–13.

Lubos E, Handy DE, Loscalzo J. 2008. Role of oxidative stress and nitric oxide in atherothrombosis. *Frontiers in Bioscience* **13**:5323–44.

Malek AM, Alper SL, Izumo S. 1999. Hemodynamic shear stress and its role in atherosclerosis. *Journal of the American Medical Association* **282**:2035–42.

Maruthamuthu V, Sabass B, Schwarz US, Gardel ML. 2011. Cell-ECM traction force modulates endogenous tension at cell-cell contacts. *Proceedings of the National Academy of Sciences U S A* **108**:4708–13.

Melchior B, Frangos JA. 2010. Shear-induced endothelial cell-cell junction inclination. *American Journal of Physiology. Cell Physiology* **299**:C621–9.

van Nieuw Amerongen GP, Beckers CML, Achekar ID, Zeeman S, Musters RJP, van Hinsbergh VWM. 2007. Involvement of Rho kinase in endothelial barrier maintenance. *Arteriosclerosis, Thrombosis, and Vascular Biology* **27**:2332–2339.

Ogunrinade O, Kameya GT, Truskey GA. 2002. Effect of fluid shear stress on the permeability of the arterial endothelium. *Annals of Biomedical Engineering* **30**:430–46.

Rüchel R, Steere RL, Erbe EF. 1978. Transmission-electron microscopic observations of freeze-etched polyacrylamide gels. *Journal of Chromatography A* **166**:563–575.

Shyy JY, Chien S. 1997. Role of integrins in cellular responses to mechanical stress and adhesion. *Current Opinion in Cell Biology* **9**:707–13.

Sottile J, Hocking DC. 2002. Fibronectin polymerization regulates the composition and stability of extracellular matrix fibrils and cell-matrix adhesions. *Molecular Biology of the Cell* **13**:3546–3559.

Suetsugu S, Yamazaki D, Kurisu S, Takenawa T. 2003. Differential roles of WAVE1 and WAVE2 in dorsal and peripheral ruffle formation for fibroblast cell migration. *Developmental Cell* **5**:595–609.

Thomas SR, Witting PK, Drummond GR. 2008. Redox control of endothelial function and dysfunction: molecular mechanisms and therapeutic opportunities. *Antioxidants & Redox Signaling* **10**:1713–65.

VanderLaan PA, Reardon CA, Getz GS. 2004. Site specificity of atherosclerosis: site-selective responses to atherosclerotic modulators. *Arteriosclerosis, Thrombosis, and Vascular Biology* **24**:12–22.

Yan SF, D'Agati V, Schmidt AM, Ramasamy R. 2007. Receptor for Advanced Glycation Endproducts (RAGE): a formidable force in the pathogenesis of the cardiovascular complications of diabetes & aging. *Current Molecular Medicine* **7**:699–710.

Zieman S, Kass D. 2004. Advanced glycation end product cross-linking: pathophysiologic role and therapeutic target in cardiovascular disease. *Congestive Heart Failure* **10**:144–9.

APPENDIX A

PERMEABILITY MEASUREMENTS OF ENDOTHELIAL CELLS ON POLYACRYLAMIDE GELS

Materials:

Timer

Forceps

35 mm petri dishes

10 μM 40 kDa FITC-dextran in L-15 media

Protocol:

1. Culture endothelial cells to 100% confluency on 18 mm circular polyacrylamide gels in 6-well plates.
2. Two-days post-confluence, refresh cells with warm Leibovitz's L-15 media and place in a non-CO_2 incubator at 37 °C. Allow to equilibrate for at least 4 hours.
3. Make enough 10 μM solution of 40 kDa FITC-dextran for all of your samples. Each sample requires 2 ml of dextran solution. For example, for 25 samples, make 50 ml of dextran solution by dissolving 0.02 g 40 kDa FITC-dextran into 50 ml L-15 media. Mix by vortexing.
4. For each sample, aliquot 2 ml of dextran solution into a 35 mm petri dish. Place these petri dishes in the non-CO_2 incubator to warm to 37 °C.
5. Turn on the Leica TCS SP2 confocal microscope. Only turn on the 488 laser and bring the power to the 9 o'clock position.
6. Open the Leica software and move the objective to the 40x dipping lens. Set

the beam to the “FITC” configuration. Move the laser power up to ~50%. Set the mode to “xzy”. Set line averaging to 4. Ensure the pinhole is of airy 1. See Fig. A.1 below.

7. Using forceps, move a gel from the 6-well plate into a dextran-filled 35 mm petri dish. Start a timer for 5 minutes. Place everything back in the incubator.
8. When you have ~1.5 minutes left, place the 35 mm petri dish on the confocal microscope using the metal dish holder or a glass microscope slide. Insert the dipping lens into your sample. Start live scanning on the confocal software. Locate your gel by moving the stage up and down.
9. Using the Q-LUT, adjust your gain and offset so that there are just a few overexposed pixels (blue) for the FITC-dextran solution and underexposed pixels (green) for the glass beneath the gel. The gain is usually around 550 V, and offset around -4%.
10. Once the timer hits 0:00, acquire 4 images in quick succession near the center of the polyacrylamide gel.
11. Repeat with all samples.
12. Pro-tip: while waiting for timer to count down before step 8, you can place another gel in dextran and start a second timer to stagger your samples every ~3 minutes.

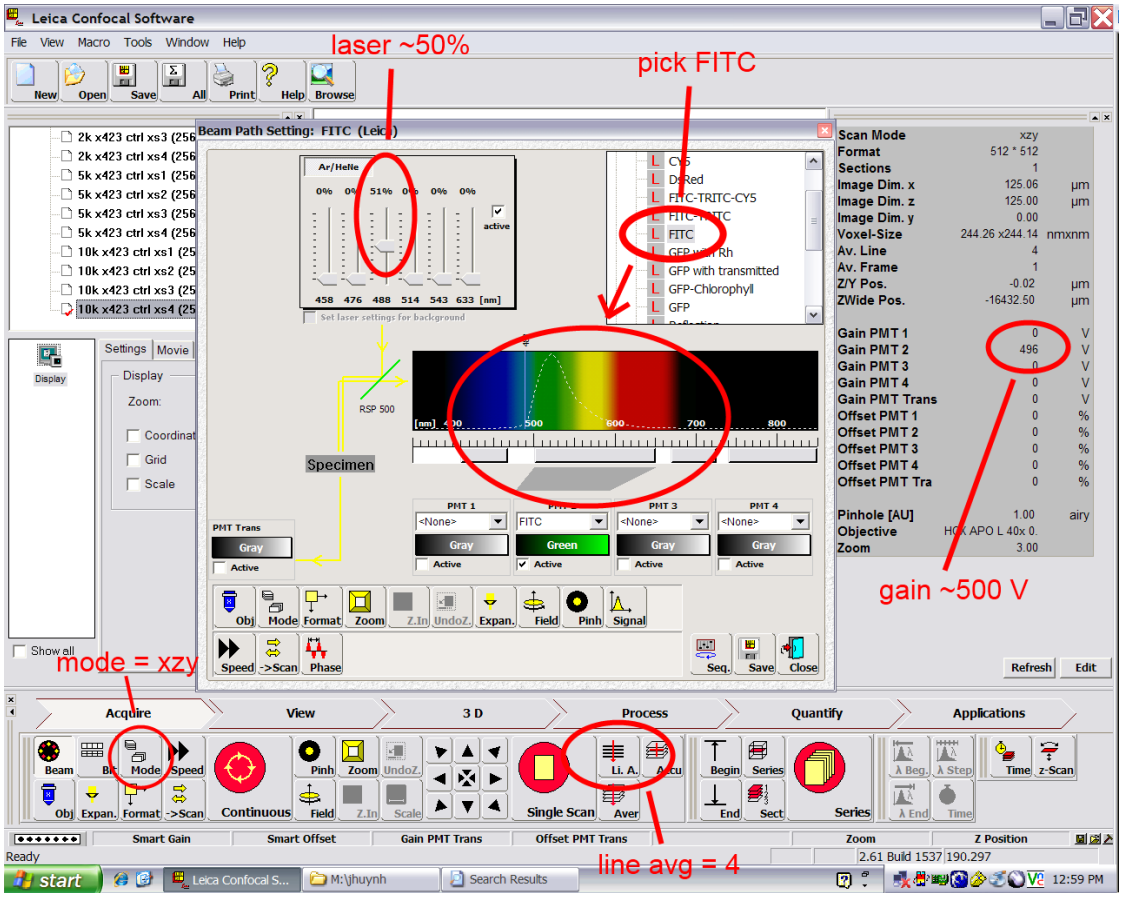

Figure A.1. Settings for Leica TCS SP2 confocal for permeability image acquisition.

APPENDIX B

SEEDING AND LYSING CELLS ON POLYACRYLAMIDE GELS FOR WESTERN BLOTTING ANAYLSIS

Materials:

For cell seeding:

Cell suspension

Kimwipes

Razor blade

100 mm petri dishes

For cell lysing:

Ice cold PBS

Ice cold lysis buffer

Ice cold 100 mm petri dishes

Razor blade

Kimwipe

Labeled ice cold 1.7 ml centrifuge tubes

Cell scrapers

Liquid nitrogen

Protocol:

1. Make 48 x 65 mm polyacrylamide gels by using 300 µl of gel solution per activated glass slide. Store at 4 °C until ready to use.
2. Remove gel from storage using a razor blade. Dry edges and the glass backing

of gels using a Kimwipe.

3. Place gel in a new, dry 100 mm petri dish.
4. Seed 2 ml of cells onto the polyacrylamide gel, creating a “bubble” of media on top of the gel.
5. Carefully place in incubator without disrupting the bubble of media.
6. Allow cells to attach for ~4 hours. Then add 8 ml media to the culture dish and culture normally.
7. When ready to lyse, prepare ice cold lysis buffer. Chill new 100 mm petri dishes at -20 °C. Chill PBS to ice cold temperature.
8. Place a chilled 100 mm petri dish on ice. Add 150 µl lysis buffer to the center of the petri dish.
9. Using a razor blade, remove polyacrylamide gel from culture and rinse both sides of the gel several times with at least 8 ml ice cold PBS.
10. Dry the glass backing and edges of the gel using a Kimwipe. Invert gel cell-side down onto lysis buffer.
11. Using a cell scraper, gently rotate the gel around in the petri dish, mechanically shearing cells off the gel.
12. Remove the gel from lysis buffer using a razor blade and collect as much lysate off the gel using the cell scraper, adding it to the petri dish.
13. Collect as much lysate as possible from the petri dish using the cell scraper.
14. Aspirate cell lysate and place in an ice cold 1.7 ml contribute tube.
15. Centrifuge at desired speed (14,000 x g) for desired time (5 min) at 4 °C.
16. Collect supernatant and place in a fresh 1.7 ml centrifuge tube.
17. Snap-freeze in liquid nitrogen and store at -80 °C until ready for Western blot analysis.

APPENDIX C

siRNA TRANSFECTION OF BOVINE AORTIC ENDOTHELIAL CELLS

Materials:

20 μM siRNA

Lipofectamine 2000

15 ml centrifuge tubes

Complete media without pen/strep

OptiMEM

Protocol:

1. Grow endothelial cells to desired confluency (90%) in 6-well plates.
2. Refresh cells with 2 ml complete media without pen/strep and place cells back in incubator.
3. In the hood, per sample, combine 250 μl OptiMEM with 5 μl Lipofectamine 2000 in a 15 ml centrifuge tube. Mix well by pipetting. In another centrifuge tube, combine 250 μl OptiMEM with 1.25 μl siRNA per sample and mix by pipetting. Allow these two tubes to incubate at room temperature for 15 minutes.
4. Combine the Lipofectamine solution with the siRNA solution. Mix well by pipetting and incubate at room temperature for 15 minutes.
5. Add 500 μl of the siRNA/Lipofectamine solution to each well of your 6-well plate.
6. Incubate cells at 37 °C for 4 hours to allow for transfection.
7. Refresh cells with complete media (with pen/strep).

8. Run experiments two-days post-confluency.
9. Pro-tip: The concentration of siRNA described above is 10 nM (stock 20 μM siRNA * 1.25 μl / 2.5 ml total media = 10 nM). You may have to play with the concentration of siRNA to optimize transfection.

APPENDIX D

CO-IMMUNOPRECIPITATION

Materials:

Ice cold PBS

Ice cold lysis buffer

Ice cold 100 mm petri dishes

Razor blade

Kimwipe

Labeled ice cold 1.7 ml centrifuge tubes

Cell scrapers

Rotator

Protein A or protein G agarose beads

Protocol:

1. On ice, lyse cells on 48 x 65 mm gels using 200 µl lysis buffer. Collect lysate into an ice cold 1.7 ml centrifuge tube.
2. Centrifuge for 10 minutes at 14,000 x g at 4 °C. Move supernatant to a newly labeled ice cold tube.
3. On ice, add 200 µl lysis buffer and 2 µl antibody to lysate (1:200 dilution).
4. Incubate 1-12 hr or overnight at 4 °C under gentle agitation/rotation.
5. Using a cut pipette tip, add 8 µl protein A or G beads (for 400 µl lysate) and incubate at 4 °C on rocker/rotator for 2 hr to overnight
6. Collect immunoprecipitates by centrifugation at 1,000 x g (2,500 rpm) for 5 min at 4 °C. Discard supernatant.

7. Wash pellet 3 times with 500 µl lysis buffer by mixing with beads and centrifuging as described in step 6.
8. Discard supernatant. Add 30 µl lysis buffer and 10 µl 5X SDS and heat/boil sample at 100 °C for 5 min.
9. Centrifuge beads at 1,000 x g and run the supernatant on SDS-PAGE.
10. Pro-tip: Antibody dilution in step 3 may need optimization. Check antibody product sheet for starting dilution (typically 1:100).

APPENDIX E

GK-12 TEACHING MATERIALS

E.1.1 Cornell BME CLIMB Module

The Mechanics of Atherosclerosis

Authors:	John Huynh and Stacey Coston
Date Created:	2010
Subject:	Biology, Chemistry
Level:	Grades 9-12
Standards:	The Living Environment: 1-Scientific Inquiry: 1.1a, 1.2a, 1.3b; 2-Scientific testing: 2.1, 2.3, 2.4; 3-Analysis of results: 3.1; 4-Content: 1-Living Things: 1.2a,b,c,d,e,f; 5-Dynamic Equilibrium: 5.2a,h,j, 5.3.
Schedule:	**Polymer lab: 90 minutes or two class periods** **Blood flow lab: 45 minutes or one class period**

Objectives:

To understand the mechanical mechanisms that underlie the progression of atherosclerosis

Students will:

Vocabulary:

Atherosclerosis
Cardiovascular Disease
Aneurysm
Polymer
Cross linker
Young's modulus

Materials:

For Each Group:
Polymer Lab:
Sharpie
10 Zip lock bags
One cup of 50% Elmer's glue
One cup of 4% Borax
2 Plastic spoons
Timer/stopwatch
Ruler
Food coloring
Activity Sheet #1 for each student

• Be introduced to polymer chemistry • Fabricate gels of varying stiffness • Design experiments to quantify gel stiffness • Understand how arterial stiffness contributes to disturbed blood flow and the progression of atherosclerosis • Communicate their findings to group mates and the class	**Blood Flow Lab:** Basketball pump with nozzle attachment 600 mL Beaker half filled with water Clear PVC tubing (5/16" I.D. x 1/2" O.D.) Amber latex tubing (1/2" I.D. x 5/8" O.D.) Non-lubricated condoms Cable ties Activity Sheet #2 for each student Safety: Be careful not to get Borax in the eyes. If this happens, please flush eyes with water for 10 minutes. Alternatively, wear safety goggles. Students who are allergic to latex should not handle latex.

Science Content for the Teacher:

Cardiovascular diseases are the leading cause of death in the United States, claiming more lives than cancer, car accidents, and HIV combined in 2006. Approximately 25% of Americans have some form of cardiovascular disease. Atherosclerosis is a disease of the arteries where the accumulation of lipids, cholesterol, and white blood cells harden the blood vessel. These atherosclerotic plaques may lead to the formation of a thrombus that occludes the artery. Atherosclerosis is considered a "silent killer" since it is typically asymptomatic and manifests itself as catastrophic events such as heart attacks or strokes.

Recent research suggests that mechanical stresses experienced in the vasculature may contribute to the progression of atherosclerosis. Atherosclerosis is often found in areas with disturbed blood flow which resemble turbulent whirlpools instead of steady streams of flow. These areas are predominantly found where blood vessels branch or bifurcate. Imagine a stream of water that encounters a large rock. The water will crash into the rock and then flow turbulently around it.

In response to disturbed blood flow, cells remodel their microenvironment by changing the composition of their extracellular matrix (collagen, elastin, laminin), which leads to increases in blood vessel stiffness. This increase in stiffness may act as a feedback loop that causes cells to continue to remodel and stiffen their microenvironment. Interestingly, as we age, 100% of the population exhibits vessel stiffening which correlates with risk of cardiovascular disease.

Healthy, elastic arteries stretch and store fluid as a pulse of blood is pumped by

the heart. As the vessels recoil, blood is continuously moved through the vasculature. Stiffened arteries lose their elasticity which results in elevated blood pressures and dysregulated blood flow.

To study the effects of mechanical stiffness on cell behavior, scientists culture cells on gels with tunable mechanical properties. By simply varying the ratio of polymer to its cross-linker (hardener), scientists can synthesize gels of varying Young's moduli, a measure of stiffness. Gels can be made with a stiffness of a few hundred Pascals which resembles brain or fat tissues, or several thousand Pascals which resemble muscle tissues or collagenous bone.

Preparation:

Pre-lab lecture: A day before the labs, the teacher should introduce the concept of cardiovascular diseases and describe the progression of atherosclerosis. The effects of blood flow and blood vessel stiffness on atherosclerosis progression should be emphasized. Additionally, the use of gels of varying stiffness in scientific research should be mentioned. See "Science Content" above and lecture slides link.

Polymer Lab:

1. Make 50% Elmer's glue solution by adding a 1:1 ratio of Elmer's glue and water in large container, such as a 1 quart plastic jar, and shaking/stirring vigorously until there are no clumps of glue. Label this "Solution A."
   Recommended: 6 bottles of Elmer's glue to the same volume of water.
2. Make 4% Borax solution by adding 4g of Borax per 100 ml warm water and mixing well. This can be approximated by adding 2 teaspoons of Borax to 1 cup of warm water. Label this "Solution B."
   Note 1: Warm water helps Borax dissolve completely.
   Note 2: Borax (sodium tetraborate) can be found online at Amazon.com or grocery stores in the household cleaners section. A commonly labeled brand is "20-Mule Team."
3. Provide for each group (3-4 students) 1 Sharpie, ~10 zip lock bags, a plastic cup half filled with Solution A, a plastic cup half filled with Solution B, 2 plastic spoons, a timer/stopwatch, a ruler, and some food coloring.
4. Provide each student with Activity Sheet #1

Blood Flow Lab:

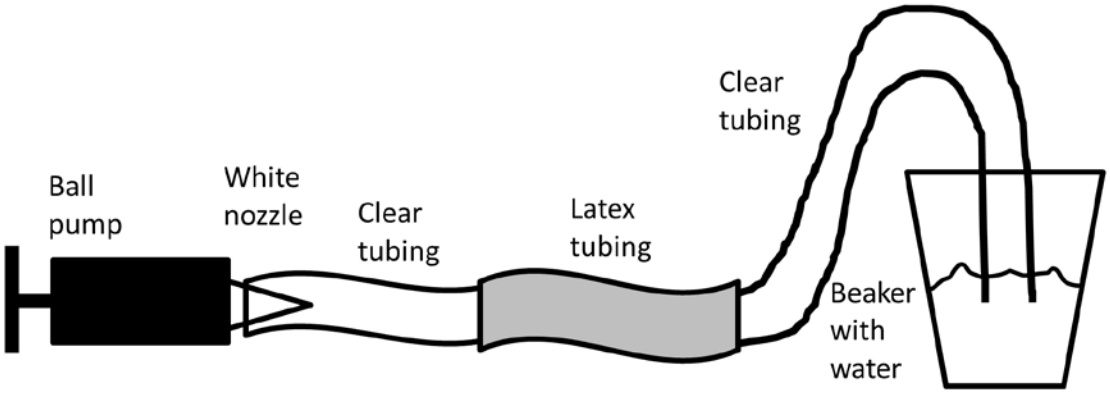

1. Each group needs 2 pieces of clear PVC tubing, one that is 1foot long, and another that is 3 feet long. Cut enough for the class. Tubing is available through Amazon.com (I.D. 5/16" x O.D. 1/2", ASIN# B000FN0OMQ for 25 ft, ASIN# B000FMULGQ for 100 ft)
2. Cut amber latex tubing into 6 inch pieces. Tubing is available through Amazon.com (I.D. 1/2" x O.D. 5/8", ASIN# B001UI1208)
3. Cut each prophylactic into 6 inch tubes.
4. Provide for each group a basketball pump with the white nozzle attachment, a one foot long piece of clear tubing, a three foot long piece of clear tubing, 1 amber latex tubing, 1 cut prophylactic, 4 cable ties, and 1 beaker half filled with water.
5. Provide each student with Activity Sheet #2

Classroom Procedure:

Polymer Lab:

Engage (Time: 5 min)

Introduction to concepts should have been discussed previously. Have all materials set out for student groups. Explain to students that they will assume the role of scientists and explore a chemical reaction that results in the synthesis of a gel. Emphasize that they will be designing their own experiments.

Explore (Time: 50 min)

Allow students to work through Activity Sheet #1. Be aware of students who are too busy playing with the gels and not progressing through the worksheet. Help students brainstorm ways to design their own experiments; remind them that they are allowed to use timers and rulers. If additional materials are available in the classroom, let students use them to design experiments.

Examples:

1. Record the time it takes for a gel to stretch 10 inches when held in mid-air.
2. Record the length a gel stretches over 30 seconds.
3. Turn the gel into sphere and measure its initial diameter. Let the ball sit on a table for 60 seconds and then measure its diameter.
4. Turn the gel into a sphere and drop from table height. Record the height the ball bounces.

Explain (Time: 35 min)

Allow groups to present their experiments to the rest of the class. Have groups present their method of quantification and their results. Have the rest of the class ask questions and critique methods. Example question: “Did you make sure all gels were equal size and shape before letting them stretch?”

See if data from one group agrees with data from another group. Does the entire class agree to a single conclusion about how polymer ratio affects gel stiffness? Oftentimes there will be conflicting data. Explain that discrepancies do exist in science and how improving future experiments (by devising better control and experimental conditions) is necessary to advance scientific knowledge.

Blood Flow Lab:

Engage (Time: 10)

Explain that the experimental setup models the circulatory system. Ask students to hypothesize how vessel stiffness would affect blood flow.

Explore (Time: 25)

Allow students to work through Activity Sheet #2.

Explain (Time: 10)

Work with students to help them answer critical thinking questions. Ask students to brainstorm ways they would treat or prevent vessel hardening.

Supplemental Information:

1. http://www.sciencebuddies.org/mentoring/project_ideas/Chem_p012.shtml
2. http://cibt.bio.cornell.edu/labs/dl/BPHY.PDF

Safety:

Be careful not to get Borax in the eyes. If this happens, please flush eyes with water for 10 minutes.
Students who are allergic to latex should not handle latex.

E.1.2 Atherosclerosis lecture slides

Atherosclerosis: a bioengineer's perspective

Cardiovascular disease (CVD)

- #1 cause of death in the United States
- In 2006, claimed more lives than cancer, car accidents, and HIV (AIDS) combined
- About 25% of Americans have some form of CVD
- 100% of people exhibit vessel stiffening which correlates with risk of CVD

americanheart.org

Atherosclerosis

- What is it?

- Where does it occur?

  Primarily in arteries

Risk Factors

- High Cholesterol
- Hypertension
- Diabetes
- Smoking
- Inactivity
- Obesity

Detection?

- Atherosclerosis is typically asymptomatic!
- It is most often found after it manifests itself as a heart attack or stroke
- Measure of LDL within the blood as a predictor
- 20% of events occur in individuals with no major risk factors

The major cellular events in the progression of atherosclerosis

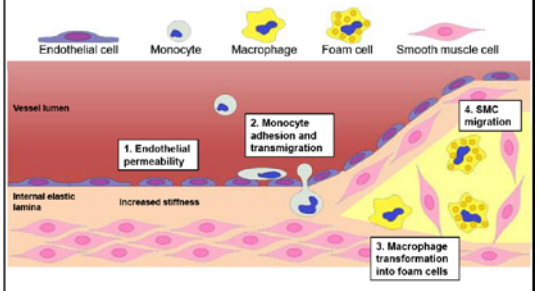

Histology of a normal artery

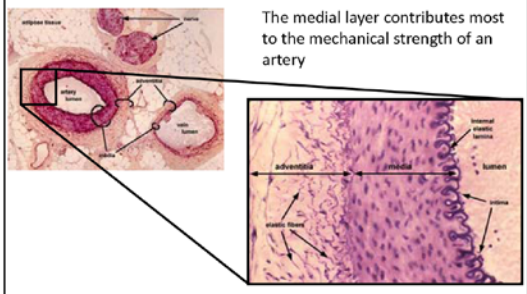

The medial layer contributes most to the mechanical strength of an artery

http://www.siumed.edu/~dking2/crr/cvguide.htm

Stresses in the vasculature

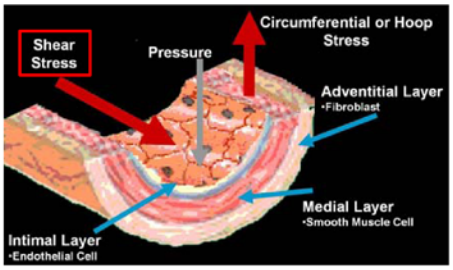

Effect of shear stress of endothelial cell orientation

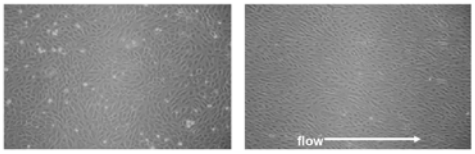

Hemodynamics within arterial lesions: A longstanding bioengineering problem

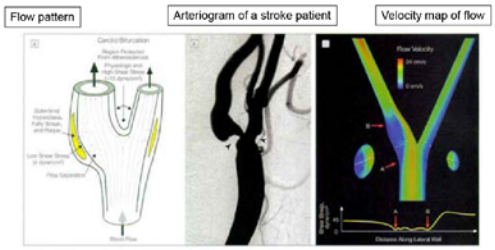

Malek AM *et al* (1999)

Streamlines at a carotid bifurcation

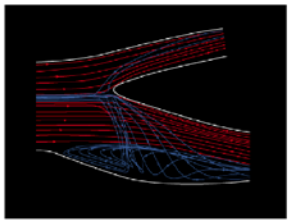

Lifeforcehospital.org

Young's modulus: measuring stiffness

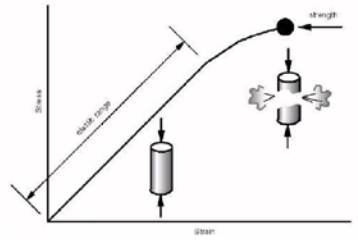

$$Young's\ modulus = \frac{stress}{strain} \quad \text{or} \quad E = \frac{\sigma}{\varepsilon}$$

Young's modulus of soft tissues

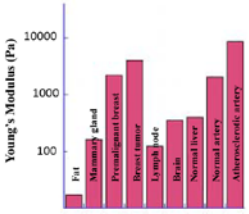

Modified from Levental, et al. *Soft Matter* 2007

We can mimic blood vessel stiffness using gels

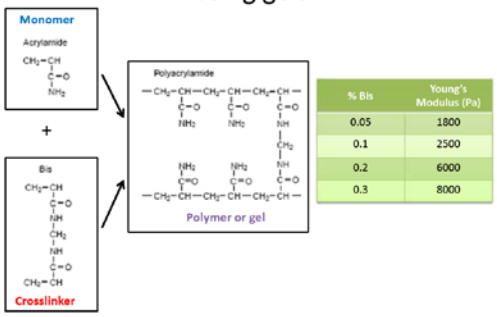

% Bis	Young's Modulus (Pa)
0.05	1800
0.1	2500
0.2	6000
0.3	8000

E.1.3 Elasticity of blood vessels lab

Introduction

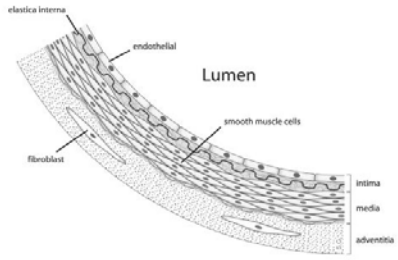

In the circulatory system, blood that is pumped by the heart flows through blood vessels and provide tissues with nutrients and oxygen. This flow, which is created by each heartbeat, is pulsatile; that is, the flow created is a series of discontinuous pulses. However, for optimal function, our body requires a steady, continuous flow of blood. How do blood vessels control this?

In addition to controlling blood flow, blood vessels are subject to mechanical stress during the pumping of blood. Thus, blood vessels must have mechanical properties that can withstand these stresses. Again, the mechanical properties of blood vessels are a function of the underlying tissue structure. Since blood vessels are soft collagenous tissues (with a good deal of elastin, another biomolecule), their stress-strain behavior resembles that of other soft collagenous tissues like ligaments and tendons.

Blood vessel tissue structure can change due to aging, disease, or altered mechanical load. Sometimes it is a combination of all three factors. For example, hypertension or high blood pressure is a disease that raises the mechanical load on the blood vessel. Due to higher stresses, the structure of the blood vessel is altered. In disease states such as atherosclerosis, arteries lose their elastic properties which results in the disruption of continuous blood flow. Additionally, blockages of blood vessels may lead to aneurysms, which are localized balloon-like dilations of the vessel. Aneurysms are often fatal if they rupture. Therefore, changes in mechanical properties may have dire consequences!

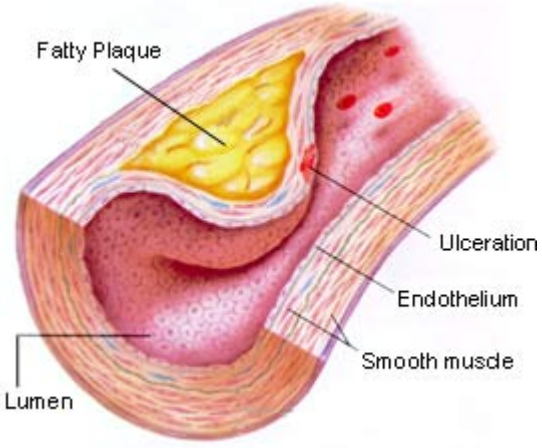

Objective

In this lab, we will use various tubing and a ball pump to model the circulatory system and observe how the mechanical properties of blood vessels alters blood flow.

Materials

- Ball pump and white nozzle
- 2 pieces of clear, stiff tubing
- 1 piece of amber, latex tubing
- 1 piece of pink, latex tubing
- 2 cable ties
- 1 beaker

Procedure

1. *Fill beaker halfway with water. Set up the circulatory system as follows: Screw the white nozzle into the ball pump. Connect the clear tubing to the pump. Then connect the amber latex tubing to the clear tubing. Finally, connect the other piece of clear tubing to the latex tubing and place the other end into the beaker.*

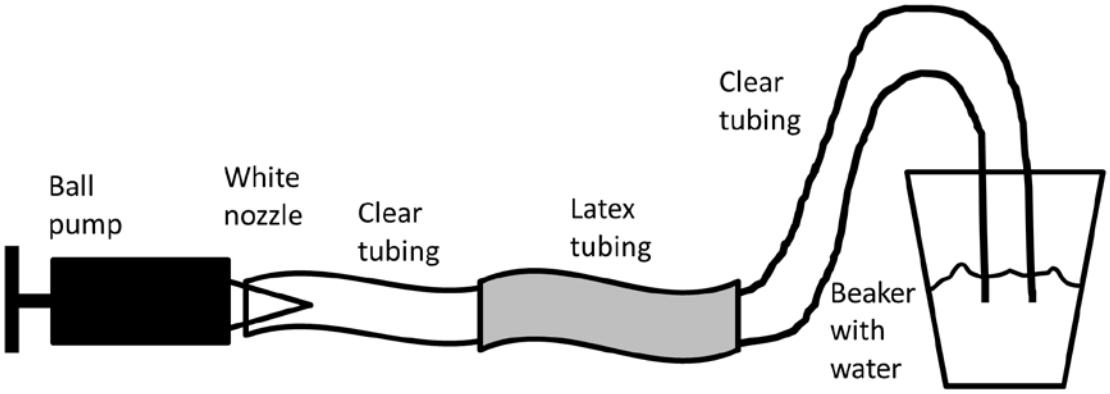

2. *Briskly pump the ball pump several times. Note how violently the bubbles appear in the beaker of water.* What does each pump (down-stroke) represent?

Heartbeat

3. *Disassemble the amber latex tubing and now replace it with the thinner pink latex tubing. Tie this onto the clear tubing with two cable ties. Make sure the connection is air-tight and there is no air leakage. Now pump several times.* Do bubbles still form? If yes, how do they compare to the amber latex?

Yes, but much less violently.

Which latex tubing results in higher pressure? How do you know?

Amber, the bubbles that formed were much more violent, meaning the air pressure was much higher.

What happens to the pink tubing during each down-stroke and upstroke?

The swells during the down-stroke and recoils during the upstroke.

In our tube model, which component represents…

a. the heart? **Pump**

b. blood? **Air**

c. a healthy artery? **Pink latex**

d. an atherosclerotic artery? **Amber latex**

From your observations, how does the elasticity of a blood vessel affect blood pressure?

The less elastic, the higher the blood pressure.

How does the elasticity of a blood vessel control the continuous flow of blood when the heart only contracts in pulses?

Elastic vessels can expand during the down-stroke and recoil normally, moving blood continuously. Stiff vessels do not expand or recoil so blood moves at higher pressures.

4. *Empty your beaker into the sink. Now, instead of allowing air to flow into water, plug the end of the tubing with your thumb. Now pump several times.* What happens to the pink latex tubing?

Balloons.

What does your thumb represent?

A thrombus (blood clot) or some kind of occlusion.

What does the expanded pink latex tubing represent?

An aneurysm.

5. *Gently squeeze the air-filled pink latex with your fingers.* How does this feel compared to an unfilled chamber?

Much less elastic due to high pressure.

What can you say about the thickness of the latex as it expands?

Gets thinner.

What about its stiffness?

Stiffer.

Conclusion:

Describe how the function of a blood vessel is altered when the mechanical properties of the blood vessel are altered.

Loses its ability to expand and recoil normally, and therefore, its ability to regulate blood pressure flow.

If an individual has atherosclerosis what happens to mechanical properties of their arteries?

The arteries stiffen.

Explain how atherosclerosis could lead to an aneurysm in a patient.

Fatty plaques can rupture and cause clots that occlude the artery.

How would you design a drug or treatment for atherosclerosis?

A drug that can reverse artery stiffening. A drug that prevents lipids or cholesterol from sticking and hardening arteries. A drug that helps the body clear plaques.

E.1.4 Polymer science: physical properties of gels lab

Introduction

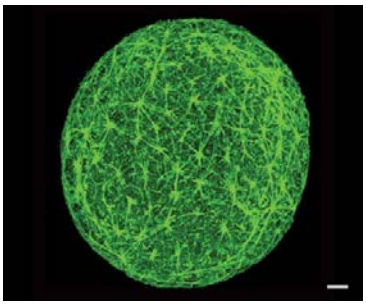

According to Wikipedia, gels are "jelly-like materials that can have properties ranging from soft and weak to hard and tough." They are found in almost all homes in different forms. For example, there is probably some hair gel in your bathroom. If you are wearing contact lenses, then there is a gel sitting on your eyeball. In biology labs, scientists can run an electrical current through gels in order to separate DNA or protein based on their size. Cells can be grown on gels that are comprised of various amounts of collagen.

Gels have many important physical characteristics. One interesting mechanical property of gels is their compliance, or stiffness. Obviously, hair gel is less stiff than contact lenses. In the growing field of mechanobiology, researchers study how cells respond to their mechanical environment by culturing them on soft or stiff gels. This kind of research will help to understand how to fight diseases that are caused by altered mechanical environments such as atherosclerosis, cancer, and cirrhosis. To make gels that have different stiffnesses, scientists vary the ratio of polymer to its crosslinker, which is a molecule that bonds one polymer to the next.

Objective

In this lab, we will make gels of varying compliances by altering the ratios of a polymer with its crosslinker and examine their physical characteristics.

Materials

- 5 zip lock bags
- A cup of "solution A"
- A cup of "solution B"
- Plastic teaspoons
- Permanent marker
- Food coloring

Procedure

1. *By varying the ratio of polymer to crosslinker, gel can be made with different compliances. To start off, make a gel that has a 4 to 1 ratio of solution A to solution B. To accomplish this, label a zip lock bag with "4:1." Add 4 teaspoons of solution A to the bag. Then add 1 teaspoon of solution B to the bag. Zip up the bag and mix thoroughly with your fingers. After a few minutes, you should get a gel. Take this out of the bag and kneed with your hands.* Write down some properties of the gel (stiffness, stickiness, bounciness, elasticity, etc.)

2. *What happens when you pull the gels apart* slowly?

Gel stretches.

What happens when you pull the gels apart quickly?

Gel breaks.

Think about the molecular structure of the gel. How do the polymer chains rearrange as you pull the gel apart slowly?

Polymer chains align parallel to one another.

How is this different when you pull the gel apart quickly?

There is not enough time to allow for polymer chain alignment.

How does molecular rearrangement of polymer chains affect the gel's mechanical properties?

Polymer alignment gives the gel its elastic strength since all the polymer chains are now parallel to one another. They act together similar to rope made of individual fibers.

3. *Make a ball out of the gel and let it sit on the table for a few minutes.* What happens?

The gel flattens out.

Would you characterize your gel as a solid or liquid? Why?

Both. It has properties of a solid in that it has structure but is liquid-like since it can flow.

4. *From this point on, you will be* ***designing an experiment****. Make two to four new gels with different ratios of solution A to solution B. Do not go lower than a 2:1 ratio or higher than a 10:1 ratio or you will not get a nice gel to play with. Remember to label your zip lock bags with the correct ratios!* Compare the properties of your new gels to the 4:1 ratio gel.

5. Based on your observations, how does adding more/less solution A affect gel properties?

This depends on the ratios the students choose. Some may find the gels get stiffer whereas others find the gels get less stiff. Remember that students may find data that do not support one another. Remind groups that discrepancies exist in science. Oftentimes this is due to inability to maintain proper controls or experimental conditions (such as size of the gel).

6. *In science, it is very important to quantify results by using numbers to describe and analyze data. Quantify one physical property of your gels as a function of its polymer ratio. Write down and explain the procedure of your quantification method. Create a chart or graph of this data.* To get you started, a sample graph is included. In this example, how would you quantify stiffness? (Hint: you can use rulers and/or stopwatches)

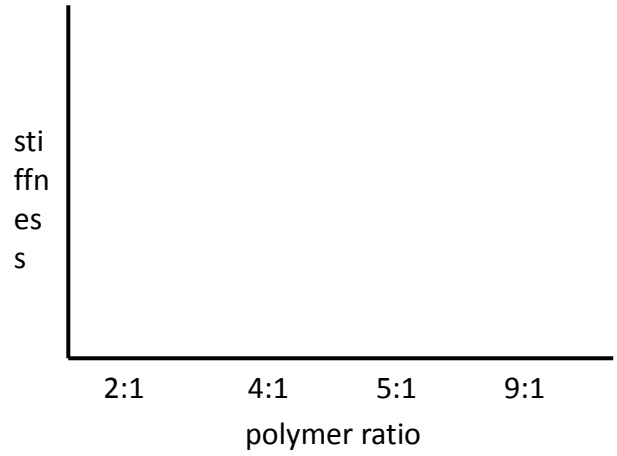

ATTACH to your LAB

Examples of experiments:

1. **Record the time it takes for a gel to stretch 10 inches when held in mid-air.**
2. **Record the length a gel stretches over 30 seconds.**
3. **Turn the gel into sphere and measure its initial diameter. Let the ball sit on a table for 60 seconds and then measure its diameter.**
4. **Turn the gel into a sphere and drop from table height. Record the height the ball bounces.**

7. If you were to engineer an implantable blood vessel using gels, which mechanical

properties would you consider and why are they important?

They should resemble the stiffness of native blood vessels in that they are not very stiff but have enough strength to regulate steady blood flow. They should not be sticky or it may lead to disturbed blood flow and the formation of clots.

E.1.5 Quiz: Atherosclerosis

1. Atherosclerosis occurs primarily in _____.

    A. veins
    B. capillaries
    C. arteries
    D. all of the above

2. Which is considered the first cellular event in the progression of atherosclerosis?

    A. Macrophage transformation
    B. Monocyte transmigration
    C. Smooth muscle cell migration
    D. Endothelial cell permeability

3. What type of mechanical stress causes endothelial cells to orient themselves in the same direction?

    A. hoop/circumferential stress
    B. shear stress
    C. compressive stress
    D. tensile stress

4. In what percent of the population does stiffening of the blood vessels occur?

    A. 25%
    B. 40%
    C. 80%
    D. 100%

5. Which is not a risk factor for atherosclerosis?

    A. cancer
    B. diabetes
    C. smoking
    D. hypercholesterolemia

6. The _____ of an artery contributes most to its mechanical strength.

A. intima
B. media
C. adventitia
D. lumen

7. Vessel stiffening results in _____.

A. increased blood pressure
B. decreased blood pressure
C. increased cholesterol
D. laminar blood flow

8. The ratio of stress to strain is called _____.

A. Young's modulus
B. Poisson's ratio
C. Creep
D. Bending strength

9. A liquid polymer solution can easily be turned into a gel by adding _____.

A. a detergent
B. an emulsifier
C. a crosslinker
D. an organic solvent

10. Blood vessels are similar to gels in that they act as _____ materials.

A. viscoelastic
B. elastic
C. isotropic
D. compressible

E.2 Cell-Cell communications lecture slides

Cell communication

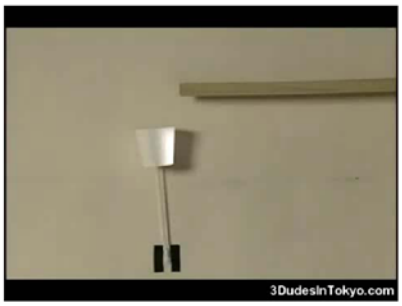

How do cells communicate?

- Electrically
  - Nerves
  - Cardiac
- Mechanically
- Chemically

Chemical signaling

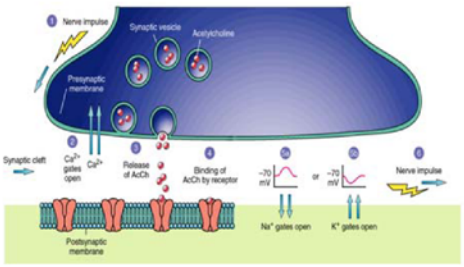

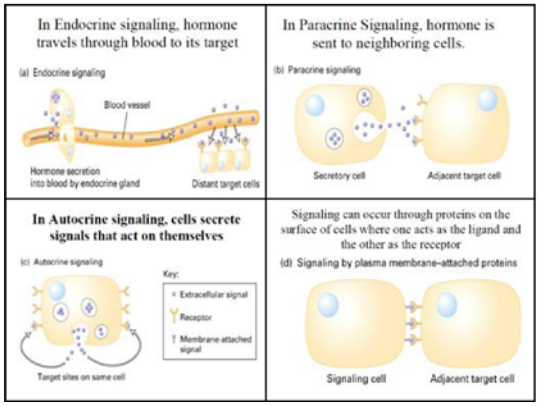

How important is cell communication?

Touch

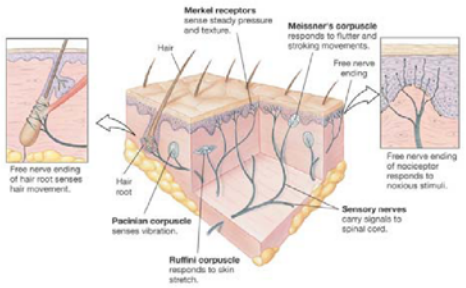

Smell

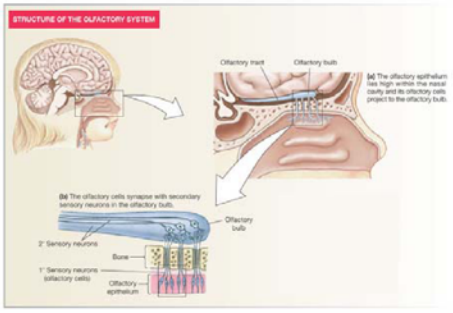

Taste

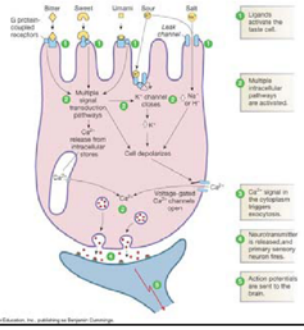

Hearing

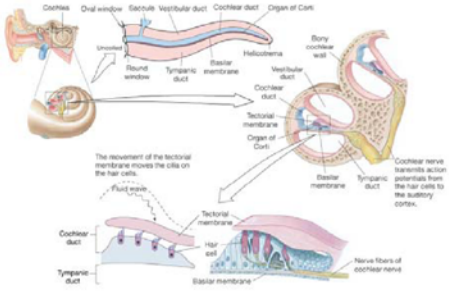

Sight

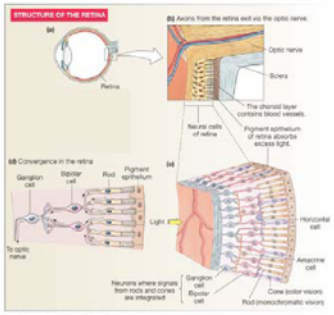

Immune system

Mechanical signaling

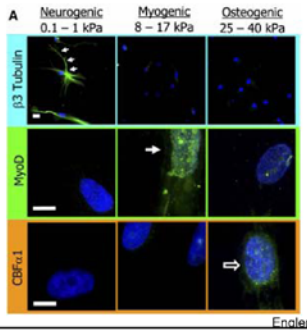

Engler, et al. Cell 2006.

Wound healing

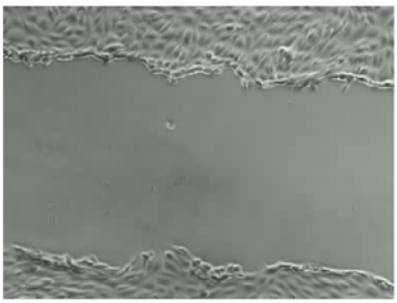

Diseases related to defective cell communication

- Cardiovascular disease
  - Stroke
  - Heart attack
- Cancer
- Diabetes
- Neurological disorders
  - Alzheimer's
  - Multiple Sclerosis

Cardiovascular disease (CVD)

- #1 cause of death in the United States
- In 2005, claimed more lives than cancer, car accidents, and HIV (AIDS) combined
- > 80 million Americans have one or more forms of cardiovascular disease
- > 12 million exhibit arterial occlusion

americanheart.org

Atherosclerosis – the hardening of arteries

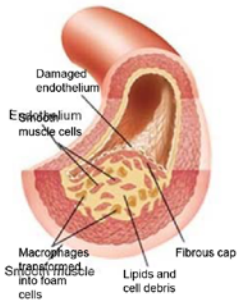

Cancer

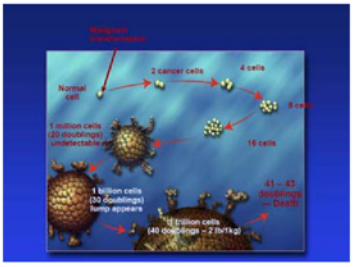

Diabetes

- As of 2007, 24 million Americans have diabetes (~8% of the population)
- Leads to CVD, kidney failure, neuropathy

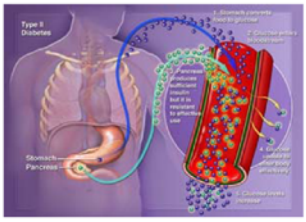

Multiple Sclerosis

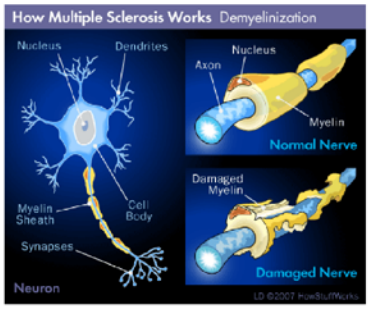

Neural Engineering

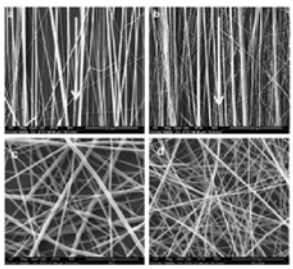

Gupta, et al. Acta Biomat 2009.

Mechanical cues align neurons

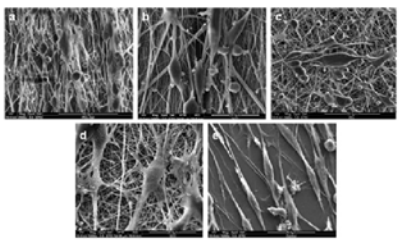

Gupta, et al. Acta Biomat 2009.

E.3 Bioterrorism lecture slides

Bioterrorism and toxins

The Rock (1996)

Hollywood Pictures

VX nerve agent

- Texture of motor oil
- Stays in the environment
- Odorless and tasteless

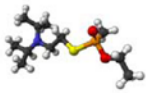

- Median lethal dose is ~1/100 of a gram through skin
- Causes muscular twitching, nausea and vomiting, tightness in the chest, shortness of breath
- Sustained paralysis of the diaphragm muscle results in death by asphyxiation

How does it work?

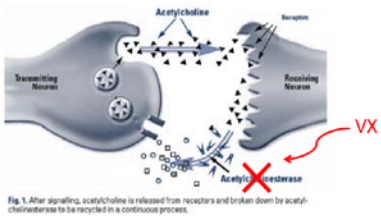

www.vrp.com

How would you counter VX?

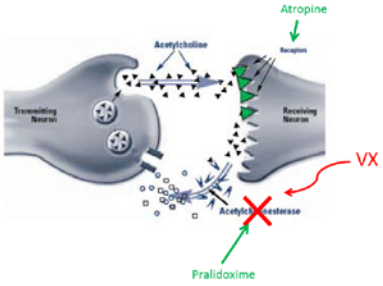

ATNAAA – antidote treatment nerve agent auto-injector

- Military use only
- Injects both pralidoxime and atropine
- VX has been used to kill only one person so far, but…

meridianmeds.com

Sarin attacks in Tokyo, 1995

- Works in the same manner as VX
- Terrorists brought bags of sarin onto the subway system
- Used umbrellas with sharpened tips to puncture the bags
- Resulted in 13 deaths and over 6000 injuries


metro.tokyo.jp and nih.gov

Animal neurotoxins acts on the same pathway


King cobra


Black widow spider

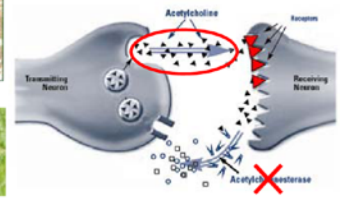

snakesting.blogspot.com and nationalgeographic.com

Other type of toxins

- <u>Cardiotoxins</u> – prevents heart contraction
- <u>Hemotoxins</u> – destroys red blood cells, disrupts blood clotting, leads to hemorrhaging
- <u>Cytotoxins</u> – rips holes into cell membranes, prevents protein synthesis, causes cell death


Rattlesnake


Castor beans → Ricin

botswanagallery.org and globalsecurity.org

Toxins in clinical use

- Botulinum toxin (Botox)
- Used to treat:
  - Excessive blinking
  - Excessive sweating
  - Spasms
  - Dystonias (sustained muscle contractions)
  - Prevents the formation of wrinkles



nature.com and freerepublic.com

How does Botox work?


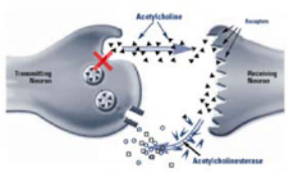

- Prevents the release of acetylcholine
- Results in paralysis

biology.clc.uc.edu

Summary

- Toxins affect many different pathways in the body which may result in tissue damage or death
- Animals use toxins as predatory (snakes, scorpions) or defense mechanisms (poison dart frogs, bees)
- Toxins have been researched as potential biological weapons
- Toxins can be used for good, such as treating neuromuscular disorders or pain

E.4 Cancer lecture slides

Treating cancer

What is cancer?

What causes cancer?

- Smoking
- Poor diet
- Genes
- Age

Cancer pathways

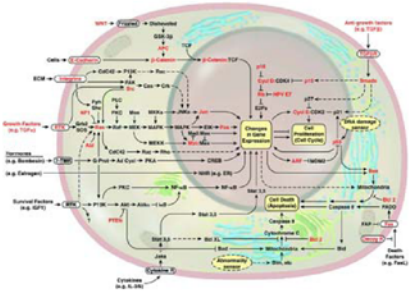

Tumor cell heterogeneity

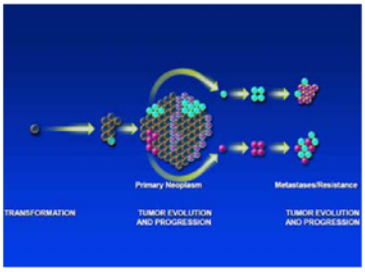

Tumor development

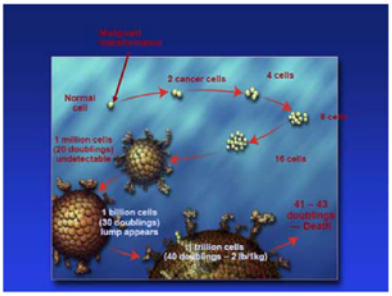

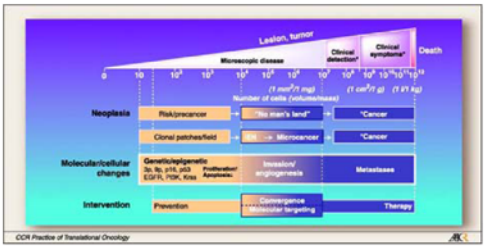

How do we treat cancer?

- Chemotherapy
  - Drugs that kill cancer cells
- Radiotherapy
  - X-rays
- Immunotherapy
  - Manipulating the immune system to seek and destroy cancer cells

Action sites of cytotoxic agents

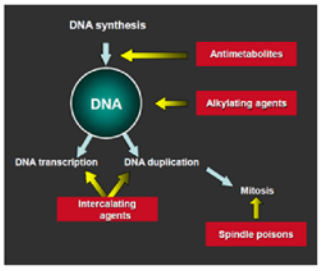

Chemotherapy may fail

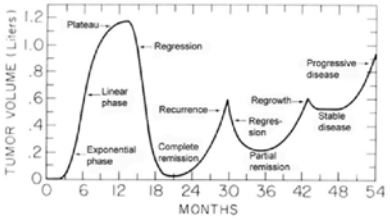

Why chemotherapy fails…

- Cancer cells become insensitive to drugs
  - Death becomes unregulated
  - Cancer cells can repair themselves
- Wrong dose of drugs
- Physical barriers prevent drugs from getting to the cancer

Angiogenesis: double-edged sword

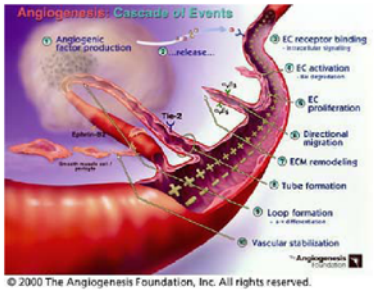

E.5 Heart valves lecture slides

The heart

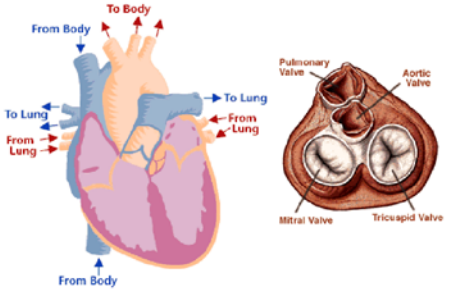

Heart valve problems

- Stenosis
  - Does not open fully
  - Stiffened valve tissue
  - Heart needs to do more work to push blood through the valve
- Incompetence
  - Inefficient blood circulation
  - Backflow of blood in the heart

Mechanical heart valves

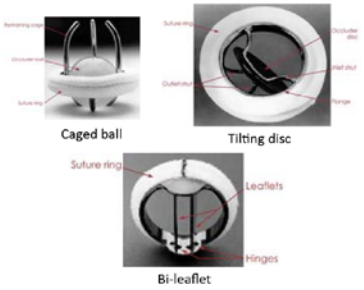

Mechanical heart valves

- Advantages
  - High durability
- Disadvantages
  - Increased risk of blood clotting
  - High probability of heart attack or stroke
  - Require anti-coagulants

Bioprosthetic tissue valves

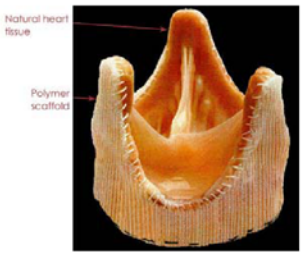

Transplants

- Human
- Animal
  - Excellent hemodynamics
  - Durability of 10-15 years
  - Can undergo calcification
  - Leads to stenosis or tears

E.6 Nanotechnology lecture slides

Nanotechnology

Carbon

Prior to 1980s, two forms:

diamond

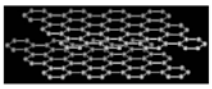

graphite

In 1985:

buckminsterfullerene
buckyball

Carbon nanotube

Nanoscale

- How big is a nanometer?

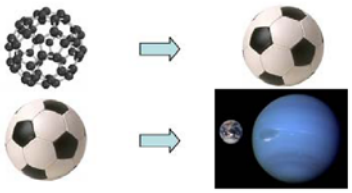

Gold nanoparticles

Gold nanoparticles

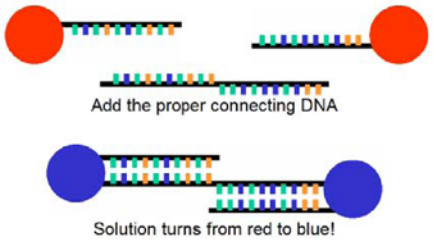

Magnetism – ferrofluid

Magnetite suspended in liquid

www.mrsec.wisc.edu

Magnetism – ferrofluid

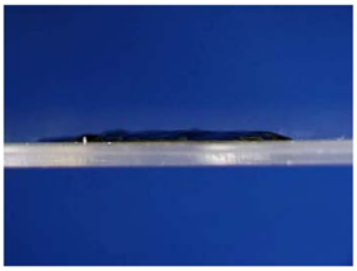

www.mrsec.wisc.edu

Medical applications

Coat with drugs, antibodies, peptides, or oligonucleotides

Use magnetic fields to position
- Deliver drugs to targets (especially for chemotherapy)
- "Tag and drag" removal (especially for toxins)

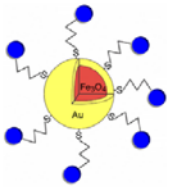

Nanoparticles absorb wavelengths the human body does not

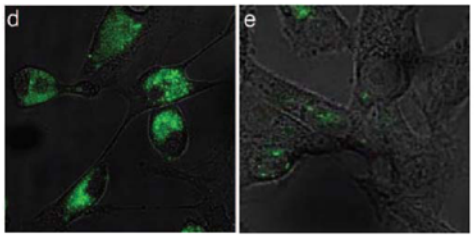

Cancer cells Normal cells

NWS Kam et al. PNAS 2005.

Window glass containing nanoparticles

- Absorb UV light and break down dirt
- Water spreads out on surface to rinse off
- "Self-cleaning" windows

activglass.com

2006 World Cup – Germany

Self-cleaning surfaces

Nanotechnology in clothing

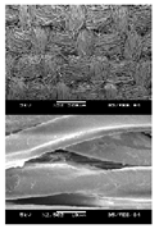

Nano-Care™ Fabric

www.eddiebauer.com

10 nm fiber coating not wet by oil or water

Nanotechnology in sports

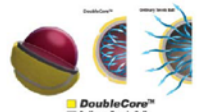

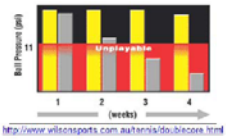

http://www.wilsonsports.com.au/tennis/doublecore.html

Nanocomposite oriented vermiculite platelets in latex polymer inhibits air permeation but remains flexible.

Nanobiotechnology

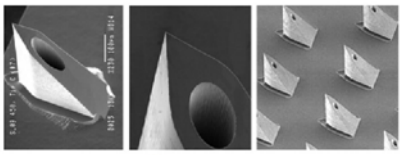

- Microneedle drug delivery
- Painless injections

nanopass.com

Nanobiotechnology

- "Nano-tattoo"
- One tiny pinprick
- Yellow and fluorescent when glucose is low
- Purple and non-fluorescent when glucose is high

earthsky.org

E.7 Tissue engineering lecture slides

Stem cells and tissues: research and applications

Tissue Engineering

"an interdisciplinary field that applies the principles of engineering and life sciences toward the development of biological substitutes that restore, maintain, or improve tissue function or a whole organ"

-Robert Langer & Joseph Vacanti, Science 1993

Tissue Engineering

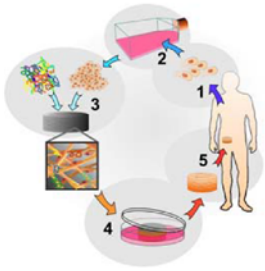

- 1. Cell isolation
- 2. Cell expansion
- 3. Load scaffold
- 4. Engineer tissue
- 5. Implant

Electrospun polymer scaffold

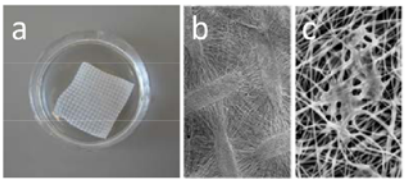

(a) Macroscopic image
(b) Scanning electron micrograph
(c) Cells seeded onto the scaffold

Polymer scaffold

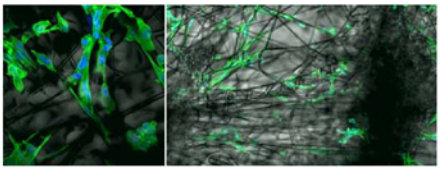

Endothelial cells attached to a PLA scaffold
Green: cytoskeleton
Blue: nucleus

Case study: Neural engineering

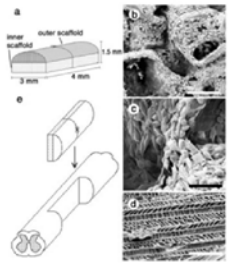

Teng YD, *et al.* PNAS 2002.

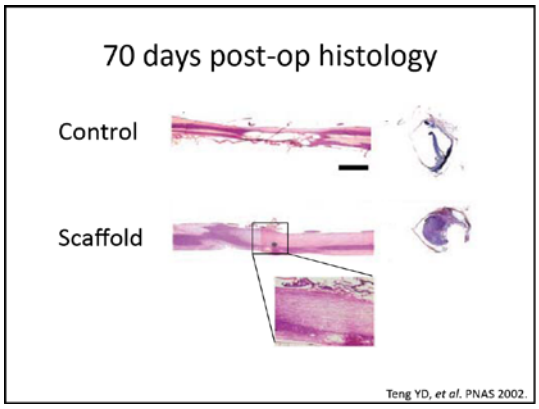
70 days post-op histology
Control
Scaffold
Teng YD, et al. PNAS 2002.

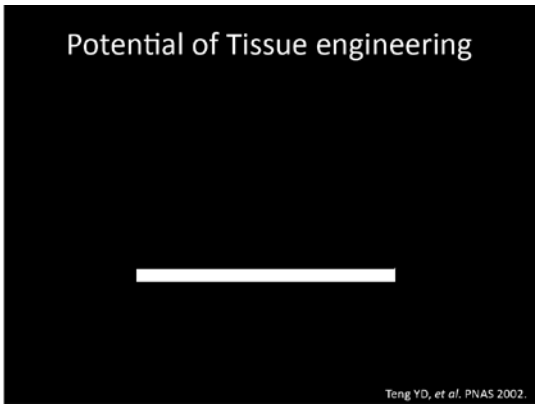
Potential of Tissue engineering
Teng YD, et al. PNAS 2002.

APPENDIX F

VASCULAR ENDOTHELIAL (VE)-CADHERIN WIDTH MEASUREMENTS

Protocol:

1. Open image in ImageJ.
2. Draw a line across the widest gap per junction perpendicular to the junction.
3. Press ‘k’ to pull up the pixel intensity profile of the line just drawn.
4. Save the graph values by clicking ‘Save…’ and saving with the naming convention data001.dat, data002.dat, etc.
5. Once all of the lines are saved, place all data files in the same folder. Also place mainpixel3.m and PixelSSR2.m into the same folder.
6. Open MATLAB. Set your ‘Current Folder’ as the folder with all of your data files.
7. Edit line 7 of mainpixel3.m to match the number of data files you have. Edit line 41 if necessary to account for microscope objective magnification.
8. Run mainpixel3.m.
9. Go through the figures MATLAB generated. If there are plots where the fit is incorrect, edit lines 24 through 27 by changing i and the guesses for fminsearch. Additional if-statements can be added for additional incorrect fits.

```
%mainpixel3.m
%this program fits to TWO gaussians
%put files into same directly as program, with naming scheme:
%data001.dat, data002,dat etc. No text on first line, just #
clear
global data
Nfiles=60;   %number of files, maximum is 999
for i=1:Nfiles

    num=num2str(i);
    if length(num)==1
        filename=['data00',num,'.dat'];
    elseif length(num)==2
        filename=['data0',num,'.dat'];
    else
        filename=['data',num,'.dat'];
    end
    load(filename)
    data=eval(filename(1:7));

    A=fminsearch('PixelSSR2',[18,25,4,500,120],
    optimset('MaxFunEvals', 5000,'MaxIter', 5000));
    %A1=mu1, A2=mu2, A3=sig, A4=a1 (rescale), A5=a2 (baseline)

    if (i==61)
    A=fminsearch('PixelSSR2',[14,25,4,500,250],
    optimset('MaxFunEvals', 5000,'MaxIter', 5000));
        checkme=i
    end

    x=[1:.1:length(data)];
    figure(i)
    plot(data(:,1),data(:,2),'bo',x,...
        A(4).*(1/sqrt(2*pi*A(3).^2)*exp(-(x-
        A(1)).^2/(2*A(3).^2))+...
    1/sqrt(2*pi*A(3).^2)*exp(-(x-A(2)).^2/(2*A(3).^2)))+A(5),'r-')

    if (A(1)<1 | A(2)<1 | A(1)>length(data) | A(2)>length(data) )
        A6=A(3)*3.585; %the width at 20% above baseline is
                       =3.585*sigma+abs(mu1-mu2)
        A(2)=A(1); % added
    else
        A6=A(3)*3.585+abs(A(1)-A(2));
    end
    A6=A6*0.3225; % for 20x images on the fluorescent scope
    A7=abs(A(1)-A(2));
    A8=A7./A(3);
    Alarge(i,:)=[A,A6,A7,A8];


end
%these numbers can be used to recreate the Gaussian curves.
%columns: mu1 | mu2 | sigma | rescale | baseline | width | Dmu |
Dmu/sigma
saving_results=xlswrite('widths.xls', Alarge);
```

```
51
52 avg_width_at_20_percent_in_um=mean(Alarge(:,6))
```

```
1 % PixelSSR2.m
2 % fit pixel intensity data to 2 Gaussian functions of the form:
3 % f = a1*(1/sqrt(2*pi*sig^2)*exp(-(x-mu1)^2/(2*sig^2))+...
4 % 1/sqrt(2*pi*sig^2)*exp(-(x-mu2)^2/(2*sig^2))) + a2
5 %we are constraining the two sigmas to be equal
6 %a1 rescales the distribution and a2 is the baseline
7
8  function SSR = PixelSSR(A)
9  global data
10 mu1=A(1);    mu2=A(2);   sig=A(3);   a1=A(4);    a2=A(5);
11
12 SSR=sum((data(:,2)-a1.*(1/sqrt(2*pi*sig.^2)*exp(-(data(:,1)-
13 mu1).^2/(2*sig.^2))+...
14 1/sqrt(2*pi*sig.^2)*exp(-(data(:,1)-mu2).^2/(2*sig.^2)))-a2).^2);
```